



MINISTÉRIO DA
CIÊNCIA, TECNOLOGIA,
INOVAÇÕES E COMUNICAÇÕES



sid.inpe.br/mtc-m21c/2020/02.12.12.28-TDI

**DIFFUSION FLAMES WITH CONTINUOUS CHANGE
IN PROPERTIES: FROM COUNTERFLOW REGIME
(TSUJI FLAME) TO COFLOW REGIME
(BURKE-SCHUMANN FLAME)**

Matheus de Pádua Severino

Master's Dissertation of the
Graduate Course in Space
Engineering and Technology,
guided by Dr. Fernando Fachini
Filho, approved in February 28,
2020.

URL of the original document:

<<http://urlib.net/8JMKD3MGP3W34R/3UTT928>>

INPE
São José dos Campos
2020

PUBLISHED BY:

Instituto Nacional de Pesquisas Espaciais - INPE
Gabinete do Diretor (GBDIR)
Serviço de Informação e Documentação (SESID)
CEP 12.227-010
São José dos Campos - SP - Brasil
Tel.:(012) 3208-6923/7348
E-mail: pubtc@inpe.br

**BOARD OF PUBLISHING AND PRESERVATION OF INPE
INTELLECTUAL PRODUCTION - CEPPII (PORTARIA Nº
176/2018/SEI-INPE):****Chairperson:**

Dra. Marley Cavalcante de Lima Moscati - Centro de Previsão de Tempo e Estudos
Climáticos (CGCPT)

Members:

Dra. Carina Barros Mello - Coordenação de Laboratórios Associados (COCTE)
Dr. Alisson Dal Lago - Coordenação-Geral de Ciências Espaciais e Atmosféricas
(CGCEA)
Dr. Evandro Albiach Branco - Centro de Ciência do Sistema Terrestre (COCST)
Dr. Evandro Marconi Rocco - Coordenação-Geral de Engenharia e Tecnologia
Espacial (CGETE)
Dr. Hermann Johann Heinrich Kux - Coordenação-Geral de Observação da Terra
(CGOBT)
Dra. Ieda Del Arco Sanches - Conselho de Pós-Graduação - (CPG)
Sílvia Castro Marcelino - Serviço de Informação e Documentação (SESID)

DIGITAL LIBRARY:

Dr. Gerald Jean Francis Banon
Clayton Martins Pereira - Serviço de Informação e Documentação (SESID)

DOCUMENT REVIEW:

Simone Angélica Del Ducca Barbedo - Serviço de Informação e Documentação
(SESID)
André Luis Dias Fernandes - Serviço de Informação e Documentação (SESID)

ELECTRONIC EDITING:

Ivone Martins - Serviço de Informação e Documentação (SESID)
Cauê Silva Fróes - Serviço de Informação e Documentação (SESID)



MINISTÉRIO DA
CIÊNCIA, TECNOLOGIA,
INOVAÇÕES E COMUNICAÇÕES



sid.inpe.br/mtc-m21c/2020/02.12.12.28-TDI

**DIFFUSION FLAMES WITH CONTINUOUS CHANGE
IN PROPERTIES: FROM COUNTERFLOW REGIME
(TSUJI FLAME) TO COFLOW REGIME
(BURKE-SCHUMANN FLAME)**

Matheus de Pádua Severino

Master's Dissertation of the
Graduate Course in Space
Engineering and Technology,
guided by Dr. Fernando Fachini
Filho, approved in February 28,
2020.

URL of the original document:

<<http://urlib.net/8JMKD3MGP3W34R/3UTT928>>

INPE
São José dos Campos
2020

Cataloging in Publication Data

Severino, Matheus de Pádua.

Se83d Diffusion flames with continuous change in properties: from counterflow regime (Tsuji flame) to coflow regime (Burke-Schumann flame) / Matheus de Pádua Severino. – São José dos Campos : INPE, 2020.

xx + 91 p. ; (sid.inpe.br/mtc-m21c/2020/02.12.12.28-TDI)

Dissertation (Master in Space Engineering and Technology) – Instituto Nacional de Pesquisas Espaciais, São José dos Campos, 2020.

Guiding : Dr. Fernando Fachini Filho.

1. Double Tsuji Diffusion Flame 2. Cylindrical Burner in Impinging Flows 3. Transition from Transient to Stationary Regime 4. Asymptotic Analysis 5. Characteristic Scales. I.Title.

CDU 662.612



Esta obra foi licenciada sob uma Licença [Creative Commons Atribuição-NãoComercial 3.0 Não Adaptada](https://creativecommons.org/licenses/by-nc/3.0/).

This work is licensed under a [Creative Commons Attribution-NonCommercial 3.0 Unported License](https://creativecommons.org/licenses/by-nc/3.0/).

Aluno (a): **Matheus de Pádua Severino**

Título: "DIFFUSION FLAMES WITH CONTINUOUS CHANGE IN PROPERTIES: FROM COUNTERFLOW REGIME (TSUJI FLAME) TO COFLOW REGIME (BURKE-SCHUMANN FLAME)"

Aprovado (a) pela Banca Examinadora em cumprimento ao requisito exigido para obtenção do Título de **Mestre** em

**Engenharia e Tecnologia
Espaciais/Combustão e Propulsão**

Dr. Fernando Fachini Filho

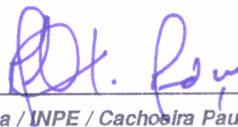


Presidente / Orientador(a) / INPE / Cachoeira Paulista - SP

() Participação por Vídeo - Conferência

Aprovado () Reprovado

Dr. Márcio Teixeira de Mendonça



Membro da Banca / INPE / Cachoeira Paulista - SP

() Participação por Vídeo - Conferência

Aprovado () Reprovado

Dr. Wladimir Mattos da Costa Dourado



Membro da Banca / IAE/DCTA / São José dos Campos - SP

() Participação por Vídeo - Conferência

Aprovado () Reprovado

Dr. Vinicius Maron Sauer



Convidado(a) / CSUN / California - USA

Participação por Vídeo - Conferência

Aprovado () Reprovado

Este trabalho foi aprovado por:

() maioria simples

unanimidade

São José dos Campos, 28 de fevereiro de 2020

“I fear the animals regard man as a being like themselves, seriously endangered by the loss of sound animal understanding; they regard him perhaps as the absurd animal, the laughing animal, the crying animal, the unfortunate animal.”

FRIEDRICH WILHELM NIETZSCHE

“The Gay Science : Third Book, 224. Animal Criticism”, 1882

*For all those who seek to rid themselves of the darkness
of ignorance and attain the true light provided by
knowledge and wisdom.*

*For the brave who have dared to leave the calm waters of
nescience and enter the turbulent and dangerous waters
of intellectual development.*

ACKNOWLEDGEMENTS

My sincere gratitude to my master's degree advisor, Dr. Fernando Fachini Filho, for the valuable learning in the Science of Combustion and for the philosophical discussions, essential for the search of knowledge about the exterior universe and, mainly, about the interior universe. An extremely professional and ethical person, who "breathes science".

Thanks to the Instituto Nacional de Pesquisas Espaciais (INPE) for the opportunity to complete the master's degree and, more specifically, to the Laboratório Associado de Combustão e Propulsão (LCP) and to every professor and collaborator who contributed directly or indirectly with this work and with this "battle of my personal war".

It was an enormous privilege to have Gabriel Silva Dias and Jorge Henrique Gagliarde as classmates and now friends.

I salute Coordenação de Aperfeiçoamento de Pessoal de Nível Superior (CAPES) for the financial support by granting a scholarship, which made this academic study possible.

I express my thankfulness to my sister, Beatriz de Padua Severino, for providing a computer to assist in numerical processing and, foremost, for the conversations and debates that always results in precious reflections.

Thank you very much, Aline Bueno Lopes, my inamorata and friend at all times!

Finally, I am very grateful to my father, Luiz Carlos Severino, and to my mother, Rosi de Padua Severino, for their unconditional support.

ABSTRACT

Understanding any phenomenon at the most fundamental level is essential for the later comprehension of more complex phenomena, because they are nothing more than a set of elementary phenomena, influencing each other. Diffusion flame established around a cylindrical burner is inherently two-dimensional. Tsuji and his partners worked for more than 20 years on cylindrical burners. Theirs experiments aimed, notably, to determine the influence of the strain rate on the flame stability. Recently, Tsuji flame has received more attention, but examining the entire flame and not only the region near the point of stagnation, under forced and natural convection. The present work endeavors to analyze a similar problem but considering a cylindrical burner in impinging flows. The objective is to determine the influence of burner, flow field and stoichiometry on the flame, developing and implementing numerically a mathematical model and determining analytical solutions. Making the model simple and without loss of generality, potential flow is assumed. According to the hypotheses considered, the mixture fraction and the excess of enthalpy describe the evolution of fuel mass fraction, oxidant mass fraction and temperature. The flame spends most of its lifetime in a region of the flow field scaled with the reciprocal of square root of strain rate and velocities are scaled with the square root of strain rate. The results demonstrate that the initial flame displacement is controlled by radial transport of fuel into the region nearby the burner, in which the impinging flows have a negligible influence. After that period, the flame is strongly influenced by the impinging flows, when its acceleration is observed. The flame length is proportional to the stoichiometric coefficient, ejecting velocity and reciprocal to square root of strain rate. Meanwhile, the flame width is only dependent on the reciprocal of square root of strain rate. Moreover, the proposed asymptotic solution underlines the most significant transport mechanisms for the flame in different conditions and allows the deduction of important properties such as stagnation points, strain rate, approximate solutions and gradients.

Keywords: Double Tsuji diffusion flame. Cylindrical burner in impinging flows. Transition from transient to stationary regime. Asymptotic analysis. Characteristic scales. Continuous change flame.

CHAMAS DIFUSIVAS COM MUDANÇA CONTÍNUA NAS PROPRIEDADES: DO REGIME DE CONTRAFLUXO (CHAMA DE TSUJI) AO REGIME DE CO-FLUXO (CHAMA DE BURKE-SCHUMANN)

RESUMO

A compreensão de qualquer fenômeno no nível mais fundamental é essencial para o entendimento posterior de fenômenos mais complexos, pois eles não passam de um conjunto de fenômenos elementares, influenciando-se mutuamente. A chama difusiva estabelecida em torno de um queimador cilíndrico é inerentemente bidimensional. Tsuji e parceiros trabalharam por mais de 20 anos em queimadores cilíndricos. Eles objetivaram, nomeadamente, determinar a influência da taxa de estiramento na estabilidade da chama. Recentemente, a chama Tsuji voltou à análise, examinando-se toda a chama e não apenas a região próxima ao ponto de estagnação, sob convecção forçada e natural. O presente trabalho procura analisar um problema semelhante, mas considerando um queimador cilíndrico em escoamentos impingentes. O objetivo é determinar a influência do queimador, escoamento e estequiometria na chama, desenvolvendo e implementando numericamente um modelo matemático e determinando soluções analíticas. Por simplicidade e sem perda de generalidade, assume-se um escoamento potencial. De acordo com as hipóteses consideradas, a fração de mistura e o excesso de entalpia descrevem a evolução da fração de massa do combustível, fração de massa do oxidante e temperatura. A chama passa a maior parte do tempo em uma região do escoamento escalonada com a recíproca da raiz quadrada da taxa de estiramento e as velocidades são escalonadas com a raiz quadrada da taxa de estiramento. Os resultados demonstram que o deslocamento inicial da chama é controlado pelo transporte radial do combustível para a região próxima ao queimador, na qual os escoamentos impingentes têm uma influência insignificante. Após esse período, a chama é fortemente influenciada pelos escoamentos impingentes, quando a sua aceleração é observada. O comprimento da chama é proporcional ao coeficiente estequiométrico, à velocidade de ejeção e à recíproca da raiz quadrada da taxa de estiramento. Entretanto, a largura da chama depende apenas da recíproca da raiz quadrada da taxa de estiramento. Além disso, a solução assintótica proposta destaca os mecanismos de transporte mais significativos para a chama em diferentes condições e permite a dedução de propriedades importantes, como pontos de estagnação, taxa de estiramento, soluções aproximadas e gradientes.

Palavras-chave: Chama duplo-Tsuji difusiva. Queimador cilíndrico em escoamentos impingentes. Transição do regime transiente ao estacionário. Análise assintótica. Escalas características. Chama com mudança contínua.

LIST OF FIGURES

	<u>Page</u>
1.1 Tsuji problem ilustration	2
1.2 Tsuji problem under natural convection	3
1.3 Proposed configuration	4
3.1 Separate visualization of the three potential flows that, superposed, constitute the flow field adopted	14
3.2 Potential flow field	16
4.1 Model schematic illustration	22
4.2 Asymptotic solution for Z	24
4.3 Asymptotic flame shape	25
4.4 Asymptotic gradient norm ($ \nabla Z $)	26
4.5 Scalar dissipation coefficient (χ)	27
4.6 Stagnation points (y_{st})	30
5.1 Comparison of the flame shape using three distinct grids.	34
5.2 Richardson's extrapolation for zero spacing grid ($h = 0$) based on the two finest grids.	35
5.3 Comparison of the asymptotic solution with numerical results	37
6.1 Temporal evolution of the flame	40
6.2 Temporal evolution of aspect ratio (\tilde{x}_f/\tilde{y}_f)	43
6.3 Temporal evolution of flame length (\tilde{x}_f) and width (\tilde{y}_f)	44
6.4 Temporal evolution of flame length (\tilde{u}_f) and width (\tilde{v}_f) velocities	45
6.5 Dynamics of the flame	46
6.6 Comparison of the asymptotic solution with numerical results	48
6.7 Diffusion flame with continuous proprieties change	49
6.8 Flow field and flame shape	51
6.9 Temperature distribution (T)	52
6.10 Flame width ($y_f \sim L_y$) - varying Pe_c	53
6.11 Flame width ($y_f \sim L_y$) - varying Pe_b	54
6.12 Flame width (y_f)	55
6.13 Flame length influence demarcator - varying S	57
6.14 Flame length influence demarcator - varying Pe_c	58

LIST OF SYMBOLS

\hat{x}	– spatial first coordinate
x	– dimensionless spatial first coordinate
\tilde{x}	– rescaled dimensionless spatial first coordinate
\hat{y}	– spatial second coordinate
y	– dimensionless spatial second coordinate
\tilde{y}	– rescaled dimensionless spatial second coordinate
\hat{r}	– spatial radial coordinate
r	– dimensionless spatial radial coordinate
\tilde{r}	– rescaled dimensionless spatial radial coordinate
θ	– spatial angular coordinate
\hat{t}	– time
t	– dimensionless time
τ	– rescaled dimensionless time
\hat{R}	– burner radius
Pe_b	– Peclet number based on the burner conditions
Pe_c	– Peclet number based on the impinging flows conditions
$Pe_c^{(1)}$	– Order unit Peclet number based on the impinging flows conditions
\hat{T}	– temperature
T	– dimensionless temperature
Z	– mixture fraction
H	– excess of enthalpy
\hat{u}	– velocity first coordinate
u	– dimensionless velocity first coordinate
\tilde{u}	– rescaled dimensionless velocity first coordinate
\hat{v}	– velocity second coordinate
v	– dimensionless velocity second coordinate
\tilde{v}	– rescaled dimensionless velocity second coordinate
\hat{Y}_n	– mass fraction of the specie n
Y_n	– normalized mass fraction of the specie n
$\hat{\rho}$	– density
$\hat{\alpha}$	– thermal diffusivity
\hat{k}	– thermal conductivity
\hat{c}_p	– specific heat at constant pressure
\hat{s}	– mass stoichiometric coefficient
S	– modified mass stoichiometric coefficient
\hat{Q}	– combustion heat released
Q	– dimensionless combustion heat released
\hat{L}_x	– estimate flame length
L_x	– dimensionless estimate flame length
\hat{L}_y	– estimate flame width

- L_y – dimensionless estimate flame width
- η – burner influence adjust coefficient
- N – flame length rescaling parameter
- χ – scalar dissipation coefficient
- y_{st} – dimensionless stagnation point

CONTENTS

	<u>Page</u>
1 PREFACE	1
1.1 Introduction	1
1.2 Objectives	4
1.2.1 Specific aims	4
1.3 Structure	5
2 LITERATURE REVIEW	7
2.1 Combustion	7
2.1.1 Diffusion flames	7
2.1.1.1 Burke-Schumann limit	8
2.1.1.2 Schvab-Zeldovich formulation	8
2.1.1.3 Liñán analysis	9
2.2 Tsuji flame	9
2.2.1 Research Group	10
3 METHODOLOGY	13
3.1 Model	13
3.1.1 Potential flow	13
3.1.2 Energy and species conservation equations	15
3.1.3 Axial symmetry	17
3.1.4 Transition $(r, t; Pe_c) \rightarrow (x, y; Pe_c)$	17
3.2 Numerical implementation	19
4 THEORETICAL ANALYSIS	21
4.1 Order of magnitude analysis	21
4.2 Asymptotic solution	23
4.2.1 Mixture fraction gradient	26
4.2.2 Point of tangency	27
4.2.3 Normal and tangential velocities	28
4.3 Stagnation points	29
4.3.1 Strain rate	30
5 NUMERICAL VALIDATION	33

5.1	Grid convergence	33
5.2	Code validation	36
6	DISCUSSION	39
6.1	Transition ($Pe_c = \varepsilon Pe_c^{(1)}, \varepsilon \ll 1$)	39
6.1.1	Asymptotic analysis	47
6.2	Flame characteristics	49
6.3	Flame properties estimation	50
6.3.1	Flame sensitivity	52
6.3.2	For $N_{min} \leq N \leq S$	56
6.3.3	For $N > S$	56
7	CONCLUSION	59
7.1	Suggestions for future work	60
	REFERENCES	61
	APPENDIX A - POTENTIAL FLOW	65
	APPENDIX B - DETAILED FORMULATION	71
B.1	Dimensionless Equations	71
B.2	Mixture Fraction (Z) and Excess Enthalpy (H)	76
	APPENDIX C - DETAILED FORMULATION OF TRANSITION PROBLEM	81

1 PREFACE

1.1 Introduction

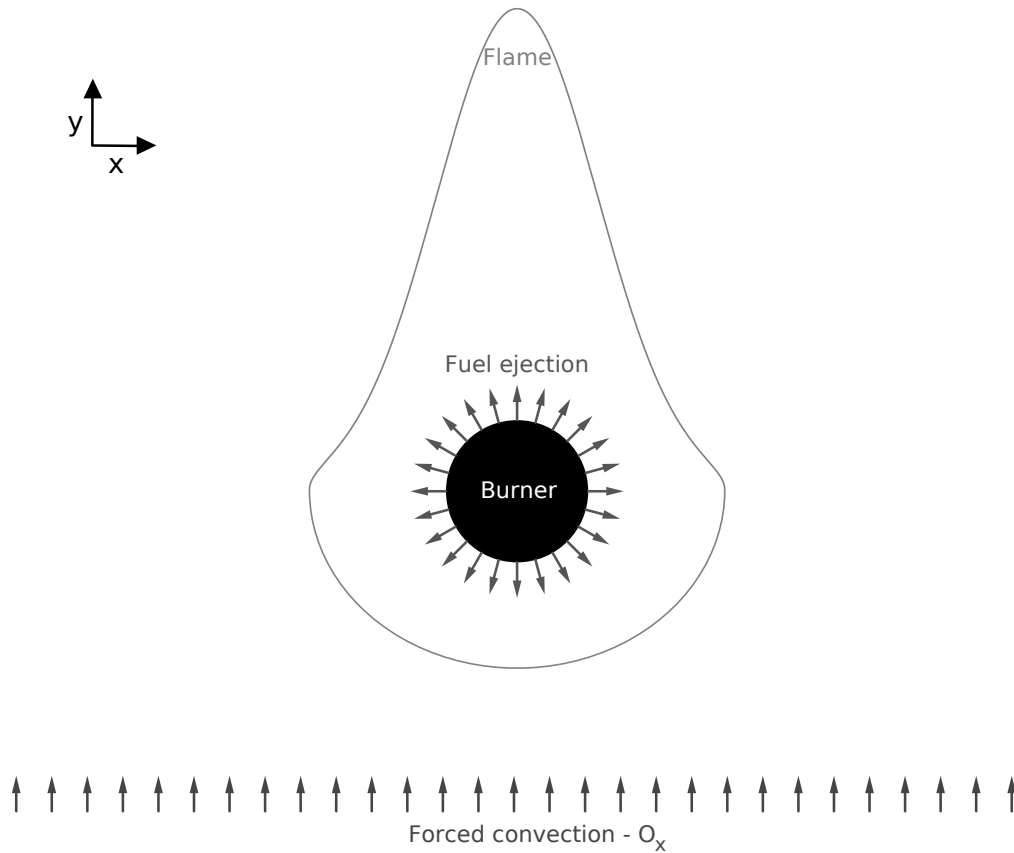
Understanding any phenomenon at the most fundamental level is essential for the later comprehension of more complex phenomena, because they are nothing more than a set of elementary phenomena, influencing each other. With a solid knowledge gained from this approach, it is possible to develop technology, and not the opposite. The objective of the present work is to study at the most fundamental level diffusion flames established in a flow field composed by cylindrically radial flow and impinging flows.

Considering the configuration with a horizontal porous cylindrical burner ejecting fuel, radially and uniformly, to the ambient atmosphere and the oxidant carried toward the burner surface by impinging flows. This burner is known as Tsuji burner and the established flame, as Tsuji flame. The objective of the studies headed by Tsuji were, notably, the influence of the strain rate¹ on the flame stability. Hence the interest region was close to the stagnation point and the backward part of the burner could be covered to avoid unnecessary fuel ejection. (TSUJI; YAMAOKA, 1967; TSUJI; YAMAOKA, 1969; TSUJI; YAMAOKA, 1971; YAMAOKA; TSUJI, 1975; YAMAOKA; TSUJI, 1979; ISHIZUKA; TSUJI, 1981; TSUJI, 1982; YAMAOKA; TSUJI, 1982; YAMAOKA; TSUJI, 1985; YAMAOKA et al., 1988; YAMAOKA; TSUJI, 1989)

The diffusion flame established around a cylindrical burner is inherently two-dimensional: either one spatial and one temporal dimensions or two spatial dimensions. In the transient case, the diffusive transport of oxidant solely is not sufficient to provide the necessary steady state conditions for the stoichiometric combustion with the fuel, transferred to the flame by diffusion but conveyed to it also by convection. Ergo, the flame is transient one-dimensional (BUCKMASTER; LUDFORD, 1982). The flame moves toward the oxidant direction, seeking for the appropriate oxidant flux to provide the stoichiometric ratio (QIAN; LAW, 1997). In the stationary case, on the other hand, the oxidant must be transported not only by the diffusive transport but also by the convective, which generates a second spatial dependence, establishing a stationary flame. This case was extensively explored by Tsuji and his collaborators, as already mentioned.

¹Strain rate is referenced as *stagnation velocity gradient* in the Tsuji's papers.

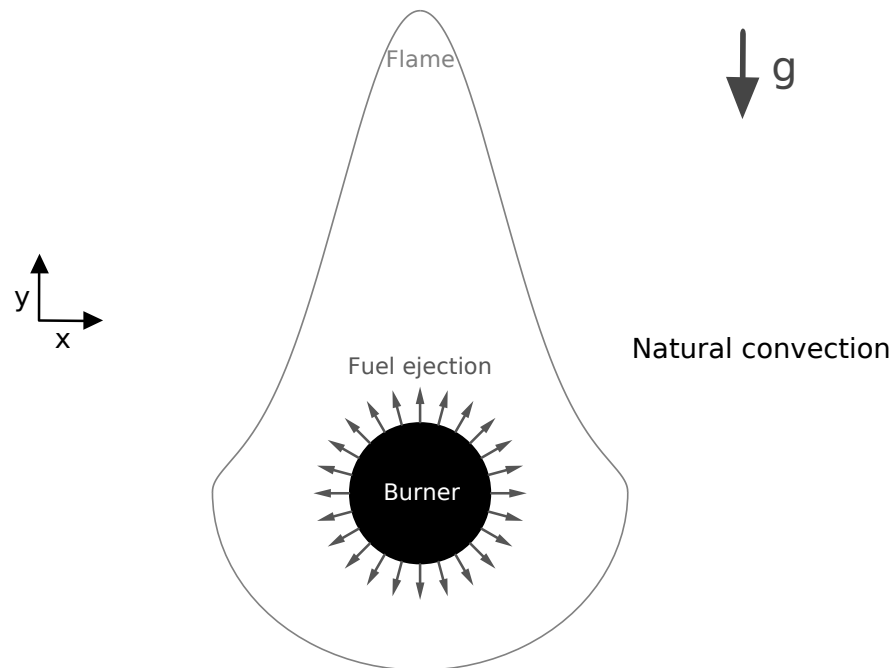
Figure 1.1 - Tsuji problem illustration



Schematic representation of the established diffusion flame in the flow field imposed by forced convection and radial flow - Tsuji burner.

Tsuji problem and derivated problems have been re-analyzed recently. One of the works investigated the diffusion flame established around a cylindrical burner, under forced convection in just one direction, essentially the Tsuji problem but analyzing whole flame, not only the stagnation region part (BIANCHIN et al., 2019), as illustrated by the Figure 1.1. Another work examined the same problem, but under natural convection (DONINI et al., 2018), according to the Figure 1.2. One striking difference between the two problems is that, under natural convection, more oxidant is taken to the flame by the buoyancy effect and, therefore, the flame is narrower and shorter. The next step is to further increase the oxidant availability, which is obtained here adding another forced flow but in the opposite direction of the first one (impinging flows).

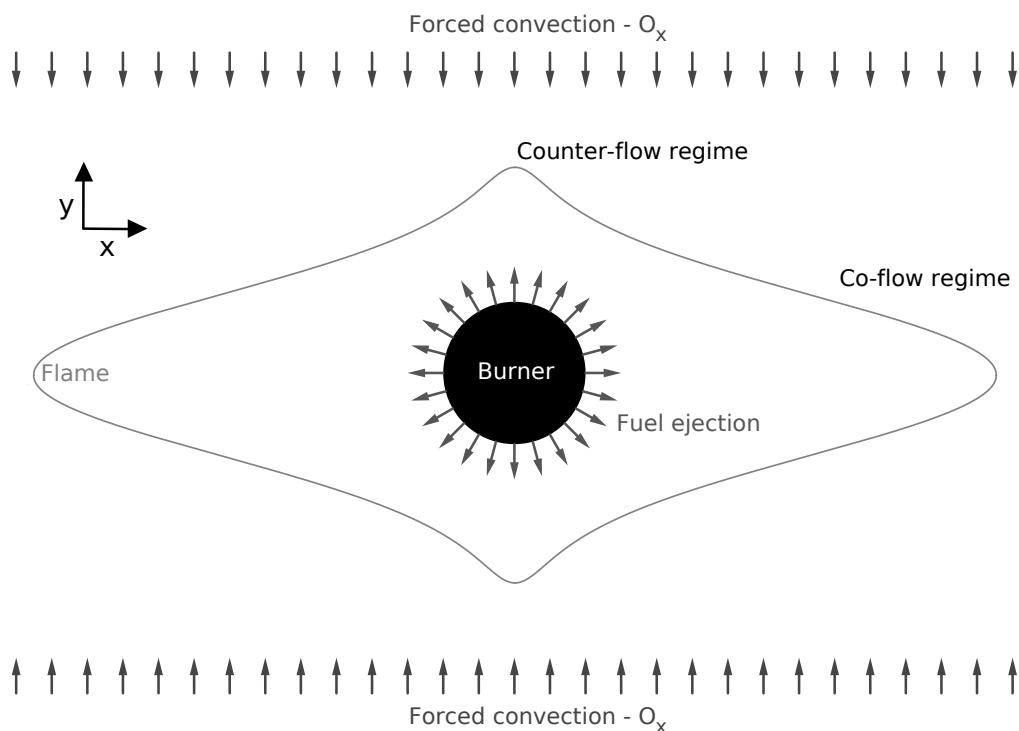
Figure 1.2 - Tsuji problem under natural convection



Schematic representation of the established diffusion flame in the flow field imposed by natural convection and radial flow.

The present work endeavors to analyze the established laminar diffusion flame in the flow field imposed by the combination of impinging rectangular flows and the flow coming out a porous cylindrical burner. The fuel is ejected, radially and evenly, and the oxidant is carried towards the flame, from the ambient atmosphere, by impinging flows, as depicted in Figure 1.3. This configuration consists in a modified Tsuji burner, however, unlike it (in which there is a single stagnation point), the flow field presents a couple of stagnation points. It is worth to mention that, like original Tsuji problem, one of the most important parameters is the strain rate, since it determines the stability conditions. Additionally, this configuration provides the behavior of the diffusion flames in a wide spectrum of conditions - with a continuous transition among them - from counterflow diffusion flame (Tsuji flame) in the vertical symmetry axis to coflow diffusion flame (Burke-Schumann Flame) in the horizontal symmetry axis.

Figure 1.3 - Proposed configuration



Schematic representation of the established diffusion flame in the flow field imposed by impinging flows and radial flow.

1.2 Objectives

The objective of this work is the theoretical study of laminar diffusion flames around modified Tsuji burner or, more precisely, the theoretical study of the flame established in a flow imposed by the combination of a burner, ejecting fuel radially and evenly, and impinging flows. Aiming at understanding of the physics involved in such reactive flow.

1.2.1 Specific aims

The thesis specific aims are:

- a) Developing the mathematical model and its numerical implementation;
- b) Developing and implementing the necessary tools for the post-processing of data;

- c) Determining analytical solutions, even if they are simplified or particular;
- d) Estimating the length and width of the flame, relating them to the flow, burner and chemical parameters;
- e) Determining the appropriate scales for the problem, in which the flame length and width have the same order of magnitude when rescaled by them;
- f) Investigating the transition from transient, one-dimensional regime to stationary, two-dimensional regime;

The study contribution is to provide an innovative configuration, in which a diffusion flame spatially changes continuously, from counterflow (Tsuji) to parallel flow (Burke-Schumann). In addition, its change is also in time and, during the evolution, the flame is accelerated. Studies of this flame can provide more information about the flow field effect on it, which could be added into the flamelet model other than strain rate of impinging flows.

1.3 Structure

Chapter 2 (LITERATURE REVIEW) presents a brief review of literature on diffusion flames, in general, up to the Tsuji flames. Chapter 3 (METHODOLOGY) introduces the methodology used in this study, including the mathematical model and numerical implementation. In Chapter 4 (THEORETICAL ANALYSIS) analytical results are presented. Chapter 5 (NUMERICAL VALIDATION) analyses numerical aspects, such as grid convergence and code validation. Chapter 6 (DISCUSSION) proposes some final discussions, with the conclusions of the study provided by Chapter 7 (CONCLUSION).

2 LITERATURE REVIEW

In this chapter a brief bibliographical review is performed, in order to obtain a solid base to develop this master's thesis satisfactorily, in addition to contribute with the advancement of diffusion flames knowledge.

2.1 Combustion

Despite growing efforts in the opposite direction, the world is extremely combustion dependent: responsible for about 90% of the world's energy production and almost 70% of the world's electric energy generation in 2016 ([INTERNATIONAL ENERGY AGENCY \(IEA\), 2016](#)). The basis of transportation systems are basically combustion: an airplane generates electric and propulsive energy by burning fuel. Moreover, most cars, ships and a significant portion of trains use combustion to generate traction. The industrial systems also depends crucially on combustion: furnaces, boilers, incinerators for production, heat treatment, drying, among others. Beyond that, combustion has an important use in waste processing ([TURNS, 2013](#)).

Given the combustion strategic importance, a solid foundation in this science becomes imperative for further technological development and advancement, which should be obtained from the knowledge of the sciences that make up the combustion: Fluid Mechanics, Transport Phenomena and Chemistry. Notwithstanding its vital importance, combustion generates pollutants that can affect people's quality of life, which reinforces the need for scientific research in the Combustion Science with the goal of mitigating the harmful effects. ([TURNS, 2013](#)).

There are basically two combustion classes, relatively to the initial spatial distribution of the reactants: the one in which fuel and oxidant were previously mixed and the one in which they are initially separated. The first kind is known as *pre-mixture combustion* and the second, as *diffusional combustion* ([ZELDOVICH et al., 1985](#)). By extension, *premixed flame*, such as that inherent in pre-mixture combustion, and *diffusion (or non-premixed) flame*, such as that inherent in diffusional combustion, are defined.

2.1.1 Diffusion flames

Diffusion flames are present and influencing people's daily lives: the use of a lamp or a candle in the blackout, forest fires, turbo-propelled planes, cars with direct injection engines, fuel droplets burning in rocket engines, and many others. As a consequence of the fuel and oxidant initial separation, combustion occurs only after

mixing due to molecular diffusion, which justifies the name. Therefore, the molecular mixing process is the prime limiting factor for diffusional combustion (unlike the pre-mixture combustion, in which external factors, such as the burner geometry and the flow field characteristics, are preponderant). At first glance, it would be possible to infer that the chemical reaction rate is generally negligible, since the reaction is limited by diffusive mixture rate (much smaller than reaction rate in the most cases) (ZELDOVICH et al., 1985; WILLIAMS, 1965). However, it is not true, because the length in which the reaction takes place is so small that the gradients of reactants are so large that the reaction rate is high enough to be used as heat source in combustion devices.

2.1.1.1 Burke-Schumann limit

The work entitled "Diffusion flames", by Burke and Schumann, ushered in an important milestone in diffusion flames theory: the first theoretical foundation. In the preceding literature, there was just purely descriptive research on this subject while the premixed flame theory had already undergone significant advances (BURKE; SCHUMANN, 1948). They proposed *the combustion (flame) surface approximation*, by supposing that the reaction zone is infinitely thin. This corresponds to the limit of very fast reactions (relatively to the diffusive transport), i.e., when Damköhler number (the characteristic reaction and diffusion times ratio) tends to infinity ($Da \rightarrow +\infty$). In this limit, the reactants can not coexist (without leakage), either there is not fuel concentration or there is not oxidant concentration for each domain point ($Y_F Y_O \rightarrow 0$). Otherwise, the reaction term tends to infinity. (ZELDOVICH et al., 1985; LIÑÁN, 1991).

2.1.1.2 Schvab-Zeldovich formulation

Taking advantage of the infinitely thin combustion zone idea, introduced by Burke and Schumann, Russian scientists Schvab and Zeldovich formalized an approach in which it is possible to eliminate the chemical reactions from the conservation equations. This is achieved performing algebraic operations in the mass balance of the chemical species and heat balance equations. At the end, two transport equations for two new scalars are obtained. One of them represents the mixture fraction (difference between oxidant and fuel concentration, divided by the respective stoichiometric coefficients) (ZELDOVICH et al., 1985). The other scalar is the modified enthalpy which involves the reactants and temperature field. The following advantages of this approach stand out: the solution of the equation is smooth in whole domain (unlike the discontinuity - a peak - presented in the solution of equations

that include the chemical reaction); Reduction in the number of conservation equations, from three to two, since the concentration of fuel and oxidant is represented by a single scalar transport equation, as presented.

2.1.1.3 Liñán analysis

Under the flame surface approximation, it is not possible to determine whether the flame is not burning. This fact occurs due to loss of information about the chemical reaction provided by this procedure. In order to avoid this problem, it is required an asymptotic analysis of the flame internal structure, like the one proposed by Liñán (1974). The latter allows to calculate the extinction conditions and, thus, to determine a combustion under specific conditions.

Liñán analysis formulation can be simplified with convenient transformations (PETERS, 1984; PETERS, 1988).

2.2 Tsuji flame

In order to establish a non-premixed flame, the oxidant diffusion, alone, is not able to supply the steady state conditions for the stoichiometric reaction with the fuel, carried towards the flame not only by diffusive transport but also by convection. Consequently, a 1-D stationary diffusion flame can not be established (BUCKMASTER; LUDFORD, 1982). The flame seeks for the appropriate oxidant flux to provide the stoichiometric ratio, moving towards the oxidant direction (QIAN; LAW, 1997). On the other hand, it is possible to add, to the oxidant, the convective transport besides the diffusive, which generates a second spatial dependence, establishing stationary flame. Thus, diffusion flame established around a cylindrical burner is inherently 2-D: either one spatial and one temporal dimensions or two spatial dimensions.

Hiroshi Tsuji¹ and his partners worked for more than 20 years in counterflow flame experiments, in both, diffusional and pre-mixture combustion. The terms *Tsuji burner* and *Tsuji flame* were originated in Tsuji honor by the relevance of his work. Tsuji burner is a porous cylindrical burner ejecting fuel, radially and uniformly, immersed in a parallel flow that takes oxidant from the ambient atmosphere towards the burner surface. Tsuji flame is any flame established under these conditions. The region of interest was close to the stagnation point (counterflow region), therefore the backward part of the burner could be coated to avoid unnecessary fuel ejection (TSUJI; YAMAOKA, 1967).

¹See http://www.combustionsociety.jp/etc/Hiroshi_Tsuji.pdf

The first experiments were on diffusion flames (TSUJI; YAMAOKA, 1967; TSUJI; YAMAOKA, 1969; TSUJI; YAMAOKA, 1971), while the later ones focused on premixed and double flames² (YAMAOKA; TSUJI, 1975; TSUJI, 1982; YAMAOKA; TSUJI, 1982; YAMAOKA; TSUJI, 1985; YAMAOKA et al., 1988; YAMAOKA; TSUJI, 1989). Besides, flammability limit study was proposed using counterflow flames (YAMAOKA; TSUJI, 1979) and the inert gases effect on extinction of laminar diffusion flames was examined (ISHIZUKA; TSUJI, 1981).

Focusing on diffusion flames, the results showed that the flames established are very stable, completely two-dimensional and that flow and thermal structure of the flame is, in general, simple. Therewithal, there is a critical strain rate beyond which the flame could not be established independently of the fuel ejection velocity. In relation to extinction, it was determined that there are two distinct mechanisms, namely extinction by chemical limitation (related with the critical strain rate) and thermal extinction (related to heat loss to the burner surface). Furthermore, it has been noted that the critical strain rate depends on the fuel composition and can be used as an estimate of the overall reaction rate. The flame always stays on the oxidant side (in relation to the stagnation point) and its separation of burner surface is correlated with the fuel ejection velocity. The conclusion is that the analyzed flame extend flame-kinetics studies by structure analysis (TSUJI; YAMAOKA, 1967). It should be noted that the experiments aimed to determine the influence of the strain rate on the flame stability.

2.2.1 Research Group

Grupo de Mecânica de Fluidos Reativos has been working, since 2017, on Tsuji flames:

Bianchin et al. (2019) investigated the Tsuji burner problem, but ejecting fuel also by the backward part of the burner and analyzing whole flame, not only the stagnation region part. Some simplifications are imposed, like constant thermodynamic and transport coefficients and it is also considered potential flow and incompressible Navier-Stokes models. In spite of the simplicity of the models, results reveal the properties of the whole Tsuji flame. In addition, an asymptotic analysis, far from the burner, makes it possible to determine the flame shape and shows the dependency of the characteristic length scales on the problem parameters: Peclet number (burner properties), free stream velocity and stoichiometry. The results show that the flame

²A combination of rich premixed and diffusion flames influencing each other.

length is proportional to a power of each parameters, as well as the flame width. An asymptotic stability analysis exposes that low-stretch flame extinction is occasioned by reactants leakage and provides the stable regime interval.

Donini et al. (2018) examined the same problem, but with natural convection, generated by low buoyancy, in place of forced convection. Their work considered a steady Navier-Stokes flow. The low buoyancy is gained equalizing difference between the flame and ambient-atmosphere densities, which is performed increasing the ambient-atmosphere temperature. Using this strategy, it is possible to control the flow strain rate, since changing the buoyancy varies the velocity field. Moreover switches on stoichiometric coefficient are imposed to adjust the forward burner flame into intended strain rate regions.

In the backward region of the burner, in the forced convection case, the oxidant is only transported towards the flame by diffusion, because the streamlines is approximately parallel to the flame in this region. Under natural convection, the buoyancy effect generates a velocity component, perpendicular to the flame surface, which implies that more oxidant is taken to the flame. Therefore, the flame is narrower and shorter.

3 METHODOLOGY

This chapter defines the methods to be used to achieve the stated objectives.

3.1 Model

Using the formulation described in Appendix B, under the hypothesis:

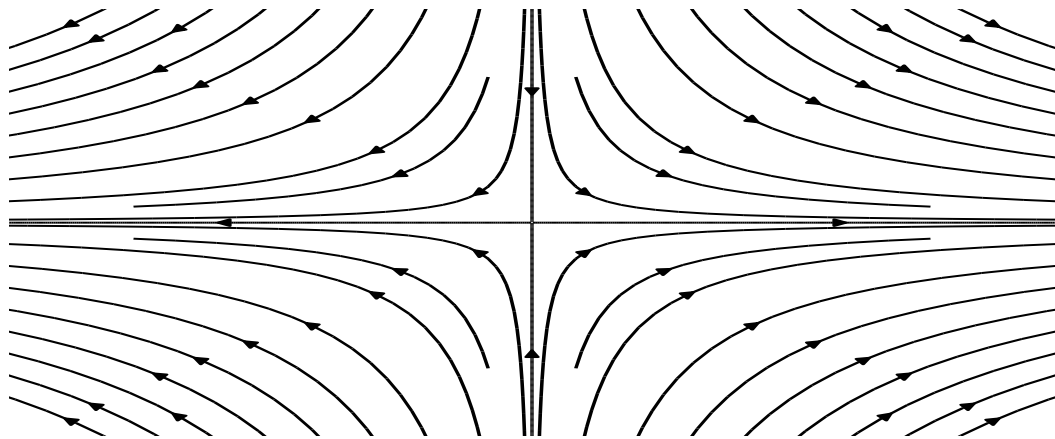
- (i) Reactants and products behave like perfect gases;
- (ii) Constant thermodynamic and transport coefficients;
- (iii) One-step irreversible reaction;
- (iv) Equivalent thermal and mass diffusivity of both species;
- (v) Negligible body forces;
- (vi) Incompressibility and irrotationality (potential flow);
- (vii) Burke-Schumann Limit;
- (viii) Schvab-Zeldovich formulation.

In this work, a simplified model is adopted in which the thermal field is decoupled from the flow field, that is, the temperature change generated by the flame does not impact on the flow field. The flow field is given by potential theory and permits the estimation of relevant properties such as stagnation points, strain rate, approximate solutions, normal and tangential flame velocities, gradients, scalar dissipation coefficient, among others. Those hypotheses permit to highlight only the effects of the species and heat transfer on the flame.

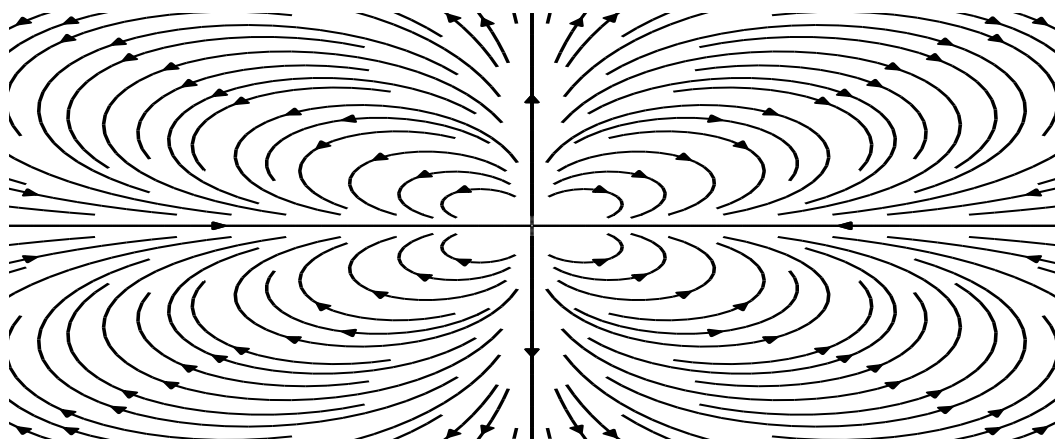
3.1.1 Potential flow

The model has the aim of revealing, with low computational cost, some aspects of the problem. In the first analysis, it is formulated using potential flow theory. This hypothesis allows the achievement of various analytical results, as mentioned, desirable for analysis of an unexplored configuration. The cylindrical burner ejecting fuel, in the middle of impinging flows, is represented by the superposition of impinging flows (Figure 3.1a), quadrupoles (Figure 3.1b) and a linear source (Figure 3.1c) (CURRIE, 2003; HOUGHTON et al., 2013):

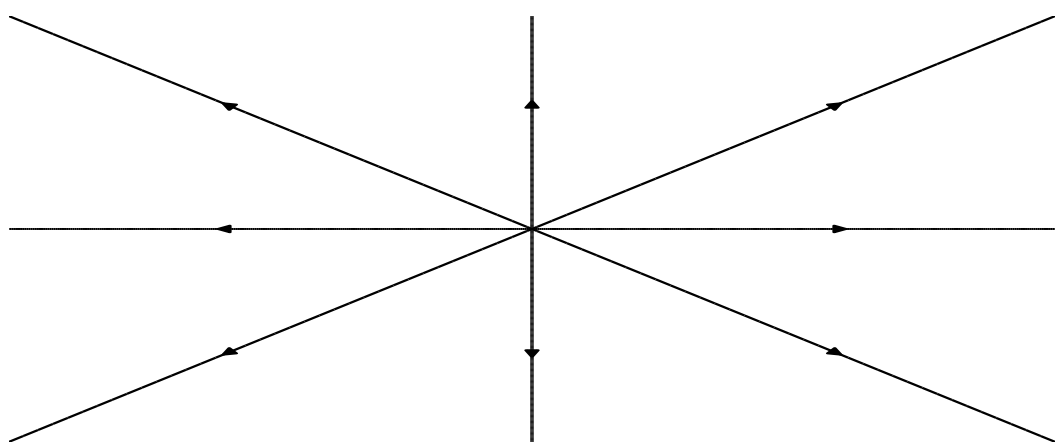
Figure 3.1 - Separate visualization of the three potential flows that, superposed, constitute the flow field adopted



(a)



(b)



(c)

Potential flow for (a) impinging flows, (b) quadrupoles and (c) linear source.

$$u = x \left(Pe_c - \frac{Pe_c(x^2 - 3y^2)}{(x^2 + y^2)^3} + \frac{Pe_b}{x^2 + y^2} \right) \quad (3.1)$$

$$v = -y \left(Pe_c + \frac{Pe_c(3x^2 - y^2)}{(x^2 + y^2)^3} - \frac{Pe_b}{x^2 + y^2} \right) \quad (3.2)$$

in which the dimensionless independent variables and velocities components are defined as $x := \hat{x}/\hat{R}$, $y := \hat{y}/\hat{R}$, $u := \hat{u}/(\hat{\alpha}/\hat{R})$ and $v := \hat{v}/(\hat{\alpha}/\hat{R})$; with \hat{R} being the burner radius and $\hat{\alpha} := \hat{k}/(\hat{\rho}\hat{c}_p)$, the thermal diffusivity.

This problem presents two Péclet numbers: one of them is based on the burner conditions (Pe_b) and, another, on the flow field around the burner (Pe_c):

$$Pe_b := \hat{u}_b \hat{R} / \hat{\alpha}, \quad Pe_c := \hat{\alpha} \hat{R}^2 / \hat{\alpha} \quad (3.3)$$

The burner Péclet number (Pe_b) is the ratio of the diffusion time in a distance of order of the burner radius, $\hat{t}_d = \hat{R}^2 / \hat{\alpha}$, to the residence time of the fuel flow in a distance of order of the burner radius, $\hat{t}_b = \hat{R} / \hat{u}_b$, in which u_b is the fuel ejection velocity. The impinging flows field Péclet number (Pe_c) is the ratio of the diffusion time in a distance of order of the burner radius, $\hat{t}_d = \hat{R}^2 / \hat{\alpha}$, to the characteristic time for changing the velocity field $\hat{t}_c = 1/\hat{a}$ (a is the strain rate).

The flow field described by Equations (3.1) and (3.2) is visualized in Figure 3.2, check Appendix A for additional background information.

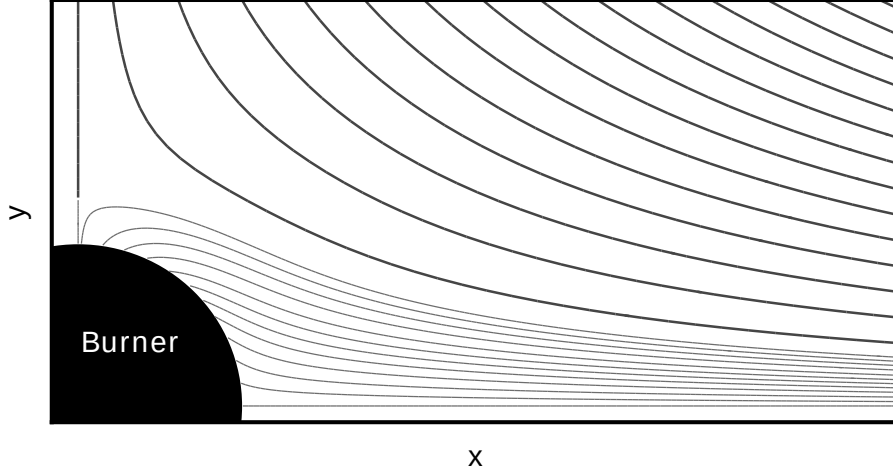
3.1.2 Energy and species conservation equations

The Burke-Schumann limit (see 2.1.1.1), $\hat{Y}_F \hat{Y}_O = 0$, permits the combination of the energy and species conservation equations in order to eliminate the chemical term (see 2.1.1.2). The result is two conservation equations (more details in Appendix B):

$$\frac{\partial Z}{\partial t} + u \frac{\partial Z}{\partial x} + v \frac{\partial Z}{\partial y} = \frac{\partial^2 Z}{\partial x^2} + \frac{\partial^2 Z}{\partial y^2} \quad (3.4)$$

$$\frac{\partial H}{\partial t} + u \frac{\partial H}{\partial x} + v \frac{\partial H}{\partial y} = \frac{\partial^2 H}{\partial x^2} + \frac{\partial^2 H}{\partial y^2} \quad (3.5)$$

Figure 3.2 - Potential flow field



The thinner and more dense streamlines are the fuel flow. $Pe_b = 1$ and $Pe_c = 1$, only the first quadrant is shown.

in which t , x and y are, respectively, the time and the first and second spatial coordinates, u and v , the first and second velocity coordinates, in this order. Besides, $Z := SY_F - Y_O + 1$ is the mixture fraction and $H := (S + 1)T/Q + Y_F + Y_O$ is the excess enthalpy, with Y_F and Y_O denoting, respectively, the mass fraction of the fuel and oxidant, and T stands for temperature. The dimensionless variables are defined as $t := \hat{t}/(\hat{R}^2/\hat{\alpha})$, $x := \hat{x}/\hat{R}$, $y := \hat{y}/\hat{R}$, $u := \hat{u}/(\hat{\alpha}/\hat{R})$, $v := \hat{v}/(\hat{\alpha}/\hat{R})$ and $T := \hat{T}/\hat{T}_\infty$, with the subscript “ b ” indicating the average conditions inside the burner, while the “ ∞ ”, in the ambient atmosphere. The fuel and oxidant mass fractions are normalized by their representative values, $Y_F := \hat{Y}_F/\hat{Y}_{F,b}$ and $Y_O := \hat{Y}_O/\hat{Y}_{O,\infty}$, $\hat{Y}_{F,b}$ is the average fuel mass fraction inside the burner and $\hat{Y}_{O,\infty}$ is the oxidant mass fraction in the ambient atmosphere. The characteristic properties used to non-dimensionalize the variables are: the radius of the burner (\hat{R}), the diffusion speed ($\hat{\alpha}/\hat{R}$), the period of time for the heat propagation over a burner radius distance with the diffusion speed ($\hat{R}^2/\hat{\alpha}$), the fuel concentration in the burner surface ($\hat{Y}_{F,b}$), the oxidant concentration in the ambient atmosphere ($\hat{Y}_{O,\infty}$) and the ambient-atmosphere temperature (\hat{T}_∞). The parameters are stoichiometricity, $S := \hat{s}\hat{Y}_{F,b}/\hat{Y}_{O,\infty}$, and heat release, $Q := \hat{Q}\hat{Y}_{F,b}/(\hat{c}_{p,\infty}\hat{T}_\infty)$, in which \hat{s} is the mass stoichiometric coefficient and \hat{Q} is the combustion heat release.

The boundary conditions are, at $x^2 + y^2 \rightarrow 1^+$,

$$Z_s - Z_b = Pe_b^{-1} \|\nabla Z\|_s, \quad H_s - H_b = Pe_b^{-1} \|\nabla H\|_s \quad (3.6)$$

and, for $x^2 + y^2 \rightarrow +\infty$,

$$Z - Z_\infty = H - H_\infty = 0 \quad (3.7)$$

The initial conditions are, for $x^2 + y^2 > 1$,

$$Z - Z_\infty = H - H_\infty = 0 \quad (3.8)$$

in which $Z_s := SY_{F,s} + 1$, $H_s := (S+1)T_s/Q + Y_{F,s}$, $Z_\infty := 0$ and $H_\infty := (S+1)/Q + 1$, with subscript “ s ” indicating the conditions at the burner surface. Moreover, the terms $Z_b := S + 1$ and $H_b := (S + 1)T_b/Q + 1$ are considered known, based on the average properties within the burner.

3.1.3 Axial symmetry

The problem presents axial symmetry in relation to x and y axes, provided by the flow field. Therefore, it is entirely represented by the solution of only one quadrant. The symmetry boundary conditions are, on the axis $x = 0$,

$$\frac{\partial Z}{\partial x} = \frac{\partial H}{\partial x} = 0 \quad (3.9)$$

on the axis $y = 0$,

$$\frac{\partial Z}{\partial y} = \frac{\partial H}{\partial y} = 0 \quad (3.10)$$

3.1.4 Transition $(r, t; Pe_c) \rightarrow (x, y; Pe_c)$

To investigate the transition from transient, one-dimensional regime to stationary, two-dimensional regime, the condition of very small flow field Péclet number must be imposed, $Pe_c \ll 1$, i.e. $Pe_c = \varepsilon Pe_c^{(1)}$, with $\varepsilon \ll 1$ and $Pe_c^{(1)} \sim 1$. This hypothesis puts in evidence the (r, t) problem, that is, decreasing ε , the (x, y) problem takes more time to be attained. Decreasing the value of Pe_c , the stationary flame condition

is found for a longer period. A straightforward analysis leads to the following re-scaling of the coordinates: $\tilde{x} := x\varepsilon^{1/2}$ and $\tilde{y} := y\varepsilon^{1/2}$; and of the velocities: $\tilde{u} := u\varepsilon^{-1/2}$ and $\tilde{v} := v\varepsilon^{-1/2}$. The region of the flow field analyzed has a size of order of $\varepsilon^{-1/2} \gg 1$ and velocities very small, of order of $\varepsilon^{1/2} \ll 1$. Therefore, the flow field is described by

$$\tilde{u} = Pe_c^{(1)}\tilde{x} + \frac{Pe_b\tilde{x}}{\tilde{x}^2 + \tilde{y}^2} + O(\varepsilon^2) \quad (3.11)$$

$$\tilde{v} = -Pe_c^{(1)}\tilde{y} + \frac{Pe_b\tilde{y}}{\tilde{x}^2 + \tilde{y}^2} + O(\varepsilon^2) \quad (3.12)$$

From the region in the domain characterized by $(x, y) \sim (\varepsilon^{-1/2}, \varepsilon^{-1/2})$, the burner is seen as a linear source of fuel and sink of heat. The reason for the burner geometry contribution disappears from the above expressions. An observer in the region $(1, 1) < (x, y) \ll (\varepsilon^{-1/2}, \varepsilon^{-1/2})$ sees the diffusion flame displacement as transient, one-dimensional problem. But, an observer in the region $(x, y) \sim (\varepsilon^{-1/2}, \varepsilon^{-1/2})$ sees the diffusion flame as a stationary, two-dimensional problem.

Not only the spatial variables must be rescaled but also the temporal variable. In this case, the re-scaling is $\tau = \varepsilon t$. Note that the Strouhal number, defined as the residence and characteristic times ratio, is very large $S_t := \varepsilon^{-1}$, which corresponds to a long period to achieve the stationary regime.

From this discussion, it is possible to evaluate the influence of the flow field on the stationary, two-dimensional flame, in which the fuel is supplied from a cylindrical burner.

Equations (3.4) and (3.5) can be rewritten as

$$\frac{\partial Z}{\partial \tau} + \tilde{u} \frac{\partial Z}{\partial \tilde{x}} + \tilde{v} \frac{\partial Z}{\partial \tilde{y}} = \frac{\partial^2 Z}{\partial \tilde{x}^2} + \frac{\partial^2 Z}{\partial \tilde{y}^2} \quad (3.13)$$

$$\frac{\partial H}{\partial \tau} + \tilde{u} \frac{\partial H}{\partial \tilde{x}} + \tilde{v} \frac{\partial H}{\partial \tilde{y}} = \frac{\partial^2 H}{\partial \tilde{x}^2} + \frac{\partial^2 H}{\partial \tilde{y}^2} \quad (3.14)$$

Refer to Appendix C for detailed formulation.

3.2 Numerical implementation

Denoting l_x and l_y two lengths not necessarily equal. A numerical domain such that $0 \leq x \leq l_x$ and $0 \leq y \leq l_y$ is selected to represent the physical domain under scrutiny, the first quadrant of a rectangular region of space where the diffusion flame is established. The discretization consists of a rectangular mesh, evenly spaced in both directions and with the same resolution ($\Delta x = \Delta y$). The FTCS (Forward-Time Central-Space) method is implemented, which consists of central finite differences in space and forward Euler method in time. Thus, the following finite difference equation is obtained, generic representation of Equations (3.4), (3.5), (3.13) and (3.14)

$$\begin{aligned} \frac{f_{i,j}^{n+1} - f_{i,j}^n}{\Delta t} + u_{i,j} \frac{f_{i+1,j}^n - f_{i-1,j}^n}{2\Delta x} + v_{i,j} \frac{f_{i,j+1}^n - f_{i,j-1}^n}{2\Delta y} = \\ = \frac{f_{i+1,j}^n - 2f_{i,j}^n + f_{i-1,j}^n}{(\Delta x)^2} + \frac{f_{i,j+1}^n - 2f_{i,j}^n + f_{i,j-1}^n}{(\Delta y)^2} \end{aligned} \quad (3.15)$$

with n , i and j being partition indexes respectively of t , x and y . It is an explicit method of first order in time and second order in space, conditionally stable. *Von Neumann Stability Theorem* provides a necessary and sufficient condition for the stability (HINDMARSH et al., 1984), which can be summarized in the sufficient condition applied

$$\Delta t \leq \min \left[\frac{1}{2} \frac{(\Delta x \Delta y)^2}{(\Delta x)^2 + (\Delta y)^2}, \frac{2}{u_{max}^2 + v_{max}^2} \right] \quad (3.16)$$

in which u_{max} and v_{max} are the maximum velocities in the x and y directions, respectively. By defining $\Delta := \Delta x = \Delta y$, it provides

$$\Delta t \leq \min \left[\frac{\Delta^2}{4}, \frac{2}{u_{max}^2 + v_{max}^2} \right] \quad (3.17)$$

The convergence criterion for the stationary solution is provided by the root-mean-square deviation (RMSD) of the interest function (f) between future ($n + 1$) and present (n) times, relatively to time variation (Δt). This can be interpreted as an approximation for temporal derivative at any point and denoted by β . Namely

$$\beta^{n+1} := \left(\frac{RMSD}{\Delta t} \right)^{n+1} \quad (3.18)$$

with

$$RMSD^{n+1} := \sqrt{\frac{1}{M_x M_y} \sum_{i=1}^{M_x} \sum_{j=1}^{M_y} (f_{i,j}^{n+1} - f_{i,j}^n)^2} \quad (3.19)$$

in which $M_x := l_x/\Delta x$ and $M_y := l_y/\Delta y$ are the cardinalities of the discrete partitions of x and y , respectively, i.e., the number of grid points in each direction.

When $\beta^{n+1} \leq \beta_{stop}$ ($\beta_{stop} \ll 1$) convergence was achieved.

The Equations (3.4) and (3.5) can be rewritten as:

$$\frac{\partial F}{\partial t} + u \frac{\partial F}{\partial x} + v \frac{\partial F}{\partial y} = \frac{\partial^2 F}{\partial x^2} + \frac{\partial^2 F}{\partial y^2} \quad (3.20)$$

in which $F := (Z - Z_\infty)/(Z_s - Z_\infty) = (H - H_\infty)/(H_s - H_\infty)$, with $F_s = 1$ and $F_\infty = 0$.

Thus, solving any of the equations, for Z , H or F , the others are determined by:

$$Z = F(Z_s - Z_\infty) + Z_\infty \quad (3.21)$$

$$H = F(H_s - H_\infty) + H_\infty \quad (3.22)$$

4 THEORETICAL ANALYSIS

In this chapter an order of magnitude analysis is performed, an asymptotic solution is determined and, from it, several results are obtained.

4.1 Order of magnitude analysis

The conditions imposed by the burner affect the properties along the entire flame. That is why the adjustment coefficient of burner influence (η) is introduced. The burner influence is maximum when $\eta \ll 1$ and minimum when $\eta \sim 1$.

To estimate length and width of the flame established in the proposed configuration, it is necessary to consider some approximations. The first one is the residence time of a center-line fuel fluid particle,

$$\hat{t}_{res} = \int_{\hat{R}}^{\hat{L}_x} \frac{d\hat{x}}{\hat{u}} = \frac{1}{\hat{\alpha}} \ln(L_x) \quad (4.1)$$

to be of the same order as the diffusion time of an oxidant fluid particle at a distance \hat{L}_y ,

$$\hat{t}_{dif} = \hat{L}_y^2 / \hat{\alpha} \quad (4.2)$$

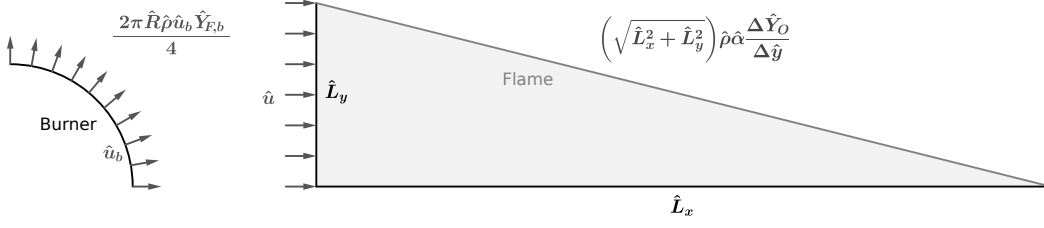
in which $L_x := (\hat{L}_x / \hat{R})$ with \hat{L}_x is the estimate flame length and \hat{L}_y is the estimate flame width. The x -direction velocity \hat{u} is approximated by the \hat{x} -component of the impinging flows velocity, $\hat{u} \sim \hat{\alpha}\hat{x}$, with \hat{x} being the first spatial coordinate (length). Thus, from Equations (4.1) and (4.2), one finds

$$\ln(L_x) = \tilde{L}_y^2 \quad (4.3)$$

in which $\tilde{L}_y := \sqrt{Pe_c} L_y$ with $L_y := (\hat{L}_y / \hat{R})$.

The second approximation is that the fuel stream coming out the burner, $2\pi\hat{R}\hat{\rho}\hat{u}_b\hat{Y}_{F,b}$, is redirected by the impinging flows from the cylindrical geometry to a stream parallel to the \hat{x} -axis, in both sides of burner. Finally, the third one is that the fuel mass flux coming out from one quadrant of the burner, $2\pi\hat{R}\hat{\rho}\hat{u}_b\hat{Y}_{F,b}/4$, is redirected to the base width (\hat{L}_y) of a rectangular triangle with height \hat{L}_x , and it is burned in the diffusion flame established on the hypotenuse. From the mass balance, considering that each unit of fuel mass is burned stoichiometrically with s mass of oxidant, one finds the relation: $s(\pi\hat{R}\hat{\rho}\hat{u}_b\hat{Y}_{F,b})/2 = \eta \left(\sqrt{\hat{L}_x^2 + \hat{L}_y^2} \right) \hat{\rho}\hat{\alpha}\nabla\hat{Y}_O$, which can

Figure 4.1 - Model schematic illustration



Only the first quadrant is shown.

be rewritten as

$$\left(\frac{L_x}{\tilde{L}_y}\right)^2 = \left[\frac{1}{\eta} \left(\frac{\pi S P e_b}{2 \sqrt{P e_c}}\right)\right]^2 \quad (4.4)$$

in which the following hypotheses are used: $\hat{L}_x \gg \hat{L}_y$, $\nabla \hat{Y}_O \sim \Delta \hat{Y}_O / \Delta \hat{y} = \eta \hat{Y}_{O,\infty} / \hat{L}_y$. \tilde{L}_y is the rescaled flame width and defined by $\tilde{L}_y := L_y \sqrt{P e_c}$ and $S := s \hat{Y}_{F,b} / \hat{Y}_{O,\infty}$ is the stoichiometric coefficient for mass of oxidant to burn stiochiometrically unity mass of a mixture of fuel and inert.

Figure 4.1 presents a schematic illustration of the proposed model.

Taking Equation (4.4) into (4.3), an estimation for the length of the flame is determined by:

$$\ln(\tilde{N} \tilde{L}_x) = \tilde{L}_x^2 \quad (4.5)$$

with $\tilde{L}_x := L_x / \tilde{N}$, $\tilde{N} := N / \eta$ and

$$N := \frac{\pi S P e_b}{2 P e_c^{1/2}} \quad (4.6)$$

Then, using the rescaled width and length of the flame, Equation (4.4) can be rewritten as $\tilde{L}_x = \tilde{L}_y$.

Looking for the position $\tilde{L}_{x,T}$ in which the two curves $\ln(\tilde{N} \tilde{L}_x)$ and \tilde{L}_x^2 have the same inclination (tangency point), one finds

$$\tilde{L}_{x,T} = 2^{-1/2} \quad (4.7)$$

In addition, for the two curves meet themselves at that point, the value of the \tilde{N} ,

called \tilde{N}_{min} , must be

$$\tilde{N}_{min} = (2e)^{1/2} \quad (4.8)$$

From Equations (4.7) and (4.8), the minimum flame length is determined $L_{x,min} = e^{1/2}$.

For $\tilde{N} < \tilde{N}_{min}$, the analysis has no solution. For $\tilde{N} > \tilde{N}_{min}$, Equation (4.5) has two solutions, the smallest one is defined in the interval $0 < \tilde{L}_x \leq \tilde{L}_{x,T}$ and the largest one is defined in $\tilde{L}_x > \tilde{L}_{x,T}$.

As will be seen ahead, the parameter N rescales very well the flame length for the cases in which the problem properties lead to $N > S$.

4.2 Asymptotic solution

Despite the double convective transport, based on previous work (BIANCHIN et al., 2019; DONINI et al., 2018) and estimates from the former section, it is still possible to expect long flames, in this case in x -direction. Thus, away from the burner, it is possible to neglect the small diffusive process in x -direction (boundary layer approximation) in the equation for Z :

$$Pe_c x \frac{\partial Z}{\partial x} - Pe_c y \frac{\partial Z}{\partial y} = \frac{\partial^2 Z}{\partial y^2} \quad (4.9)$$

Performing the spatial coordinate transformation $\tilde{y} = y\sqrt{Pe_c}$, one finds

$$x \frac{\partial Z}{\partial x} - \tilde{y} \frac{\partial Z}{\partial \tilde{y}} = \frac{\partial^2 Z}{\partial \tilde{y}^2} \quad (4.10)$$

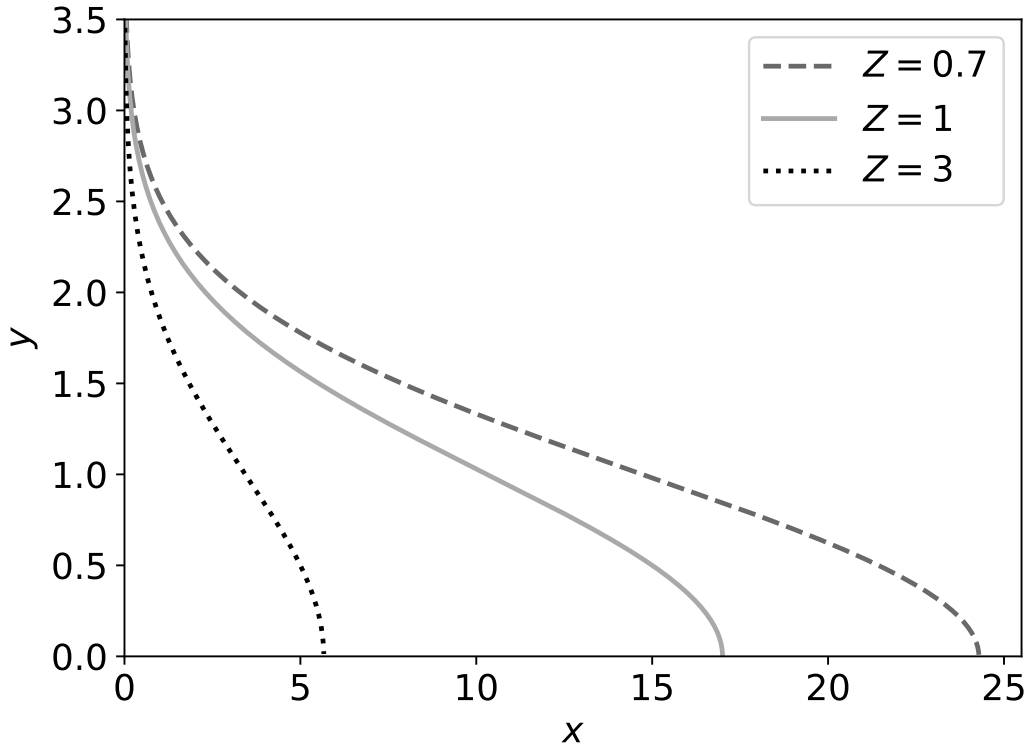
Proposing a solution by separating variables $Z = F(x)G(\tilde{y})$, functions F and G satisfy $x F' / F = (G'' + \tilde{y} G') / G = -c$ whose solution in (x, y) is

$$Z = \frac{A}{x} \exp \left[- \left(y \sqrt{Pe_c / 2} \right)^2 \right] \quad (4.11)$$

The flame is determined by the level curve $Z(x, y) = 1$. Applying the boundary condition $Z(x_f, 0) = 1$, $A = x_f$ is obtained, in which $x_f = x_f(S, Pe_b, Pe_c)$ is the total length of the flame, which transmits the conditions near the burner to the asymptotic solution, such as fuel flow. Thus, the expression

$$\frac{x}{x_f} = \exp \left[- \left(y \sqrt{Pe_c / 2} \right)^2 \right] \quad (4.12)$$

Figure 4.2 - Asymptotic solution for Z



The contours $Z = 0.7$, $Z = 1$ and $Z = 3$ are shown, with $Pe_c = 1$ and $x_f = 17$.

determines the flame position far from the burner as a function of the flame length (x_f). An illustration of the asymptotic solution for Z is provided by Figure 4.2 which already evidences the low concentration at the flame tip.

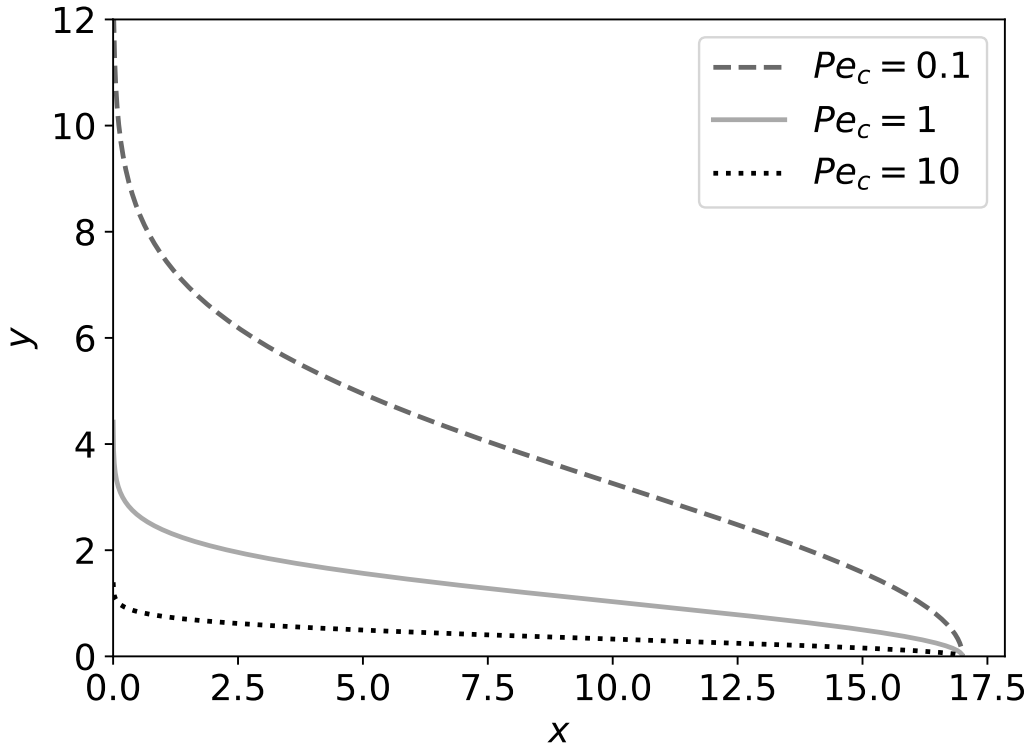
It is worth to mention that the analysis of order of magnitude is able to capture the relation between the flame length and flame width, Equation (4.3), given by the asymptotic solution, Equation (4.12).

Rewriting conveniently Equation (4.12), the following relation is found

$$y = \pm \left[\frac{2}{Pe_c} \ln \left(\frac{1}{Z} \frac{x_f}{x} \right) \right]^{1/2} \quad (4.13)$$

Note that $x_f > 0$ in the first and fourth quadrants and $x_f < 0$ in the second and third quadrants. This curve, in the first quadrant, is plotted in Figure 4.3 for three distinct Pe_c .

Figure 4.3 - Asymptotic flame shape



The cases $Pe_c = 0.1$, $Pe_c = 1$ and $Pe_c = 10$ are shown, with $Pe_c = 1$ and $x_f = 17$.

In the first quadrant, the inclination of the curve describing the flame is

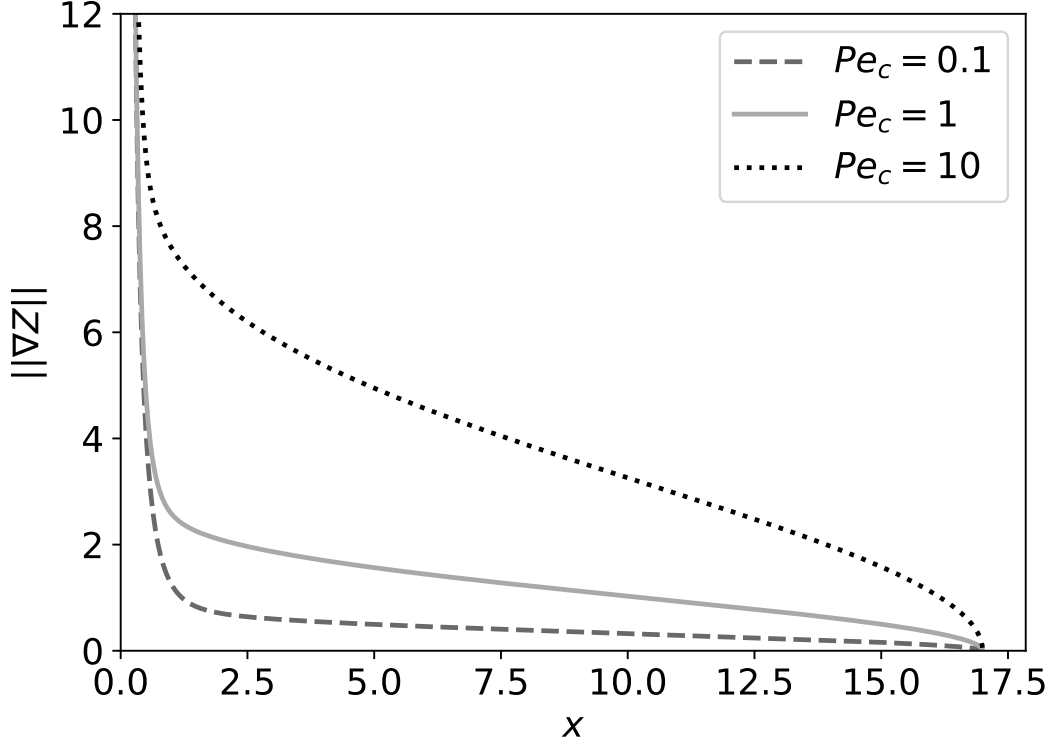
$$y' = \frac{1}{\sqrt{2Pe_c}} \left\{ -\frac{1}{x} \left[\ln \left(\frac{x_f}{x} \right) \right]^{-1/2} \right\} \quad (4.14)$$

and the curvature of that is

$$y'' = \frac{1}{2\sqrt{2Pe_c}} \frac{1}{x^2} \left[\ln \left(\frac{x_f}{x} \right) \right]^{-1/2} \left\{ 2 - \left[\ln \left(\frac{x_f}{x} \right) \right]^{-1} \right\} \quad (4.15)$$

Note that there is a point ($x = x_f e^{-1/2}$) where $y'' = 0$.

Figure 4.4 - Asymptotic gradient norm ($\|\nabla Z\|$)



The cases $Pe_c = 0.1$, $Pe_c = 1$ and $Pe_c = 10$ are shown, with $Pe_c = 1$ and $x_f = 17$.

4.2.1 Mixture fraction gradient

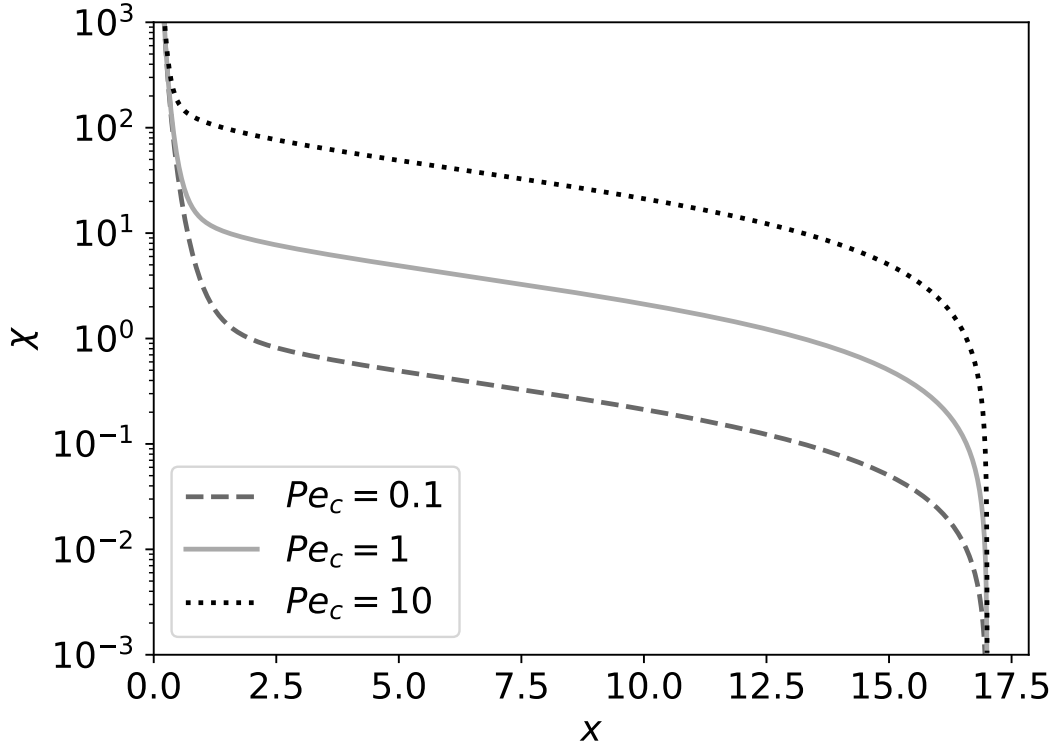
The results of the asymptotic analysis permit a good analytical estimate for the mixture fraction gradient (∇Z) far from the burner:

$$\nabla Z = -Z \left(\frac{1}{x}, \pm \left[2Pe_c \ln \left(\frac{1}{Z} \frac{x_f}{x} \right) \right]^{1/2} \right) \quad (4.16)$$

in which Equation (4.11) was used. The term in y -direction is positive in the second and third quadrants and, negative in the first and fourth. Knowing the gradient of mixture fraction on the flame ($Z = 1$), the scalar dissipation coefficient χ is found,

$$\chi/2 = (\nabla Z \cdot \nabla Z)|_{Z=1} = \frac{1}{x^2} + 2Pe_c \ln \left(\frac{x_f}{x} \right) \quad (4.17)$$

Figure 4.5 - Scalar dissipation coefficient (χ)



The cases $Pe_c = 0.1$, $Pe_c = 1$ and $Pe_c = 10$ are shown, with $Pe_c = 1$ and $x_f = 17$.

Illustrations for the gradient norm ($\|\nabla Z\|$) and the scalar dissipation coefficient (χ) are given in Figure 4.4 and 4.5, respectively, showing that dissipation grows with the increase of Pe_c .

4.2.2 Point of tangency

Since the gradient of the curve $Z(x, y) = 1$ (on the flame) is a normal vector to the flame surface, then $\vec{u} \cdot \nabla Z = 0$ determines where the velocity vector is parallel to the flame. From Equation (4.16) and its associated flow field $(u, v) = Pe_c(x, -y)$,

$$\vec{u} \cdot \nabla Z = -Pe_c + y^2 Pe_c^2 = -Pe_c + 2Pe_c \ln\left(\frac{x_f}{x}\right) = 0 \quad (4.18)$$

leads to

$$(x, y)_T = (x_f e^{-1/2}, Pe_c^{-1/2}) \quad (4.19)$$

The subscript T represents the tangency of flow field to the flame. Equation (4.19) shows the position of separation between counterflow regime and coflow regime. For all cases it is at the boarder of the molecular transport zone, $y_T = Pe_c^{-1/2}$, and at about 60% of the flame length, $x_T \approx 0.607x_f$. It is worth to mention that for $x_T < x < x_f$ the streamlines are practically parallel to the flame, except in the region very close to the tip $x \sim x_f$, where the streamlines cross the flame with high angle. The convective transport close to the tip creates a very narrow molecular transport zone, that imposes high enough fuel flux to the flame in spite of very low fuel concentration.

From Equations (4.14) and (4.15), at the tangency point the inclination of the flame is

$$y' = -\frac{1}{\sqrt{Pe_c}} \frac{e^{1/2}}{x_f} \quad (4.20)$$

and the curvature is zero, $y'' = 0$. The curvature for the flame before the tangent point is positive and after that is negative.

4.2.3 Normal and tangential velocities

It is possible to decompose the velocity \vec{u} into normal (u_N) and tangential (u_T) components. The normal component is given by the projection of \vec{u} in the direction of unit vector, normal to the flame. The normalized gradient has this property (ARFKEN; WEBER, 2005), ie. $u_N = \vec{u} \cdot (\nabla Z / \|\nabla Z\|_{Z=1})$. The velocity and the gradient tends asymptotically to $\vec{u} = (xPe_c, -yPe_c)$ and $\nabla Z = -(1/x, Pe_c y)$. Furthermore, considering Equation (4.13), limited to the first quadrant,

$$u_N = Pe_c \frac{1 - 2 \{ \ln(x_f/x) \ln[(1/Z)(x_f/x)] \}^{1/2}}{\sqrt{1/x^2 + 2Pe_c \ln(x_f/x)}} \quad (4.21)$$

or, on the curve $Z = 1$ (on the flame):

$$u_N = Pe_c \frac{1 - 2 \ln(x_f/x)}{\sqrt{1/x^2 + 2Pe_c \ln(x_f/x)}} \quad (4.22)$$

The tangential component is given by the relation $u_T^2 = \|\vec{u}\|^2 - u_N^2$, then

$$u_T = Pe_c \left[x^2 + \frac{2}{Pe_c} \ln \left(\frac{1}{Z} \frac{x_f}{x} \right) - \left(\frac{1 - 2 \{ \ln(x_f/x) \ln[(1/Z)(x_f/x)] \}^{1/2}}{\sqrt{1/x^2 + 2Pe_c \ln(x_f/x)}} \right)^2 \right]^{1/2} \quad (4.23)$$

or, on the flame:

$$u_T = Pe_c \left[x^2 + \frac{2}{Pe_c} \ln \left(\frac{x_f}{x} \right) - \left(\frac{1 - 2 \ln(x_f/x)}{\sqrt{1/x^2 + 2Pe_c \ln(x_f/x)}} \right)^2 \right]^{1/2} \quad (4.24)$$

Perceive that at the point of tangency ($x = x_T$), one finds $u_N = 0$ and $u_T = \|\vec{u}\|$. On the other hand, at the top of the flame ($x = x_f$), one finds $u_N = \|\vec{u}\|$ and $u_T = 0$. Although, as x decreases, it is necessary to use the numerical solution, since the influence of the burner becomes relevant, which is not included in the assumptions employed in the asymptotic solution.

4.3 Stagnation points

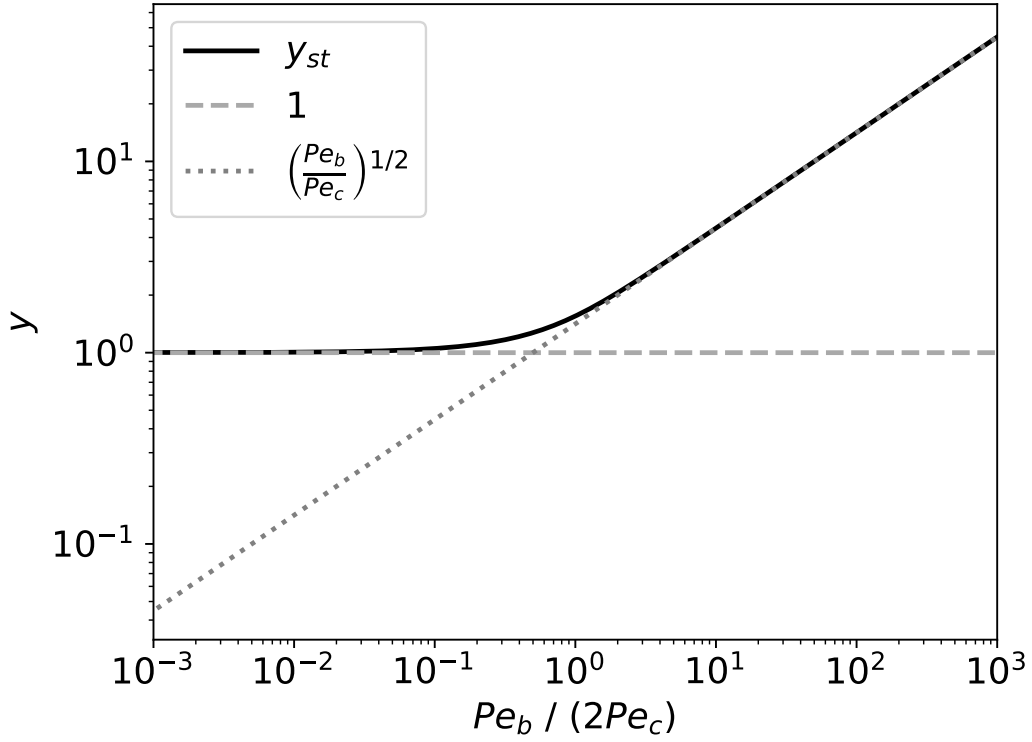
According to the geometry of the problem, there are two stagnation points, one in each side of the burner on $x = 0$. Imposing the condition $v = 0$ into Equation (3.2) and solving the resulting quadratic equation for y_{st}^2 , the stagnation points $y = \pm y_{st} \neq 0$ are determined by

$$y_{st}^2 = \frac{Pe_b}{2Pe_c} + \sqrt{\left(\frac{Pe_b}{2Pe_c} \right)^2 + 1} \quad (4.25)$$

For the conditions leading to the distinguished limit $Pe_b/(2Pe_c) \ll 1$, the stagnation points are at the burner surface $y_{st} \rightarrow \pm 1$. For the other distinguished limit $Pe_b/(2Pe_c) \gg 1$, the stagnation points are far from the burner, $y_{st} \rightarrow \pm (Pe_b/Pe_c)^{1/2}$.

Figure 4.6 shows the behavior prescribed by Equation (4.25). Note that y_{st} quickly tends to its asymptotic behavior for $Pe_b/(2Pe_c) \gg 1$, just over $Pe_b/(2Pe_c) = 0.5$. Moreover, y_{st} tends to its asymptotic behavior for $Pe_b/(2Pe_c) \ll 1$, just below $Pe_b/(2Pe_c) = 0.5$.

Figure 4.6 - Stagnation points (y_{st})



The stagnation points (y_{st}) are shown as a function of $Pe_b / (2Pe_c)$. The asymptotic behavior is also displayed.

4.3.1 Strain rate

Similarly, on $x = 0$, the velocity derivative is given by:

$$\frac{dv}{dy} = - \left(1 + \frac{3}{y^4} + \frac{Pe_b}{Pe_c} \frac{1}{y^2} \right) Pe_c \quad (4.26)$$

At $y = y_{st}$:

$$\frac{dv}{dy} \Big|_{y=y_{st}} = - \left[1 + \frac{3(2Pe_c/Pe_b)^2}{(1 + \sqrt{1 + (2Pe_c/Pe_b)^2})^2} + \frac{2}{1 + \sqrt{1 + (2Pe_c/Pe_b)^2}} \right] Pe_c \quad (4.27)$$

For the extreme condition $Pe_b / (2Pe_c) \gg 1$:

$$\left. \frac{dv}{dy} \right|_{y=b} \approx - \left[2 + 3 \left(\frac{Pe_c}{Pe_b} \right)^2 \right] Pe_c \quad (4.28)$$

For the other extreme condition, $Pe_b / (2Pe_c) \ll 1$:

$$\left. \frac{dv}{dy} \right|_{y=b} \approx - \left[4 + \frac{Pe_b}{Pe_c} \right] Pe_c \quad (4.29)$$

Thus, this configuration provides strain rates from two to four times higher than the counterflow flames. Which have, in comparison, a strain rate of order of Pe_c .

5 NUMERICAL VALIDATION

This chapter is dedicated to examine the grid convergence and the code validation.

5.1 Grid convergence

This section examines the grid convergence as proposed by Roache (1998) and summarized in Slater (2008), which is based on Richardson's extrapolation.

Three different grids with constant refinement ratio ($r = 2$), with normalized spacing $h_3 = 4$ ($\Delta_3 = 0.04$), $h_2 = 2$ ($\Delta_2 = 0.02$) and $h_1 = 1$ ($\Delta_1 = 0.01$), are used to solve the same problem (S, Pe_b, Pe_c) = (10, 1, 1), obtaining the flame length for each of them (f_i), parameter of relevance for the simulations, according to Table 5.1. Note that the grid spacing is normalized by most refined grid spacing, i.e., $h_i := \Delta_i/\Delta_{min}$. Besides, the flame shape is shown in Figure 5.1, for each grid.

Table 5.1 - Flame length as a function of grid refinement.

Grid (i)	Normalized grid spacing (h_i)	Flame length (f_i)
Fine (1)	1	23.0224
Medium (2)	2	22.8761
Coarse (3)	4	22.5457

The convergence order (p) can be obtained from solutions, according to

$$p = \ln \left(\frac{f_3 - f_2}{f_2 - f_1} \right) \frac{1}{\ln(r)} \quad (5.1)$$

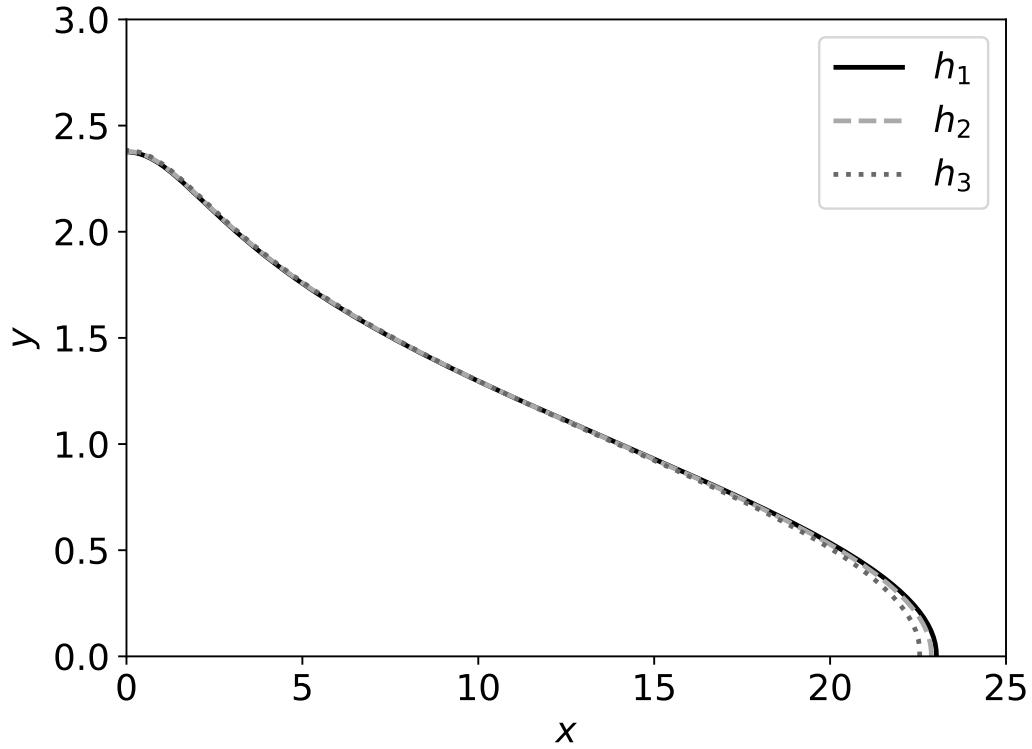
$$\implies p = 1.1753 \quad (5.2)$$

The grid convergence index (GCI) is calculated in accordance with

$$GCI_{i,j} = \frac{F_s |\varepsilon_{i,j}|}{r^p - 1} \quad (5.3)$$

in which $\varepsilon_{i,j} := (f_j - f_i)/f_i$ is the relative error and $F_s := 1.25$, a factor of safety.

Figure 5.1 - Comparison of the flame shape using three distinct grids.



The solutions are for the same problem $(S, Pe_b, Pe_c) = (10, 1, 1)$ and the normalized resolutions are $h_1 = 1, h_2 = 2, h_3 = 4$.

Between grids 1 and 2:

$$GCI_{1,2} = 0.6312\% \quad (5.4)$$

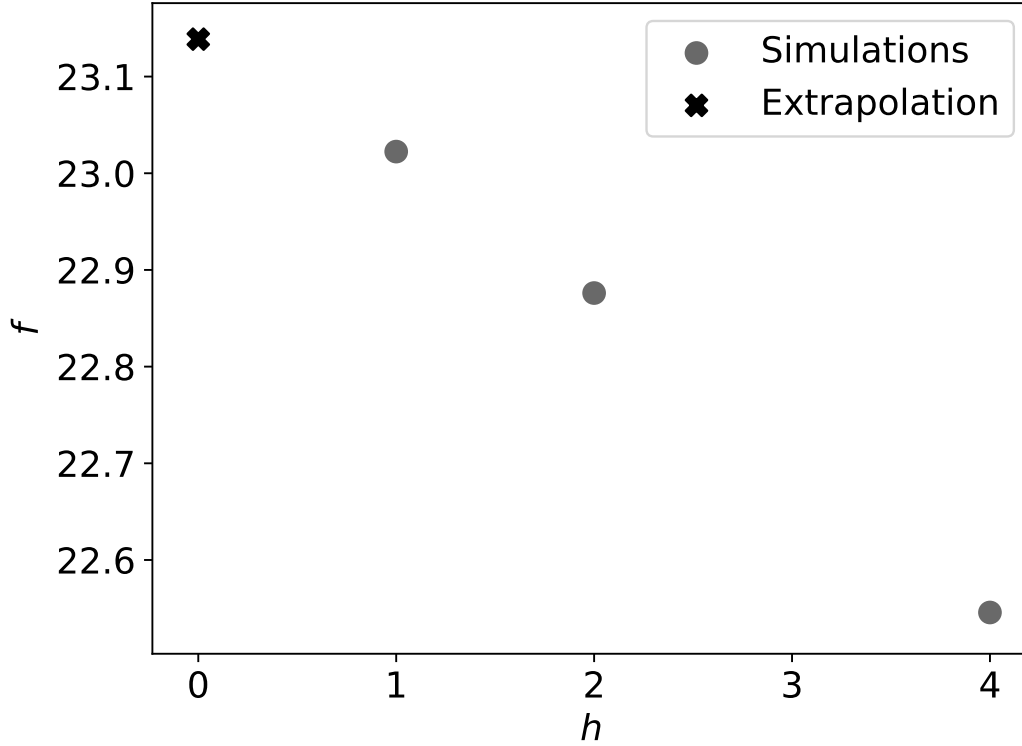
Between grids 2 and 3:

$$GCI_{2,3} = 1.4347\% \quad (5.5)$$

The refinement is adequate when the solution is in the asymptotic range of convergence. This is verified through the relationship:

$$GCI_{2,3} \approx r^p GCI_{1,2} \quad (5.6)$$

Figure 5.2 - Richardson's extrapolation for zero spacing grid ($h = 0$) based on the two finest grids.



In addition to the extrapolated value ($h = 0$), the values obtained from the simulations, $h = 1$, $h = 2$ and $h = 4$, are displayed.

or

$$\frac{GCI_{2,3}}{r^p GCI_{1,2}} \approx 1 \quad (5.7)$$

Which in fact occurs, since

$$\frac{GCI_{2,3}}{r^p GCI_{1,2}} = 1.0065 \quad (5.8)$$

Richardson's extrapolation can be applied between the two finest grids to obtain an estimate of the flame length with a zero spacing grid ($h = 0$).

$$f_{h=0} \approx f_1 + \frac{f_1 - f_2}{r^p - 1} \quad (5.9)$$

$$\implies f_{h=0} \approx 23.1387 \quad (5.10)$$

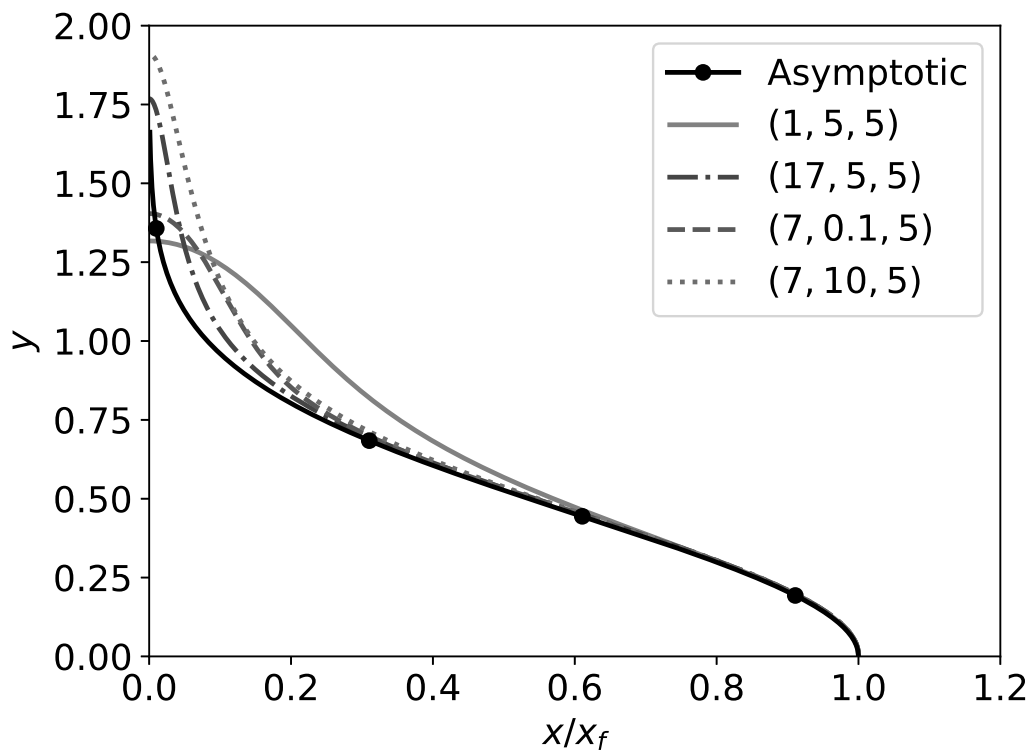
Namely, the estimated flame length is 23.1387 with an uncertainty of 0.6312%, which is depicted in Figure 5.2.

5.2 Code validation

Since this is an unexplored problem, there are no data in the literature for comparison. Ergo, validation is based on the asymptotic solution obtained in Section 4.2.

The numerical results represent very well the asymptotic solution in the part of domain where it is valid, which is ratified by Figure 5.3.

Figure 5.3 - Comparison of the asymptotic solution with numerical results



The cases $(S, Pe_b, Pe_c) = (1, 5, 5), (17, 5, 5), (7, 0.1, 5), (7, 10, 5)$ are compared with the asymptotic solution. For better observation, the results are normalized.

6 DISCUSSION

In this chapter is performed a final discussion.

First, the transient problem is examined in Section 6.1. This requires the imposition of a low strain rate and re-scaling of temporal and spatial variables, in accordance with Subsection 3.1.4. After that, in Section 6.2, the general stationary problem is reinstated and the original scales are also re-established, concluding the discussion in Section 6.3.

6.1 Transition ($Pe_c = \varepsilon Pe_c^{(1)}$, $\varepsilon \ll 1$)

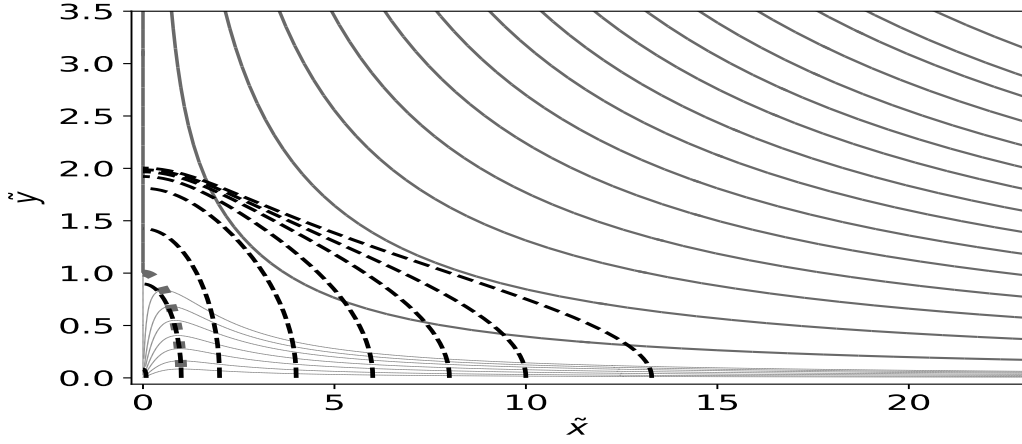
Looking at the Equations (3.13) and (3.14) in polar coordinates, $\tilde{x} := \tilde{r} \cos \theta$ and $\tilde{y} := \tilde{r} \sin \theta$, helps to visualize the deformation of the flame from its initial geometry to the final geometry.

$$\frac{\partial Z}{\partial \tau} + Pe_c^{(1)} \left[\tilde{r} \cos(2\theta) \frac{\partial Z}{\partial \tilde{r}} - \sin(2\theta) \frac{\partial Z}{\partial \theta} \right] + \frac{Pe_b}{\tilde{r}} \frac{\partial Z}{\partial \tilde{r}} = \frac{1}{\tilde{r}} \frac{\partial Z}{\partial \tilde{r}} \left(\tilde{r} \frac{\partial Z}{\partial \tilde{r}} \right) + \frac{1}{\tilde{r}^2} \frac{\partial^2 Z}{\partial \theta^2} \quad (6.1)$$

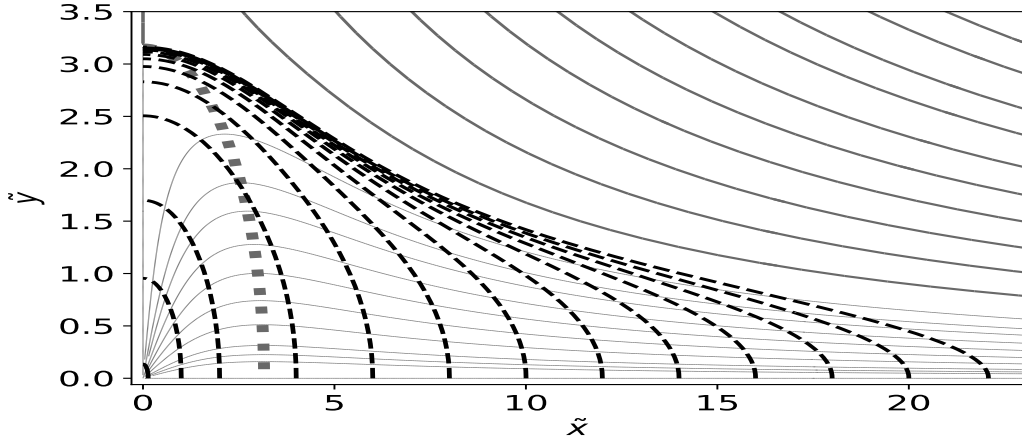
$$\frac{\partial H}{\partial \tau} + Pe_c^{(1)} \left[\tilde{r} \cos(2\theta) \frac{\partial H}{\partial \tilde{r}} - \sin(2\theta) \frac{\partial H}{\partial \theta} \right] + \frac{Pe_b}{\tilde{r}} \frac{\partial H}{\partial \tilde{r}} = \frac{1}{\tilde{r}} \frac{\partial H}{\partial \tilde{r}} \left(\tilde{r} \frac{\partial H}{\partial \tilde{r}} \right) + \frac{1}{\tilde{r}^2} \frac{\partial^2 H}{\partial \theta^2} \quad (6.2)$$

For initial conditions such that $Z = Z(\tilde{r})$ and $H = H(\tilde{r})$, the second term in the left hand side, both terms inside the bracket, and the second one in right hand side are zero. However, the first term inside the bracket, which is very small while $\tilde{r} \ll 1$, is responsible for distorting the cylindrical geometry of the flame. The flame distortion does not occur indefinitely because the flame finds its stationary form. The flow field Péclet number (Pe_c) can be interpreted as a stationarity indicator: as Pe_c increases, the steady state is reached more quickly, since the Strouhal number (S_t) decreases. Just for $Pe_c = 0$ (radial fuel ejection into inert oxidant ambient atmosphere), the flame is always in transient regime (QIAN; LAW, 1997).

Figure 6.1 - Temporal evolution of the flame



(a)



(b)

(a) $(S, Pe_b) = (10, 1)$ and (b) $(S, Pe_b) = (1, 10)$. The flow field of the impinging flows is for $Pe_c^{(1)} = 1$. The flame shapes correspond to (a) $\tau = 0.001, 0.158, 0.496, 1.187, 1.772, 2.309, 2.884, 9.856$ and (b) $\tau = 0.001, 0.051, 0.182, 0.523, 0.850, 1.139, 1.395, 1.629, 1.857, 2.092, 2.363, 2.758, 7.265$. The curve represented by square dots determines the position $\tilde{x}_0^2 + \tilde{y}_0^2 = Pe_b/Pe_c^{(1)}$ where $\tilde{v}(\tilde{x}_0, \tilde{y}_0) = 0$.

In the formulation of transition from transient, one-dimensional regime to stationary, two-dimensional regime (see Subsection 3.1.4), there is no reason for taking $Pe_c^{(1)} \neq 1$, because the value of $Pe_c^{(1)}$ different from unity could be included in the value of ε . Therefore, in all cases presented for discussions, $Pe_c^{(1)} = 1$ is assumed.

The cases were selected in such a way that the fuel flux remains the same or, in

other words, the product SPe_b is constant. Thus, in any cases in which $SPe_b = 10$, the same amount of fuel is provided to the ambient, but with different fuel ejection momentum.

The discrete evolution of the flame for the cases (a) $(S, Pe_b) = (10, 1)$ and (b) $(S, Pe_b) = (1, 10)$ are exhibited in Figure 6.1. Due to no unique behavior of the flame velocity, the flame shapes are not displaced in regular time interval, but they are chosen to represent properly the flame evolution. Thus the flame shapes correspond to the times $\tau = 0.001, 0.158, 0.496, 1.187, 1.772, 2.309, 2.884, 9.856$ for $(S, Pe_b) = (10, 1)$ and $\tau = 0.001, 0.051, 0.182, 0.523, 0.850, 1.139, 1.395, 1.629, 1.857, 2.092, 2.363, 2.758, 7.265$ for $(S, Pe_b) = (1, 10)$. Clearly, the initial displacement of the flame is controlled by radial transport of fuel into the region close to the burner, where the impinging flows has a negligible influence.

In addition, considering in this figure the position $(\tilde{x}_0, \tilde{y}_0)$ defined by $\tilde{r}_0^2 = \tilde{x}_0^2 + \tilde{y}_0^2 = Pe_b/Pe_c^{(1)}$, the velocity in the y -direction (\tilde{v}) is zero. In particular, there are two stagnation points at the positions $\tilde{y}_{st} := (0, \pm|\tilde{y}_0|)$. The convective transport is only in the x -direction over the curve specified by the points $(\tilde{x}_0, \tilde{y}_0)$. For $\tilde{r} < \tilde{r}_0$, the flow field is practically radial. Nevertheless, for $\tilde{r} > \tilde{r}_0$, the convective term in y -direction deflects the streamlines from the burner to parallel to the x -axis, as seen in Figure 6.1. Once the flame passes by the radius $\tilde{r} = \tilde{r}_0$, it enters in the flow field region influenced by the impinging flows and starts to distort in x -direction, because its displacement in y -direction - against y -direction convection transport of oxidant - is at a velocity that decreases with time.

The thick-line streamlines describe the region of influence of the impinging flows. Moreover, the thin-line streamlines, from the cylindrical burner, describe the region of influence of fuel ejection, as shown in Figure 6.1. Observing the flame position relatively to the flow field in Figure 6.1a, it is observed that the location of flame is in the region where the flow field is imposed mainly by the impinging flows. This fact indicates the influence of the diffusion. The fuel species is diffusively transported into the impinging flows region. Consequently, the fuel consumption is larger than the other case, $(S, Pe_b) = (1, 10)$, and the flame length is smaller, as seen in Figure 6.1b.

The most significant result depicted by Figure 6.1b is the flame to be very close to the frontier from the flow field imposed by the burner fuel ejection and the flow field imposed by the impinging flows. The diffusive transport is limited to a layer around that frontier. As consequence, the flame must be very long to permit the

fuel consumption.

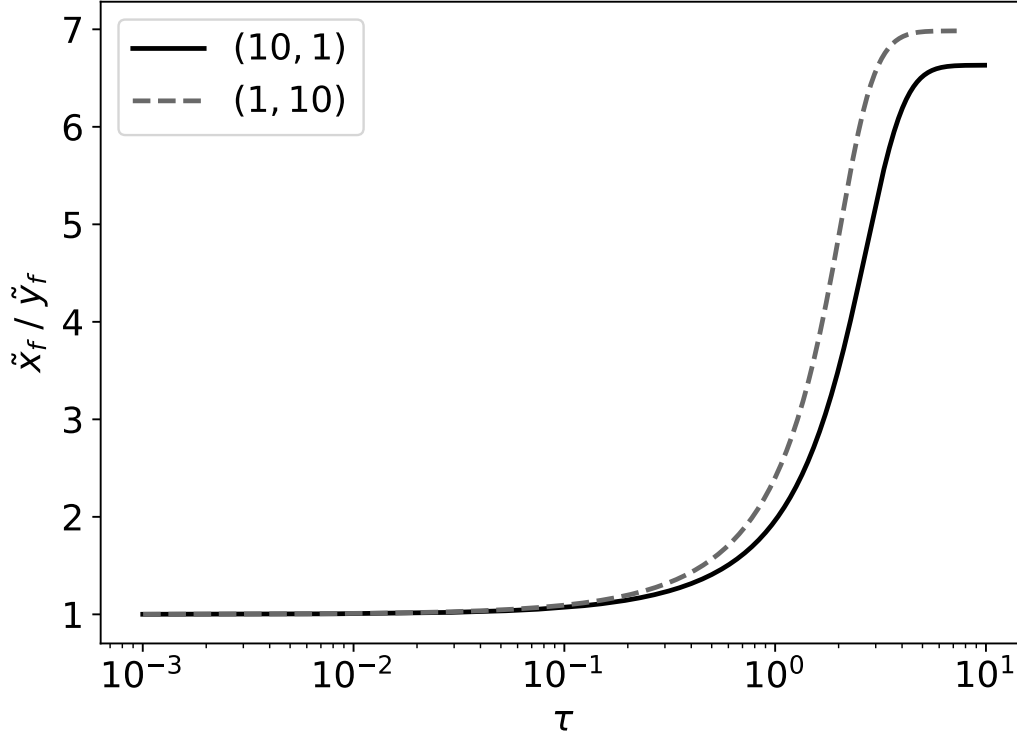
Denoting \tilde{x}_f as the flame position on the x -axis (length), \tilde{y}_f as the flame position on the y -axis (width), from Figure 6.1, it can be seen the final position (\tilde{y}_f) with respect to the stagnation point (\tilde{y}_{st}) on both sides of the burner. For the case $(S, Pe_b) = (1, 10)$, the stationary flame width (\tilde{y}_f) is at the stagnation point, $\tilde{y}_{st} = 10^{1/2}$. This result shows that the molecular transport layer is very thin: the diffusion does not transport fuel beyond the stagnation point (\tilde{y}_{st}), i.e. $\tilde{y}_f - \tilde{y}_{st} \ll 1$. This result would be expected for $Pe_b \gg 1$ because the thickness of the molecular transport layer is of order $Pe_b^{-1/2}$. Then, for $Pe_b = 10$, the diffusion could transport fuel to a distance of $10^{-1/2}$ beyond the stagnation point. However, fuel penetration is not observed because the fuel concentration is very low in the case $S = 1$, $Y_{F,b} = Y_{O,\infty}/s \ll 1$.

Besides, the circular behavior in the beginning of the flame displacement is observed clearly, which was expected because the radial transport of the fuel controls the flame dynamics. To demonstrate this behavior, the aspect ratio (\tilde{x}_f/\tilde{y}_f) of the flame is quantified and exhibited in Figure 6.2. In the time interval $\tau < 0.1$, the flame is circular. Therefore, depending on the chosen spatial and temporal scales, $\tilde{r}_c \ll 1$ and $\tau_c \ll 1$ ($r_c \ll \varepsilon^{-1/2}$ and $t_c \ll \varepsilon^{-1}$), the flame can be considered circular and transient (QIAN; LAW, 1997).

The dynamics of the flame is basically separated into three periods: initial ($0 < \tau < 0.1$), intermediate ($0.1 \leq \tau < \tau_s$) and final ($\tau \geq \tau_s$), in which τ_s is the time to attain stationary regime. The flame aspect ratio for $(S, Pe_b) = (1, 10)$ is larger than that for $(S, Pe_b) = (10, 1)$. Additionally, time τ_s is shorter for $(S, Pe_b) = (1, 10)$, $\tau_s = 4.198$, than that for $(S, Pe_b) = (10, 1)$, $\tau_s = 6.800$, with τ_s considered the time when the major component of velocity is approximately 10^{-2} . The initial period is predominantly governed by molecular transport while the intermediate period is also influenced by convection. The final period is also governed by molecular transport, but the small spatial scale close to the flame, wherein that transport is important, is imposed by the convective transport.

Denoting \tilde{u}_f as the velocity of \tilde{x}_f and \tilde{v}_f as the velocity of \tilde{y}_f . Thus, in the initial period, \tilde{x}_f and \tilde{y}_f are proportional to $\tau^{1/2}$, as well as \tilde{u}_f and \tilde{v}_f are inversely proportional to the same temporal power, $\tau^{-1/2}$. Figures 6.3 and 6.4 show this behavior for both, position and velocity, of flame length and flame width, in cases $(S, Pe_b) = (10, 1)$ (continuous line) and $(S, Pe_b) = (1, 10)$ (dashed line).

Figure 6.2 - Temporal evolution of aspect ratio (\tilde{x}_f/\tilde{y}_f)

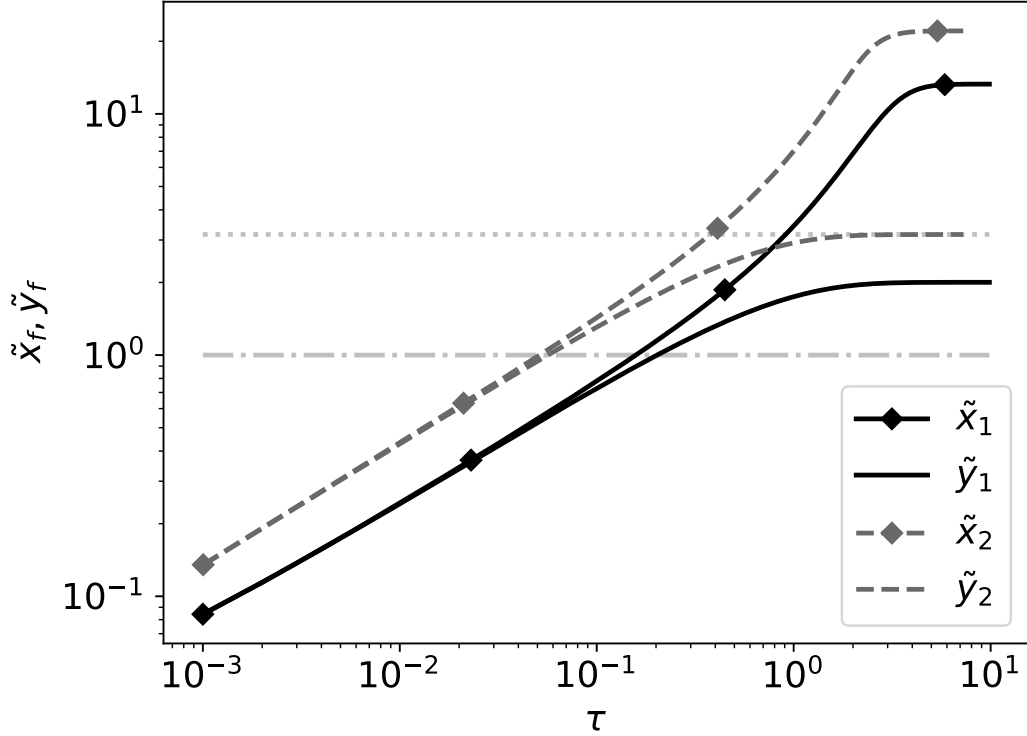


For both cases, $(S, Pe_b) = (10, 1), (1, 10)$.

Since $(S, Pe_b) = (10, 1), (1, 10)$ are the extreme cases, for any other values of (S, Pe_b) that lead to $S Pe_b = 10$, the results are between the two curves exhibited in Figures 6.3 and 6.4. Therefore, the difference of results is imposed by the momentum of the fuel stream dictated by the ejection velocity.

As mentioned before, the flame aspect ratio evolution, Figure 6.2, shows that the case $(S, Pe_b) = (1, 10)$ has a shorter transient period than the case $(S, Pe_b) = (10, 1)$. Figure 6.3 reveals the same behavior for the evolution of both, flame width (\tilde{y}_f) and flame length (\tilde{x}_f). However, the flame width (\tilde{y}_f) reaches the stationary condition earlier for both cases than the flame length (\tilde{x}_f).

Figure 6.3 - Temporal evolution of flame length (\tilde{x}_f) and width (\tilde{y}_f)

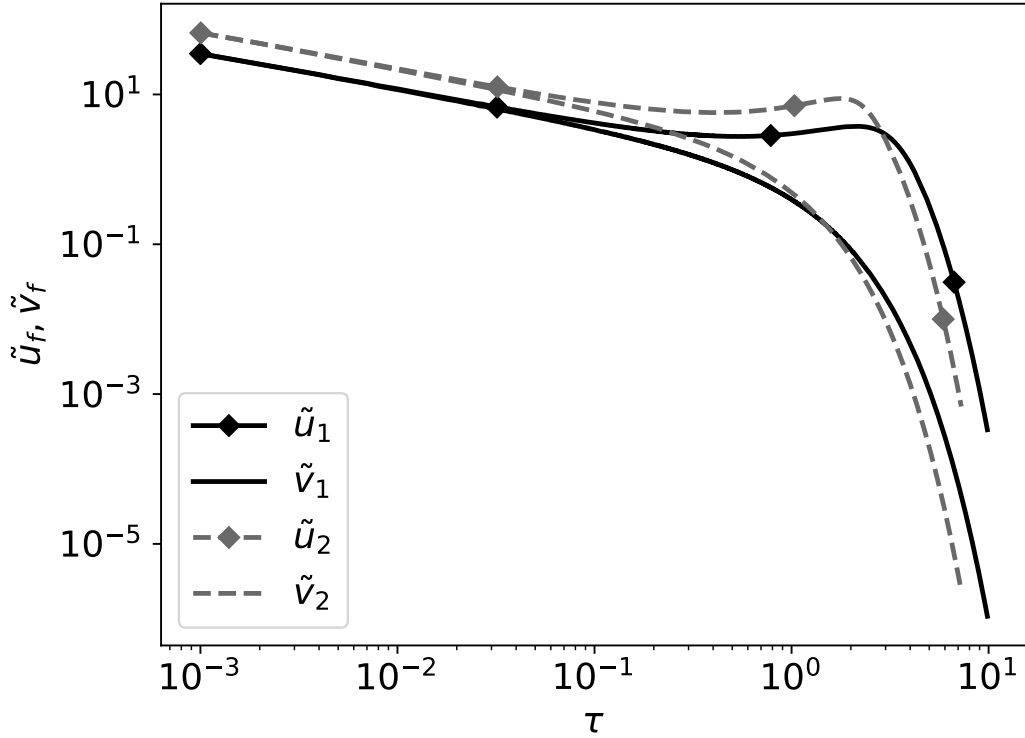


Indexes 1 and 2 stand for the cases $(S, Pe_b) = (10, 1)$ and $(S, Pe_b) = (1, 10)$, respectively. The stagnation points for each case are also displayed for referencing, $\tilde{y}_{st} = (Pe_b/Pe_c^{(1)})^{1/2}$.

In Figure 6.3, the stagnation positions (\tilde{y}_{st}) are determined by the horizontal lines. For the case $(S, Pe_b) = (10, 1)$, the stagnation point is at $\tilde{y}_{st} = 1$ and the molecular transport layer is of order unity, namely the diffusive process takes fuel into a distance of order unity beyond the stagnation point, $\tilde{y}_f - \tilde{y}_{st} = 1.003$, as seen in the figure. For the case $(S, Pe_b) = (1, 10)$, the stagnation point is at $\tilde{y}_{st} = 10^{1/2}$ and the stationary flame width (\tilde{y}_f) is practically on the stagnation point ($\tilde{y}_f - \tilde{y}_{st} = -0.001$), as explained before.

Figure 6.4 exhibits the velocity of the flame on the axes, $\tilde{u}_f(\tilde{x}, 0, \tau)$ and $\tilde{v}_f(0, \tilde{y}, \tau)$. These results confirm that the velocities, \tilde{u}_f and \tilde{v}_f , decrease according to $\tau^{-1/2}$ in the period $\tau < 0.1$. About $\tau \sim 0.5$, the velocity \tilde{v}_f is reduced and the velocity \tilde{u}_f is found constant. Approximately, in the time interval $0.5 < \tau < 2$, the flame length \tilde{x}_f first accelerates and then decelerates. The accelerating period occurs when the velocity \tilde{v}_f is reduced, indicating that the stationary regime for \tilde{y}_f is close.

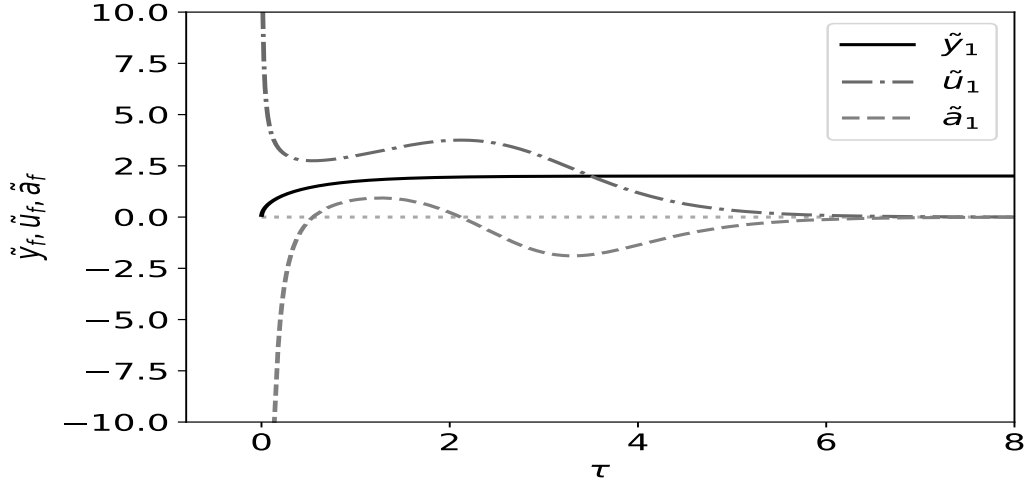
Figure 6.4 - Temporal evolution of flame length (\tilde{u}_f) and width (\tilde{v}_f) velocities



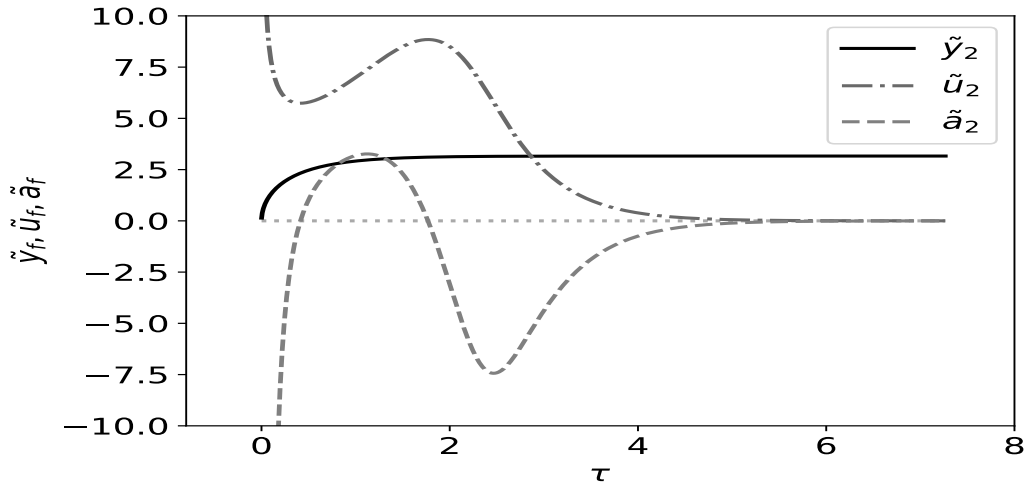
Indexes 1 and 2 stand for the cases $(S, Pe_b) = (10, 1)$ and $(S, Pe_b) = (1, 10)$, respectively.

Figure 6.5 shows the acceleration of the flame on the x -axis, defined as \tilde{a}_f . In order to facilitate the elucidation of the flame acceleration behavior, two additional lines are displayed, namely, the evolution of the flame on the y -axis (\tilde{y}_f) and of the flame velocity on the x -axis (\tilde{u}_f). As seen more clearly in the two plots, the flame accelerates in x -direction in the time interval $0.5 < \tau < 2$, practically for the two cases. However, the acceleration in the case $(S, Pe_b) = (1, 10)$ is larger than the other case, $(S, Pe_b) = (10, 1)$. The case in which the fuel diffusion has an important contribution on the flame displacement, the acceleration is smaller than the case in which the convection dominates the flame displacement since the earlier period.

Figure 6.5 - Dynamics of the flame



(a)



(b)

The evolution of the flame position (\tilde{y}_f), of the flame velocity (\tilde{u}_f) and of the flame acceleration (\tilde{a}_f) on the x -axis for (a) $(S, Pe_b) = (10, 1)$ and (b) $(S, Pe_b) = (1, 10)$.

In both cases, it is seen that the acceleration of the flame starts after the flame decreases significantly the growth in y -direction, then the flame is close to the stationary regime in y -axis. Quantitatively, for $(S, Pe_b) = (10, 1)$, x_f acceleration (\tilde{a}_f) becomes positive in the time interval $0.545 \leq \tau \leq 2.117$ and, for $(S, Pe_b) = (1, 10)$, \tilde{a}_f becomes positive in the time interval $0.414 \leq \tau \leq 1.769$.

Accordingly, these results underline the influence of the fuel ejection momentum, measured by Pe_b . Increasing Pe_b , the acceleration period starts earlier and is shorter, but its magnitude is higher.

6.1.1 Asymptotic analysis

The region where the streamlines coming out of the burner are located is very narrow and is around the x -axis. This feature justifies the application of the boundary layer approximation. Imposing the latter condition and using results from Section 4.2, the solution for the mixture fraction Z is

$$Z = \frac{x_f}{\tilde{x}} \exp \left[- \left(\tilde{y} \sqrt{Pe_c^{(1)}/2} \right)^2 \right] \quad (6.3)$$

The flame length (\tilde{x}_f) depends on the problem parameters, namely $\tilde{x}_f = \tilde{x}_f(S, Pe_b, Pe_c^{(1)})$, then the asymptotic problem shows only the behavior of the solution.

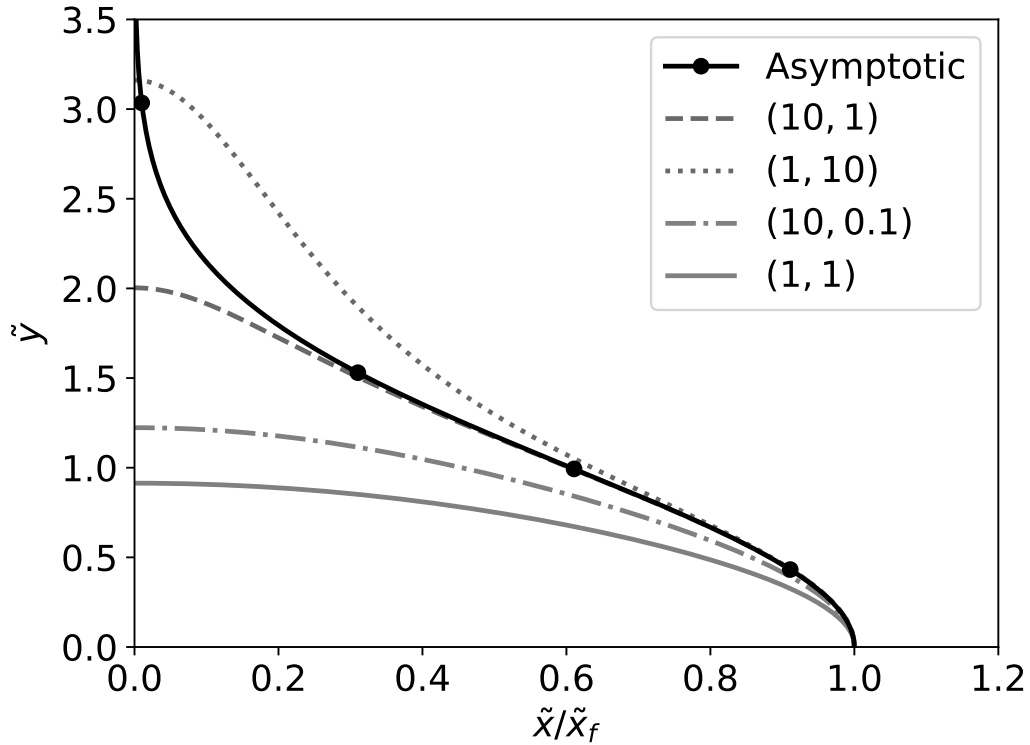
Imposing $Z(\tilde{x}, \tilde{y}) = 1$, the flame position in the first (positive) and fourth (negative) quadrant is evidenced

$$\tilde{y} = \pm \left[\frac{2}{Pe_c^{(1)}} \ln \left(\frac{\tilde{x}_f}{\tilde{x}} \right) \right]^{1/2} \quad (6.4)$$

Figure 6.6 shows a comparison between the asymptotic and the numerical solutions for the cases $(S, Pe_b) = (10, 1)$, $(1, 10)$, for which the fuel flux is $SPe_b = 10$, and for $(S, Pe_b) = (10, 0.1)$, $(1, 1)$, for which $SPe_b = 1$. To promote a compact comparative analysis, the x -coordinate is normalized by the flames length, respectively given by $\tilde{x}_f = 13.286, 22.081, 2.942, 1.634$. The asymptotic solution may fail for two reasons: the evolution of the flame depends on fuel ejection and on the diffusive transport in x -direction.

For the case $(S, Pe_b) = (10, 1)$, due to the high fuel concentration, the molecular transport is predominant and, as the fuel flow is relatively large, the flame is established away from the burner, making the diffusion in y -direction preponderant. In this case, the asymptotic solution quickly tends to the numerical solution, right after the region where the diffusion in x -direction is of the same magnitude order as the diffusion in y -direction (cylindrical symmetry region).

Figure 6.6 - Comparison of the asymptotic solution with numerical results



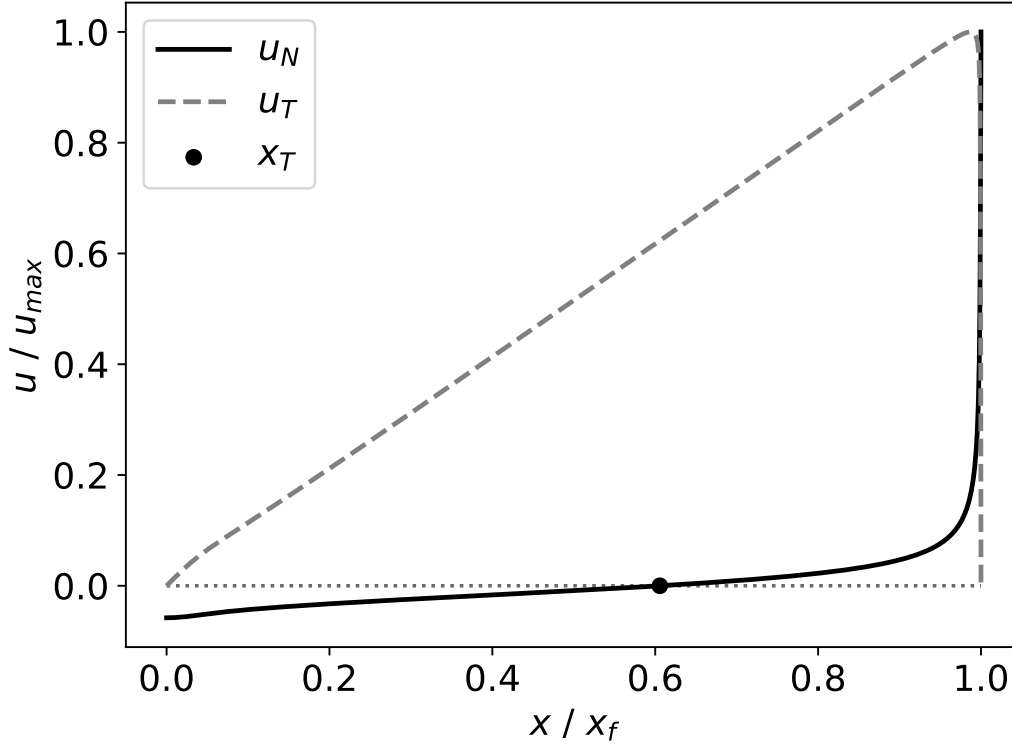
$(S, Pe_b) = (10, 1), (1, 10), (10, 0.1), (1, 1)$. For the sake of comparison, the results are normalized.

For $(S, Pe_b) = (1, 10)$, the influence of fuel ejection is significant and, as $S = 1$, the flame is established at the interface between the impinging flows and the fuel ejection flow. Thus, the numerical solution only tends to the asymptotic solution for $\tilde{x} \gg 1$, since, in this region, the impinging flows are dominant.

For the cases $(S, Pe_b) = (10, 0.1)$ and $(S, Pe_b) = (1, 1)$, because of the low fuel flow, the flame is established in the burner proximity, where the two avoided transport mechanisms are of the same order of the other transport mechanisms. However, the case $(S, Pe_b) = (1, 1)$ is the most critical, because the flame is even deeper into the region where the fuel ejection effects are not negligible.

6.2 Flame characteristics

Figure 6.7 - Diffusion flame with continuous proprieties change



Diffusion flame continuous change from counterflow diffusion flame (Tsuji flame) in the vertical symmetric axis ($x = 0$) to coflow diffusion flame (Burke-Schumann flame) in the proximity of the tangency point (x_T). It corresponds to the base case $(S, Pe_b, Pe_c) = (17, 1, 1)$ and, for the sake of comparison, the results are normalized by its maximum values ($u_{max} \approx x_f = 37.779$).

The innovative configuration proposed in this work offers the opportunity to observe continuously the behavior of diffusion flames in a complete spectrum of conditions, from counterflow diffusion flame (Tsuji flame) in the vertical symmetric axis ($x = 0$) to coflow diffusion flame (Burke-Schumann flame) from the tangency point (x_T) up to the flame tip - refer to Subsection 4.2.2 - as highlighted by Figure 6.7. In this figure it is possible to observe that at the point $x = 0$ (on the axis of vertical symmetry), the normal velocity in the flame is present and the tangential velocity, is absent, characterizing a Tsuji (counterflow) flame. As one progresses forward in x -direction, the intensity of the normal component decreases and the tangential component

increases. The normal velocity is almost zero around the point of tangency (exactly zero at this point), characterizing the beginning of the Burke-Schumann (coflow) flame. As it continues to advance in x -direction, the normal component remains continuously advancing, until it reaches its apex at the top of the flame, while the tangential component always grows (proportionally to x), until very close to the flame top, when it decreases to zero abruptly on the axis of horizontal symmetry ($y = 0$). A parallel with the Subsection 4.2.3 can help to clarify this.

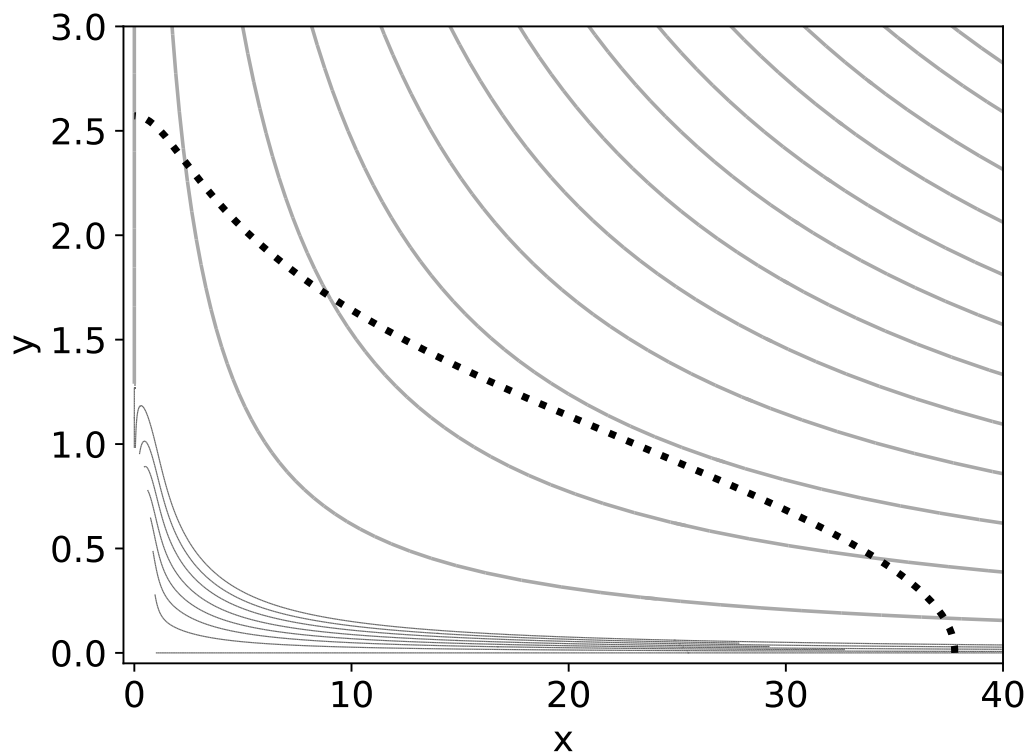
6.3 Flame properties estimation

To examine some characteristics of the flame, the case $(S, Pe_b, Pe_c) = (17, 1, 1)$ (Figure 6.8) is chosen to represent the problem generically and should act as a reference for the discussion that ensues. The flame established near to the burner consumes a significant portion of fuel and generates a reasonable amount of products, which influence the concentration of oxidant in the flame region downstream. The flame can be divided into two parts and the property used to distinguish one from another is the position where a streamline is tangent to the flame, in the Figure 6.8 this point is located at $(x, y)_T = (22.81, 1.01)$. Note the large penetration of the flame in the oxidant stream occasioned by diffusion, because of the high concentration ($S = 17$).

Between the burner and the point of tangency, the streamlines cross the flame from outside to inside. It is an indication of oxidant transport from the ambient atmosphere to the flame by the convective process. However, between the point of tangency and the tip of the flame, the streamlines cross the flame from inside to outside. In this part of the flame, the convective process takes fuel to the flame. The convective transport is the responsible to create small length scale for the diffusive transport to be high enough to sustain the flame even with very low concentration of fuel. Furthermore, the convective transport between the burner and the point of tangency carries the heat generated by the flame in this region towards the top of the flame, which generates a vast hot zone, in agreement with Figure 6.9. The presence of a high temperature zone prevents heat loss in one direction, acting as an important flame stabilizer, avoiding its extinction by heat loss. On the other hand, it favors the formation of soot which must be investigated with a proper model.

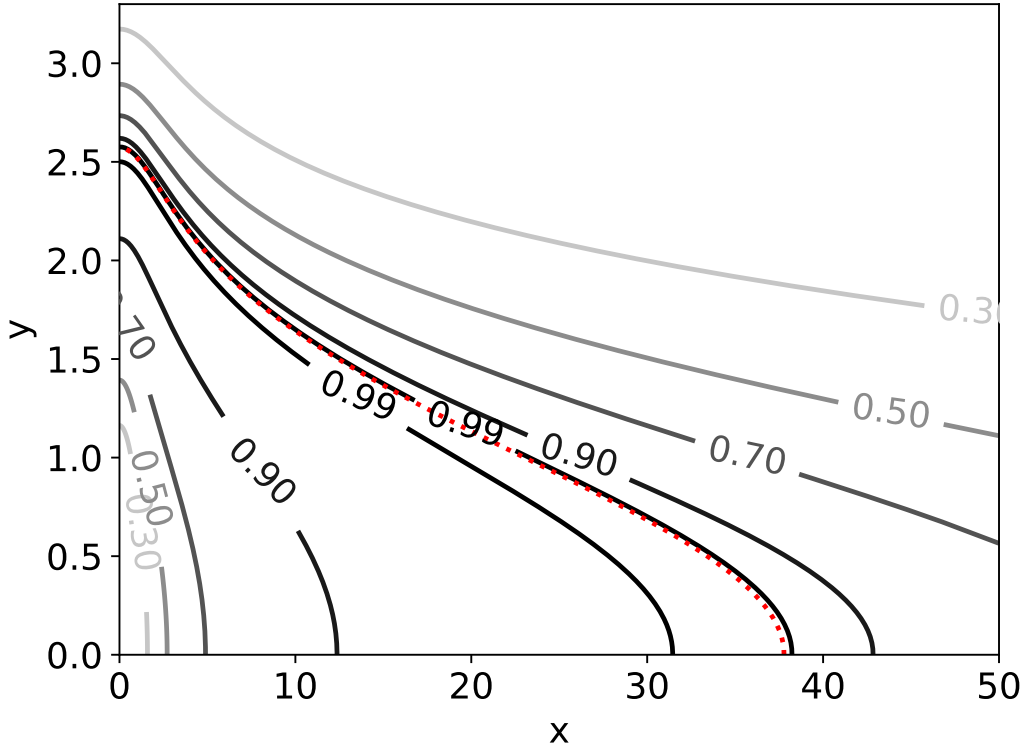
It is emphasized that the point of tangency can be considered a transition demarcator between the diffusion flame in counterflow regime (part of the convective transport of oxidant is perpendicular to the flame surface) and diffusion flame in coflow regime (convective transport of oxidant is parallel to the flame surface).

Figure 6.8 - Flow field and flame shape



Flame established in the original configuration suggested. Case $(S, Pe_b, Pe_c) = (17, 1, 1)$ is taken as a generic representation. The dotted line is the flame position and the thinner and more dense streamlines are the fuel flow.

Figure 6.9 - Temperature distribution (T)



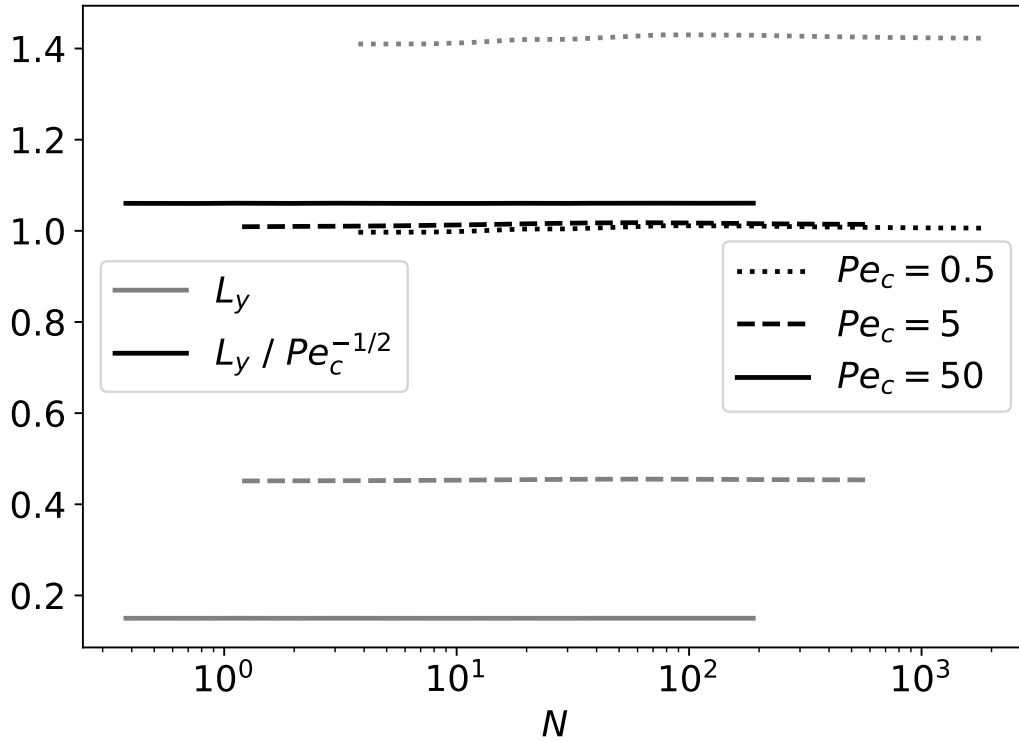
A large hot region is formed between the point of tangency and the top of the flame caused by the heat transport from the region between the burner and the point of tangency. Case $(S, Pe_b, Pe_c) = (17, 1, 1)$ is taken as a generic representation. The location of the flame is indicated in red (dotted line).

6.3.1 Flame sensitivity

Regardless of N value, the characteristic width in y -direction (see Section 4.1) is always of order of $\tilde{L}_y \sim 1$ ($L_y \sim Pe_c^{-1/2}$), that is corroborated by Figures 6.10 and 6.11. Then the flame is established in a flow field practically parallel, according to $(u, v) = (x, O(Pe_c^{-1/2}))$. Consequently, the width of the flame ($y_f \sim L_y$) is conditioned only by the impinging flows, evidenced through the dependency on Pe_c .

Similarly for flame width (y_f), but around the point of stagnation, the appropriate scale is in the order of $y_{st} + Pe_c^{-1/2}$. Figure 6.12 displays both the original and the rescaled quantities.

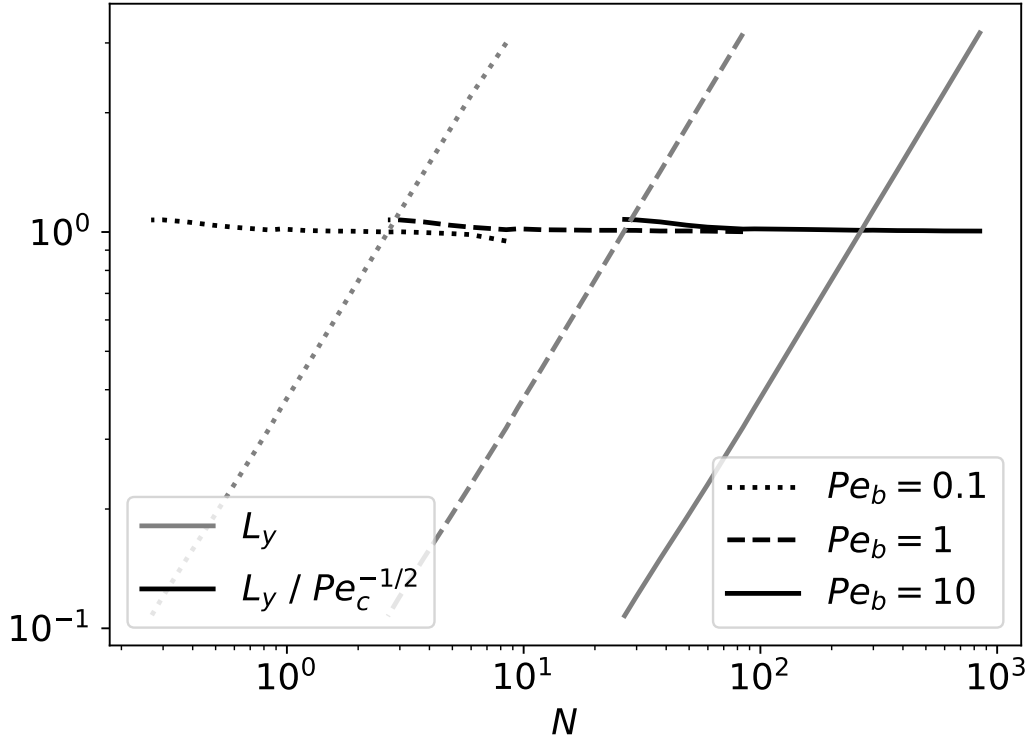
Figure 6.10 - Flame width ($y_f \sim L_y$) - varying Pe_c



Flame width ($y_f \sim L_y$) for the cases $Pe_c = 0.5$, $Pe_c = 5$ and $Pe_c = 50$, is taken as y_T , in which this parameter denotes the width of the flame at the point of tangency, i.e., at the point $(x, y) = (x_T, y_T)$ where the influence of the burner is irrelevant. $Pe_b \in [0.1, 50]$ and $S = 17$.

Depending on the flow conditions imposed by the burner geometry or fuel ejection, the shape of the flame changes in burner surroundings, including the flame width (y_f). Ergo, even ejecting the same fuel mass ($S Pe_b$), a considerably different length (x_f) can be obtained, as function of S and Pe_b , although the asymptotic behavior (far from the burner) to be the same.

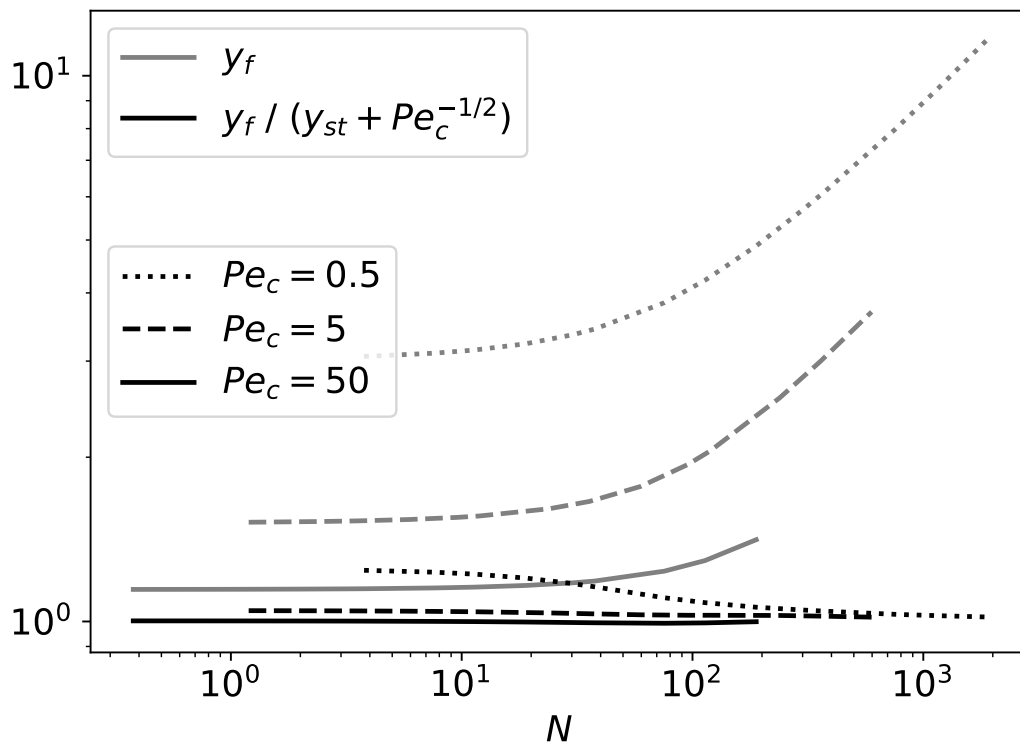
Figure 6.11 - Flame width ($y_f \sim L_y$) - varying Pe_b



Flame width ($y_f \sim L_y$) for the cases $Pe_b = 0.1$, $Pe_b = 1$ and $Pe_b = 10$, is taken as y_T , in which this parameter denotes the width of the flame at the point of tangency, i.e., at the point $(x, y) = (x_T, y_T)$ where the influence of the burner is irrelevant. $Pe_c \in [0.1, 100]$ and $S = 17$.

The numerical results indicate that $N = S$ is a demarcator between the flame highly influenced by the conditions near the burner ($N \leq S$) and the flame weakly influenced by them ($N > S$). This behavior can be clearly seen in Figures 6.13 and 6.14, whose results will be extensively discussed ahead. In order to help the data interpretation, Figures 6.13 and 6.14 gather findings of two analyses. The first one shows the dependence of the flame length (x_f) with S . In addition, the second one exhibits the dependence of the flame length (x_f) on the parameters S , Pe_b and Pe_c , grouped in N . In these figures, the dependence of x_f with S and N is clarified by rescaling x_f with these two parameters. For this reason, there are two curve patterns in each graph.

Figure 6.12 - Flame width (y_f)



For the cases $Pe_c = 0.5$, $Pe_c = 5$ and $Pe_c = 50$, with $Pe_b \in [0.1, 50]$ and $S = 17$.

6.3.2 For $N_{min} \leq N \leq S$

As seen in the numerical results, the flame length L_x is not rescaled with N for the conditions that lead to $N \leq S$, i.e., the flow field with high strain rate or very little fuel ejection. In such conditions, the flame follows the burner shape and, because of that, the burner influence is strong. This fact justifies $\eta < 1$ in the diffusive transport of Equation (4.4).

Considering $\tilde{L}_y \sim 1$, the flame length is rescaled by N/η and, accordingly, the flame length is rescaled by S - as illustrated by Figures 6.13 and 6.14 - demonstrating that it depends only on the fuel concentration at the burner surface, i.e., the flame under these conditions is governed predominantly by diffusion. Furthermore the value of η is determined as $\pi Pe_b / (2Pe_c^{1/2})$ based on the numerical results.

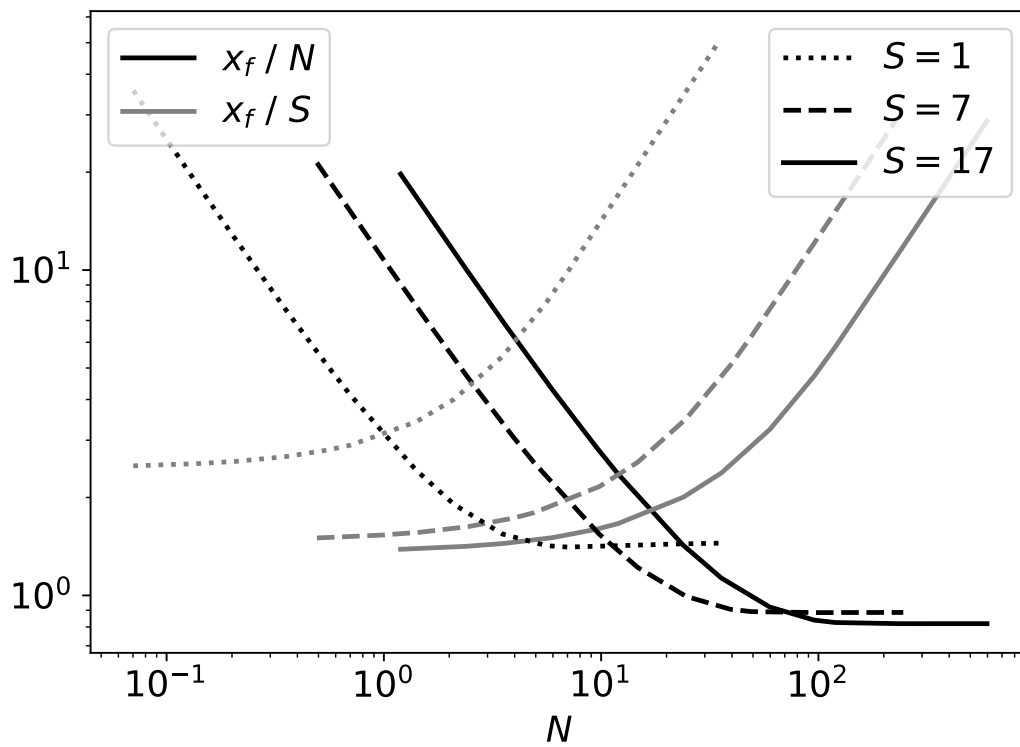
6.3.3 For $N > S$

In the cases that lead to the flow field with low strain rate or high fuel ejection ($N > S$), the flame is located far from the burner and, thereby, the burner influence is minimal, which justifies $\eta = 1$.

As confirmed by Figures 6.13 and 6.14, the flame length (x_f) is rescaled very well with N .

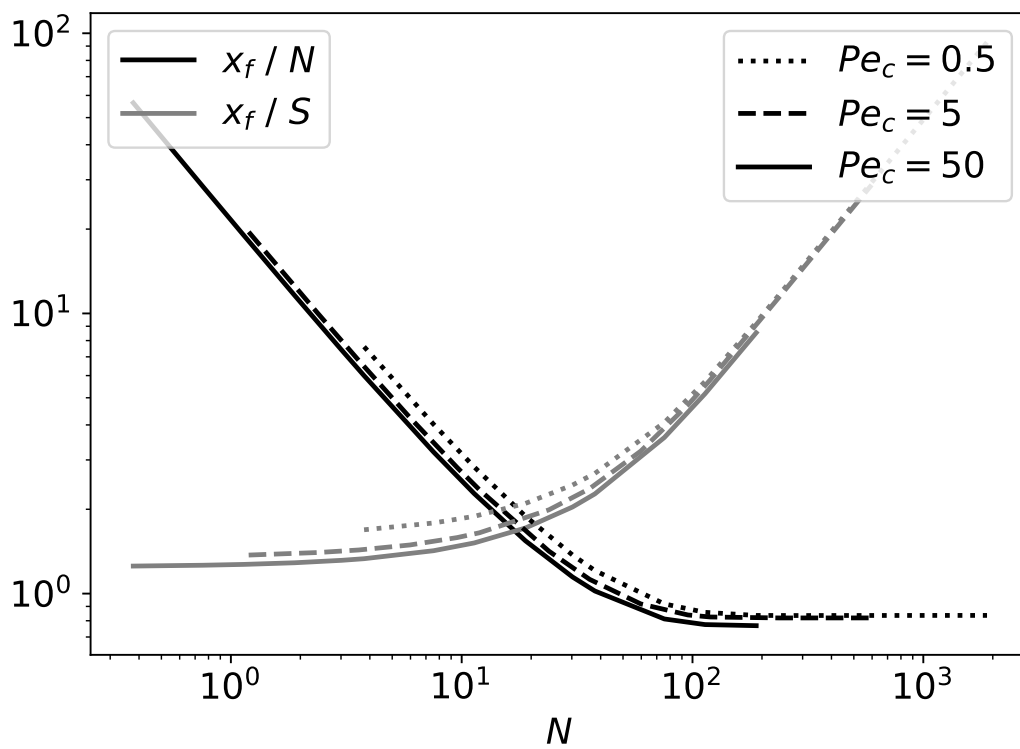
Therefore, the flame dependency - in the flow parameters (Pe_b and Pe_c) and in the chemical parameter (S) - already suggested in the physical analysis of order of magnitude is ratified in this Section.

Figure 6.13 - Flame length influence demarcator - varying S



The length of the flame for the same cases, $S = 1$, $S = 7$ and $S = 17$, is normalized by S (gray) and N (black). In both situations, $Pe_b \in [0.1, 50]$ and $Pe_c = 5$.

Figure 6.14 - Flame length influence demarcator - varying Pe_c



The length of the flame (x_f) for the same cases, $Pe_c = 0.5$, $Pe_c = 5$ and $Pe_c = 50$, is normalized by S (gray) and N (black). In both situations, $Pe_b \in [0.1, 50]$ and $S = 17$.

7 CONCLUSION

Employing a horizontal, cylindrical burner inside a very low strained flow, the established diffusion flame presents a continuous change from transient, circular behavior to stationary, two-dimensional behavior. In the stationary state, two local counterflows in y -axis are found and the flames established there are of Tsuji type, a system of double Tsuji flame. In the early stage of displacement, the diffusion flame is controlled by diffusion and fuel ejection, then the flame geometry is circular and transient. After the flame crosses the surface determined by the radius $(Pe_b/Pe_c^{(1)})^{1/2}$, where the vertical velocity (v) is zero, the flame displacement in y -direction becomes slow down and the flame starts distorting mainly in the x -direction, influenced by the impinging flows. When the flame is very close to the region of domain controlled by the impinging flows, the distortion velocity in the x -direction increases, the flame accelerates due to the restriction of the fuel flow. The period to reach the stationary regime depends on stoichiometric parameter (S) and burner Péclet number (Pe_b). For large S , the diffusion transport takes fuel deep into the region controlled by the impinging flows. In the other hand, for large Pe_b , the diffusion transport is not able to take fuel further from the interface between the region under the influence of the fuel ejection and that one under the influence of the impinging flows. The asymptotic solution emphasizes the relevant transport mechanisms for the flame in different (S, Pe_b) conditions and permits to know analytically relevant properties like, for example, stagnation points, strain rate, approximate solutions, normal and tangential flame velocities, gradients, scalar dissipation coefficient, among others.

The contribution of this master's thesis is to provide an innovative configuration, in which a diffusion flame spatially changes continuously, from counterflow (Tsuji) flame to parallel flow (Burke-Schumann) flame. In addition, its change is also in time and, during the evolution, the flame is accelerated. There are two regions in the flame, delimited by the point of tangency between the streamlines and the flame. One of them is the region between the burner and that point where the convective transport favors the oxidant flux to the flame. The other one is the region where the convective transport supports the fuel flux to the flame. Specifically, even with low fuel concentration, the convective transport generates an appropriated spatial scale close to the flame where the molecular transport of fuel sustains the stoichiometric burning. It is worth noting that the convective heat transfer creates a large hot zone in the second region, which stabilizes the flame. The width of the flame (where there is no more burner influence), $y_f \sim L_y$, is proportional to the thickness of the molecular transport layer, i.e. $y_f \propto Pe_c^{-1/2}$. The condition $N = S$ was established as

the transition demarcator of flame length (x_f) behavior. For $N \leq S$, the flame length is directly proportional to the stoichiometric parameter ($x_f \propto S$). For $N > S$, the flame length is proportional to the stoichiometric parameter ($x_f \propto S$) and the flow parameter based on the burner conditions ($x_f \propto Pe_b$) and inversely proportional to the square root of the flow parameter based on the conditions imposed by impinging flows ($x_f \propto Pe_c^{-1/2}$), which is described grouped in proportionality to the parameter $N = \pi S Pe_b / (2 Pe_c^{-1/2})$, namely $x_f \propto N$.

7.1 Suggestions for future work

The first suggestion is to determine the flow field by solving the Navier-Stokes equations.

As widely discussed, the proposed model ignores the interaction between the flame and the flow field, i.e., between the temperature field and the velocity field. It is recommended for subsequent work to add this effect by implementing a method that takes into account compressibility at low Mach number (thermal compressibility).

It is also suggested the elaboration of a model that considers heat loss by radiation.

In addition, it is recommended to include chemical kinetics in order to study triple flame problems (when a part of the flame is extinguished and then a premixed flame is established interacting with the diffusive flame, with rich and lean areas) and the formation of soot due to the vast hot zone observed.

In conclusion, the flame tip should be studied in detail.

REFERENCES

- ARFKEN, G. B.; WEBER, H. J. **Mathematical methods for physicists**. 6. ed. Amsterdam, The Netherlands: Elsevier Academic, 2005. 28
- BIANCHIN, R. P.; DONINI, M. S.; CRISTALDO, C. F. C.; FACHINI, F. F. On the global structure and asymptotic stability of low-stretch diffusion flame: forced convection. **Proceedings of the Combustion Institute**, v. 37, n. 2, p. 1903–1910, 2019. 2, 10, 23
- BUCKMASTER, J.; LUDFORD, G. **Theory of Laminar Flames**. Cambridge: Cambridge University Press, 1982. 1, 9
- BURKE, S. P.; SCHUMANN, T. E. W. Diffusion flames. **Proceedings of the Symposium on Combustion**, v. 1-2, p. 2–11, 1948. 8
- CURRIE, I. G. **Fundamental mechanics of fluid**. 3. ed. New York: Marcel Dekker, 2003. 13
- DONINI, M. S.; BIANCHIN, R. P.; CRISTALDO, C. F. C.; FACHINI, F. F. **Numerical analysis of low stretch Tsuji flames driven by low buoyant force: global structure and flow field**. São Paulo: Instituto Nacional de Pesquisas Espaciais, 2018. Work in progress. 2, 11, 23
- HINDMARSH, A.; GRESHO, P.; GRIFFITHS, D. The stability of explicit euler time-integration for certain finite difference approximations of the multi-dimensional advection–diffusion equation. **International Journal for Numerical Methods in Fluids**, v. 4, n. 9, p. 853–897, 1984. 19
- HOUGHTON, E.; CARPENTER, P.; COLLICOTT, S. H.; VALENTINE, D. T. Chapter 3 - potential flow. In: HOUGHTON, E.; CARPENTER, P.; COLLICOTT, S. H.; VALENTINE, D. T. (Ed.). **Aerodynamics for engineering students**. 6. ed. Boston: Butterworth-Heinemann, 2013. p. 149 – 207. ISBN 978-0-08-096632-8. Available from: <<http://www.sciencedirect.com/science/article/pii/B9780080966328000035>>. 13
- INTERNATIONAL ENERGY AGENCY (IEA). **World: balances for 2016**. 2016. Available from: <<https://www.iea.org/statistics/>>. Access in: May 6, 2019. 7

- ISHIZUKA, S.; TSUJI, H. An experimental study of effect of inert gases on extinction of laminar diffusion flames. **Symposium (International) on Combustion**, v. 18, n. 1, p. 695–703, 1981. 1, 10
- LIÑÁN, A. The asymptotic structure of counterflow diffusion flames for large activation energies. **Acta Astronautica**, v. 1, n. 7-8, p. 1007–1039, 1974. 9
- _____. The structure of diffusion flames. In: ONOFRI, M.; TESEI, A. (Ed.). **Fluid dynamical aspects of combustion theory**. England: Longman Pub Group, 1991. p. 11–29. 8
- PETERS, N. Laminar diffusion flamelet models in non-premixed turbulent combustion. **Progress in Energy and Combustion Science**, v. 10, n. 3, p. 319–339, 1984. 9
- _____. Laminar flamelet concepts in turbulent combustion. **Symposium (International) on Combustion**, v. 21, n. 1, p. 1231–1250, 1988. 9
- QIAN, J.; LAW, C. K. On the spreading of unsteady cylindrical diffusion flames. **Combustion and Flame**, v. 110, n. 1-2, p. 152–162, 1997. 1, 9, 39, 42
- ROACHE, P. J. **Verification and validation in computational science and engineering**. New Mexico: Hermosa Pub, 1998. 33
- SLATER, J. W. **Examining spatial (grid) convergence**. 2008. Available from: <<https://www.grc.nasa.gov/WWW/wind/valid/tutorial/spatconv.html>>. Access in: Jan 27, 2020. 33
- TSUJI, H. Counterflow diffusion flames. **Progress in Energy and Combustion Science**, v. 8, n. 2, p. 93–119, 1982. 1, 10
- TSUJI, H.; YAMAOKA, I. The counterflow diffusion flame in the forward stagnation region of a porous cylinder. **Symposium (International) on Combustion**, v. 11, n. 1, p. 979–984, 1967. 1, 9, 10
- _____. The structure of counterflow diffusion flames in the forward stagnation region of a porous cylinder. **Symposium (International) on Combustion**, v. 12, n. 1, p. 997–1005, 1969. 1, 10
- _____. Structure analysis of counterflow diffusion flames in the forward stagnation region of a porous cylinder. **Symposium (International) on Combustion**, v. 13, n. 1, p. 723–731, 1971. 1, 10

TURNS, S. R. **Introdução à combustão: conceitos e aplicações**. 3. ed. Porto Alegre: AMGH, 2013. ISBN 9788580552744. 7

WILLIAMS, F. A. **Combustion Theory of Chemically Reacting Flow Systems**. Boston: Addison-Wesley, 1965. 8

YAMAOKA, I.; TSUJI, H. The structure of rich fuel-air flames in the forward stagnation region of a porous cylinder. **Symposium (International) on Combustion**, v. 15, n. 1, p. 637–644, 1975. 1, 10

_____. An experimental study of flammability limits using counterflow flames. **Symposium (International) on Combustion**, v. 17, n. 1, p. 843–855, 1979. 1, 10

_____. Structure and extinction of near-limit flames in a stagnation flow. **Symposium (International) on Combustion**, v. 19, n. 1, p. 1533–1540, 1982. 1, 10

_____. Determination of burning velocity using counterflow flames. **Symposium (International) on Combustion**, v. 20, n. 1, p. 1883–1892, 1985. 1, 10

_____. Extinction of near-stoichiometric flames diluted with nitrogen in a stagnation flow. **Symposium (International) on Combustion**, v. 22, n. 1, p. 1565–1572, 1989. 1, 10

YAMAOKA, I.; TSUJI, H.; HARIGAYA, Y. Extinction and structure of methane/very lean methane-air counterflow diffusion flames. **Symposium (International) on Combustion**, v. 21, n. 1, p. 1837–1843, 1988. 1, 10

ZELDOVICH, Y. B.; BARENBLATT, G. I.; LIBROVICH, V. B.; MAKHVILADZE, G. M. **The Mathematical theory of combustion and explosions**. New York: Consultants Bureau, 1985. ISBN 9780306109744. 7, 8

APPENDIX A - POTENTIAL FLOW

In this appendix the potential flow field is deduced.

The cylindrical burner in the middle of impinging flows, ejecting fuel, is represented by the superposition of a linear source, quadrupoles and impinging flows. The complex function that describes those flows is $w = Pe_c(z^2 + z^{-2})/2 + Pe_b \ln z$, in which:

$$Pe_b := \frac{\hat{t}_{c3}}{\hat{t}_{c1}} = \frac{\hat{R}^2/\hat{\alpha}}{\hat{R}/\hat{U}} = \frac{\hat{U}\hat{R}}{\hat{\alpha}} = \frac{\hat{U}}{\hat{\alpha}/\hat{R}} \quad (\text{A.1})$$

$$Pe_c := \frac{\hat{t}_{c3}}{\hat{t}_{c2}} = \frac{\hat{R}^2/\hat{\alpha}}{1/\hat{\alpha}} = \frac{\hat{\alpha}\hat{R}^2}{\hat{\alpha}} = \frac{\hat{\alpha}\hat{R}}{\hat{\alpha}/\hat{R}} \quad (\text{A.2})$$

with $\hat{\alpha}$ being the strain rate, \hat{U} , the fuel ejection speed, \hat{t}_{c3} , the diffusion time, \hat{t}_{c1} , the fuel residence time, \hat{t}_{c2} , the counter-flow time, \hat{R} , the radius of the burner and $\hat{\alpha}$, the thermal diffusivity. The Péclet number Pe_b is based on the burner conditions and the Péclet number Pe_c , on the flow field around the burner.

Therefore, the velocity potential and the streamline function for the combination of three velocity field are defined as

$$w = Pe_c^* (r^2 e^{i2\theta} + r^{-2} e^{-i2\theta}) + Pe_b \ln (r e^{i\theta})$$

with $Pe_c^* := Pe_c/2$.

$$w = Pe_c^* [r^2 (\cos 2\theta + i \sin 2\theta) + r^{-2} (\cos 2\theta - i \sin 2\theta)] + Pe_b (\ln r + i\theta)$$

The velocity potential is the real part of w ,

$$\begin{aligned} \phi &= Pe_c^* (r^2 + r^{-2}) \cos 2\theta + Pe_b \ln r \\ &= Pe_c^* (r^2 + r^{-2}) (\cos^2 \theta - \sin^2 \theta) + Pe_b \ln r \end{aligned}$$

The streamline function is the imaginary part of w ,

$$\begin{aligned}\psi &= Pe_c^*(r^2 - r^{-2})\sin 2\theta + Pe_b\theta \\ &= 2Pe_c^*(r^2 - r^{-2})\sin\theta \cos\theta + Pe_b\theta\end{aligned}$$

The components of the velocity in polar coordiante are

$$\begin{aligned}u_r &= \frac{\partial\phi}{\partial r} = \frac{\partial}{\partial r} \left[Pe_c^*(r^2 + r^{-2})(\cos^2\theta - \sin^2\theta) + Pe_b \ln r \right] \\ &= Pe_c^*(2r - 2r^{-3})(\cos^2\theta - \sin^2\theta) + \frac{Pe_b}{r} \\ &= 2Pe_c^*(r - r^{-3})(\cos^2\theta - \sin^2\theta) + \frac{Pe_b}{r}\end{aligned}$$

$$\begin{aligned}u_\theta &= \frac{1}{r} \frac{\partial\phi}{\partial\theta} = \frac{1}{r} \frac{\partial}{\partial\theta} \left[Pe_c^*(r^2 + r^{-2})(\cos^2\theta - \sin^2\theta) + Pe_b \ln r \right] \\ &= \frac{Pe_c^*}{r} (r^2 + r^{-2})(-2\cos\theta\sin\theta - 2\sin\theta\cos\theta) \\ &= -4Pe_c^*(r + r^{-3})\cos\theta \sin\theta\end{aligned}$$

Also, the velocity components can be determined from the streamline function,

$$\begin{aligned}u_r &= \frac{1}{r} \frac{\partial\psi}{\partial\theta} = \frac{1}{r} \frac{\partial}{\partial\theta} \left[2Pe_c^*(r^2 - r^{-2})\sin\theta \cos\theta + Pe_b\theta \right] \\ &= \frac{1}{r} \left[2Pe_c^*(r^2 - r^{-2})(\cos^2\theta - \sin^2\theta) + Pe_b \right] \\ &= 2Pe_c^*(r - r^{-3})(\cos^2\theta - \sin^2\theta) + \frac{Pe_b}{r}\end{aligned}$$

$$\begin{aligned}u_\theta &= -\frac{\partial\phi}{\partial r} = -\frac{\partial}{\partial r} \left[2Pe_c^*(r^2 - r^{-2})\sin\theta \cos\theta + Pe_b\theta \right] \\ &= -2Pe_c^*(2r + 2r^{-3})\sin\theta \cos\theta \\ &= -4Pe_c^*(r + r^{-3})\cos\theta \sin\theta\end{aligned}$$

The components of the velocity in x and y directions are

$$\begin{aligned}u &= u_r \cos\theta - u_\theta \cos(\pi/2 - \theta) = u_r \cos\theta - u_\theta \sin\theta \\ v &= u_r \sin\theta + u_\theta \sin(\pi/2 - \theta) = u_r \sin\theta + u_\theta \cos\theta\end{aligned}$$

$$\begin{aligned}
u &= u_r \cos\theta - u_\theta \sin\theta \\
&= \left[2Pe_c^*(r - r^{-3})(\cos^2\theta - \sin^2\theta) + \frac{Pe_b}{r} \right] \cos\theta - \\
&\quad \left[-4Pe_c^*(r + r^{-3})\cos\theta \sin\theta \right] \sin\theta \\
&= 2Pe_c^*(r - r^{-3})(\cos^3\theta - \sin^2\theta \cos\theta) + \frac{Pe_b \cos\theta}{r} + \\
&\quad 4Pe_c^*(r + r^{-3})\sin^2\theta \cos\theta \\
&= 2Pe_c^*(r - r^{-3})\cos^3\theta + \frac{Pe_b \cos\theta}{r} + \\
&\quad 2Pe_c^*[2(r + r^{-3}) - (r - r^{-3})]\sin^2\theta \cos\theta \\
&= 2Pe_c^*(r - r^{-3})\cos^3\theta + \frac{Pe_b \cos\theta}{r} + 2Pe_c^*(r + 3r^{-3})\sin^2\theta \cos\theta \\
&= 2Pe_c^*r(\cos^2\theta + \sin^2\theta)\cos\theta + 2Pe_c^*r^{-3}(-\cos^2\theta + 3\sin^2\theta)\cos\theta + \frac{Pe_b \cos\theta}{r} \\
&= 2Pe_c^*r\cos\theta - 2Pe_c^*r^{-3}(\cos^2\theta - 3\sin^2\theta)\cos\theta + \frac{Pe_b \cos\theta}{r} \\
&= 2Pe_c^*x - \frac{2Pe_c^*}{(x^2 + y^2)^{3/2}} \left(\frac{x^2}{x^2 + y^2} - \frac{3y^2}{x^2 + y^2} \right) \frac{x}{\sqrt{x^2 + y^2}} + \frac{Pe_b x}{x^2 + y^2} \\
&= 2Pe_c^*x - 2Pe_c^* \left(\frac{x^2 - 3y^2}{x^2 + y^2} \right) \frac{x}{(x^2 + y^2)^2} + \frac{Pe_b x}{x^2 + y^2} \\
&= 2Pe_c^*x - 2Pe_c^* \frac{x(x^2 - 3y^2)}{(x^2 + y^2)^3} + \frac{Pe_b x}{x^2 + y^2}
\end{aligned}$$

By definition, $Pe_c^* = Pe_c/2$

$$u = Pe_c \left[x - \frac{x(x^2 - 3y^2)}{(x^2 + y^2)^3} \right] + Pe_b \frac{x}{x^2 + y^2}$$

$$\begin{aligned}
v &= u_r \sin\theta + u_\theta \cos\theta \\
&= \left[2Pe_c^*(r - r^{-3})(\cos^2\theta - \sin^2\theta) + \frac{Pe_b}{r} \right] \sin\theta + \\
&\quad \left[-4Pe_c^*(r + r^{-3})\cos\theta \sin\theta \right] \cos\theta \\
&= 2Pe_c^*(r - r^{-3})(\cos^2\theta \sin\theta - \sin^3\theta) + \frac{Pe_b \sin\theta}{r} - \\
&\quad 4Pe_c^*(r + r^{-3})\cos^2\theta \sin\theta \\
&= -2Pe_c^*(r - r^{-3})\sin^3\theta + \frac{Pe_b \sin\theta}{r} + \\
&\quad 2Pe_c^*[-2(r + r^{-3}) + (r - r^{-3})]\cos^2\theta \sin\theta \\
&= -2Pe_c^*(r - r^{-3})\sin^3\theta + \frac{Pe_b \sin\theta}{r} - 2Pe_c^*(r + 3r^{-3})\cos^2\theta \sin\theta \\
&= -2Pe_c^*r(\sin^2\theta + \cos^2\theta)\sin\theta + 2Pe_c^*r^{-3}(\sin^2\theta - 3\cos^2\theta)\sin\theta + \frac{Pe_b \sin\theta}{r} \\
&= -2Pe_c^*r\sin\theta + 2Pe_c^*r^{-3}(\sin^2\theta - 3\cos^2\theta)\sin\theta + \frac{Pe_b \sin\theta}{r} \\
&= -2Pe_c^*y + \frac{2Pe_c^*}{(x^2 + y^2)^{3/2}} \frac{y^2 - 3x^2}{(x^2 + y^2)} \frac{y}{(x^2 + y^2)^{1/2}} + \frac{Pe_b y}{(x^2 + y^2)} \\
&= -2Pe_c^*y - 2Pe_c^* \frac{3x^2 - y^2}{(x^2 + y^2)^{3/2}} \frac{y}{(x^2 + y^2)^{3/2}} + \frac{Pe_b y}{(x^2 + y^2)} \\
&= -2Pe_c^*y - 2Pe_c^* \frac{y(3x^2 - y^2)}{(x^2 + y^2)^3} + \frac{Pe_b y}{(x^2 + y^2)}
\end{aligned}$$

$$v = Pe_c \left[-y - \frac{y(3x^2 - y^2)}{(x^2 + y^2)^3} \right] + Pe_b \frac{y}{(x^2 + y^2)}$$

$$u = Pe_c x - \frac{Pe_c x(x^2 - 3y^2)}{(x^2 + y^2)^3} + \frac{Pe_b x}{x^2 + y^2} \quad (\text{A.3})$$

$$v = -Pe_c y - \frac{Pe_c y(3x^2 - y^2)}{(x^2 + y^2)^3} + \frac{Pe_b y}{x^2 + y^2} \quad (\text{A.4})$$

in which the flow field is given by the superposition of a potential counterflow ($\vec{v} = \hat{a}\vec{r}$, in which a is the strain rate), quadrupoles and a line source ($\vec{v} = u_b R \vec{r} / |\vec{r}|^2$, in which \hat{u}_b is the velocity of the fluid leaving the burner and \hat{R} is its radius) representing the cylinder, i.e.,

$$\hat{u} = \hat{a}\hat{x} - \frac{\hat{a}\hat{R}^4\hat{x}(\hat{x}^2 - 3\hat{y}^2)}{(\hat{x}^2 + \hat{y}^2)^3} + \frac{\hat{u}_b\hat{R}\hat{x}}{\hat{x}^2 + \hat{y}^2} \quad (\text{A.5})$$

$$\hat{v} = -\hat{a}\hat{y} - \frac{\hat{a}\hat{R}^4\hat{y}(3\hat{x}^2 - \hat{y}^2)}{(\hat{x}^2 + \hat{y}^2)^3} + \frac{\hat{u}_b\hat{R}\hat{y}}{\hat{x}^2 + \hat{y}^2} \quad (\text{A.6})$$

APPENDIX B - DETAILED FORMULATION

In this appendix the formulation is detailed.

B.1 Dimensionless Equations

The hat variables indicates the dimensional form of them or, in case of inherent dimensionless variables, it indicates non-normalized form, like for mass fraction of the species.

The fundamental equations are:

$$\partial_t \hat{\rho} + \hat{\nabla} \cdot \hat{\rho} \hat{\mathbf{v}} = 0 \quad (\text{B.1.1})$$

$$\partial_i \hat{\rho} \hat{v}_i + \hat{\nabla} \cdot \hat{\rho} \hat{\mathbf{v}} \hat{\mathbf{v}} = -\hat{\nabla} \hat{P} + \hat{\nabla} \cdot \hat{\mathbf{\Gamma}} + \sum_k \hat{\rho} \hat{\mathbf{f}}_k \quad (\text{B.1.2})$$

$$\partial_i \hat{\rho} \hat{Y}_n + \hat{\nabla} \cdot \hat{\rho} \hat{\mathbf{v}} \hat{Y}_n = \hat{\nabla} \cdot \hat{\rho} \hat{D}_n \hat{\nabla} \hat{Y}_n - \hat{s}_n \hat{\rho} \hat{\omega} \quad (\text{B.1.3})$$

$$\partial_i \hat{\rho} \hat{h} + \hat{\nabla} \cdot \hat{\rho} \hat{\mathbf{v}} \hat{h} = \partial_i \hat{P} + \hat{\mathbf{v}} \cdot \hat{\nabla} \hat{P} + \hat{\nabla} \hat{\mathbf{v}} : \hat{\mathbf{\Gamma}} + \hat{\nabla} \cdot \hat{\mathbf{Q}}_T + \hat{Q} \hat{\rho} \hat{\omega} \quad (\text{B.1.4})$$

in which

$$\hat{\mathbf{Q}}_T := \hat{k} \hat{\nabla} \hat{T} + \sum_n \hat{\rho} \hat{D}_n \hat{\nabla} \hat{Y}_n \hat{h}_n$$

Considering the dimensionless independent variables:

$$t = \frac{\hat{t}}{\hat{t}_c}, \quad x_i = \frac{\hat{x}_i}{\hat{l}_c},$$

In which t is time and x_i is the i^{th} spatial coordinate and the subscript "c" indicates characteristics scales.

In addition, considering the dimensionless dependent variables:

$$\rho = \frac{\hat{\rho}}{\hat{\rho}_c}, \quad Y_n = \frac{\hat{Y}_n}{\hat{Y}_{nc}}, \quad T = \frac{\hat{T}}{\hat{T}_c}, \quad P = \frac{\hat{P}}{\hat{P}_c}, \quad \mathbf{v} = \frac{\hat{\mathbf{v}}}{\hat{v}_c}, \quad h = \frac{\hat{h}}{\hat{h}_c}$$

In which ρ is density, Y_n , specie n mass fraction, T , temperature, P , pressure, \mathbf{v} , velocity, h , enthalpy.

And, even, considering the dimensionless parameters:

$$D_n = \frac{\hat{D}_n}{\hat{D}_{n_c}}, \quad \mu = \frac{\hat{\mu}}{\hat{\mu}_c}, \quad \alpha = \frac{\hat{\alpha}}{\hat{\alpha}_c}, \quad k = \frac{\hat{k}}{\hat{k}_c}$$

In which D_n is mass diffusivity, μ , viscosity, α , thermal diffusivity and k is thermal conductivity.

Thus the relations between dimensional and dimensionless operators are:

$$\begin{aligned} \partial_{\hat{t}} &= \frac{\partial}{\partial \hat{t}} = \frac{\partial}{\partial t} \frac{\partial t}{\partial \hat{t}} = \frac{1}{\hat{t}_c} \frac{\partial}{\partial t} = \frac{1}{\hat{t}_c} \partial_t \\ \hat{\nabla} &= \frac{\partial}{\partial \hat{x}_i} \mathbf{e}_i = \frac{\partial}{\partial x_i} \frac{\partial x_i}{\partial \hat{x}_i} \mathbf{e}_i = \frac{1}{\hat{l}_c} \frac{\partial}{\partial x_i} \mathbf{e}_i = \frac{1}{\hat{l}_c} \nabla \\ \hat{\Gamma} &= \hat{\mu} \hat{\nabla} \hat{\mathbf{v}} = \hat{\mu} \frac{\partial \hat{v}_j}{\partial \hat{x}_i} \mathbf{e}_i \mathbf{e}_j = \hat{\mu}_c \frac{\hat{\mu}}{\hat{\mu}_c} \frac{\partial}{\partial x_i} \frac{\partial x_i}{\partial \hat{x}_i} (\hat{v}_c v_j) \mathbf{e}_i \mathbf{e}_j = \frac{\hat{\mu}_c \hat{v}_c}{\hat{l}_c} \mu \frac{\partial v_j}{\partial x_i} \mathbf{e}_i \mathbf{e}_j = \frac{\hat{\mu}_c \hat{v}_c}{\hat{l}_c} \mu \nabla \mathbf{v} = \frac{\hat{\mu}_c \hat{v}_c}{\hat{l}_c} \mathbf{\Gamma} \end{aligned}$$

Using these definitions and their consequences in the dimensional equations:

For the mass balance equation (Equation B.1.1):

$$\begin{aligned} \frac{\hat{\rho}_c}{\hat{t}_c} \partial_t \rho + \frac{\hat{\rho}_c \hat{v}_c}{\hat{l}_c} \nabla \cdot \rho \mathbf{v} &= 0 \\ \implies \frac{\hat{l}_c / \hat{v}_c}{\hat{t}_c} \partial_t \rho + \nabla \cdot \rho \mathbf{v} &= 0 \end{aligned}$$

The Strouhal number is the residence and characteristic times ratio, defined by $S_t := (\hat{l}_c / \hat{v}_c) / \hat{t}_c = \hat{t}_{res} / \hat{t}_c$, then:

$$S_t \partial_t \rho + \nabla \cdot \rho \mathbf{v} = 0 \quad (\text{B.1.5})$$

For the momentum balance equation (Equation B.1.2):

$$\frac{\hat{\rho}_c \hat{v}_c}{\hat{t}_c} \partial_t \rho \mathbf{v} + \frac{\hat{\rho}_c \hat{v}_c^2}{\hat{l}_c} \nabla \cdot \rho \mathbf{v} \mathbf{v} = -\frac{\hat{P}_c}{\hat{l}_c} \nabla P + \frac{\hat{\mu}_c \hat{v}_c}{\hat{l}_c^2} \nabla \cdot \mathbf{\Gamma} + \hat{\rho}_c \sum_k \rho \hat{\mathbf{f}}_k$$

$$\implies \frac{\hat{l}_c/\hat{v}_c}{\hat{t}_c} \partial_t \rho \mathbf{v} + \nabla \cdot \rho \mathbf{v} \mathbf{v} = -\frac{\hat{P}_c}{\hat{\rho}_c \hat{v}_c^2} \nabla P + \frac{\hat{\mu}_c/\hat{\rho}_c}{\hat{l}_c \hat{v}_c} \nabla \cdot \mathbf{\Gamma} + \frac{\hat{l}_c \hat{\rho}_c}{\hat{\rho}_c \hat{v}_c^2} \sum_k \rho \hat{\mathbf{f}}_k$$

Considering the constitutive equation ($\hat{P}_c = \hat{\rho}_c \hat{r}_0 \hat{T}_c$) and, since the Mach number $Ma := \hat{v}_c / \sqrt{\gamma \hat{r}_0 \hat{T}_c}$, note that: $\hat{P}_c / (\hat{\rho}_c \hat{v}_c^2) = \hat{\rho}_c \hat{r}_0 \hat{T}_c / (\hat{\rho}_c \hat{v}_c^2) = \gamma \hat{r}_0 \hat{T}_c / (\gamma \hat{v}_c^2) = 1 / (\gamma M^2)$, in which \hat{r}_0 is the universal gas constant and γ is the ratio of specific heat of a gas at a constant pressure to heat at a constant volume. Furthermore the Reynolds number, the inertial and viscous forces ratio, is defined by $Re := \hat{l}_c \hat{v}_c / (\hat{\mu}_c / \hat{\rho}_c) = \hat{l}_c \hat{v}_c / \hat{\nu}_c$, in which ν is kinematic viscosity ($\nu := \mu / \rho$). Then,

$$S_t \partial_t \rho \mathbf{v} + \nabla \cdot \rho \mathbf{v} \mathbf{v} = -\frac{1}{\gamma M^2} \nabla P + \frac{1}{Re} \nabla \cdot \mathbf{\Gamma} + \sum_k \rho \mathbf{f}_k \quad (\text{B.1.6})$$

with $\mathbf{f}_k = (\hat{l}_c / \hat{v}_c^2) \hat{\mathbf{f}}_k$.

For the mass balance equation of the chemical species (Equation B.1.3):

$$\begin{aligned} \frac{\hat{\rho}_c \hat{Y}_{n_c}}{\hat{t}_c} \partial_t \rho Y_n + \frac{\hat{\rho}_c \hat{v}_c \hat{Y}_{n_c}}{\hat{l}_c} \nabla \cdot \rho \mathbf{v} Y_n &= \frac{\hat{\rho}_c \hat{D}_{n_c} \hat{Y}_{n_c}}{\hat{l}_c^2} \nabla \cdot \rho D_n \nabla Y_n - \frac{\hat{l}_c \hat{\rho}_c}{\hat{\rho}_c \hat{v}_c \hat{Y}_{n_c}} \hat{s}_n \rho \hat{\omega} \\ \implies \frac{\hat{l}_c / \hat{v}_c}{\hat{T}_c} \partial_t \rho Y_n + \nabla \cdot \rho \mathbf{v} Y_n &= \frac{\hat{\alpha}_c \hat{D}_{n_c}}{\hat{\alpha}_c \hat{l}_c \hat{v}_c} \nabla \cdot \rho D_n \nabla Y_n - \frac{\hat{Y}_{F_c}}{\hat{Y}_{n_c}} \hat{s}_n \rho \hat{\omega} \frac{\hat{l}_c}{\hat{v}_c \hat{Y}_{F_c}} \end{aligned}$$

Peclet number and the Lewis number are defined by $Pe := \hat{l}_c \hat{v}_c / \hat{\alpha}_c$ and $Le_n := \hat{\alpha}_c / \hat{D}_{n_c}$, respectively, thus:

$$S_t \partial_t \rho Y_n + \nabla \cdot \rho \mathbf{v} Y_n = \frac{1}{Pe Le_n} \nabla \cdot \rho D_n \nabla Y_n - s_n \rho \omega \quad (\text{B.1.7})$$

with $s_n := (\hat{Y}_{F_c} / \hat{Y}_{n_c}) \hat{s}_n$ and

$$\omega := \frac{\hat{l}_c}{\hat{v}_c \hat{Y}_{F_c}} \hat{\omega} = \frac{\hat{l}_c B \hat{Y}_{F_c} \hat{Y}_{O_c}}{\hat{v}_c \hat{Y}_{F_c}} Y_F Y_O e^{-\beta/T} = \frac{\hat{l}_c B \hat{Y}_{O_c}}{\hat{v}_c} Y_F Y_O e^{-\beta/T} = Da Y_F Y_O e^{-\beta/T}$$

In which B is a pre-exponential factor. Ergo,

$$\omega := Da Y_F Y_O e^{-\beta/T}$$

with Da being Damköhler number:

$$Da := (\hat{l}_c B Y_{O_c}) / \hat{v}_c$$

For the thermal enthalpy balance equation (Equation B.1.4):

$$\begin{aligned} \frac{\hat{\rho}_c \hat{h}_c}{\hat{t}_c} \partial_t \rho h + \frac{\hat{\rho}_c \hat{v}_c \hat{h}_c}{\hat{l}_c} \nabla \cdot \rho \mathbf{v} h &= \frac{\hat{P}_c}{\hat{t}_c} \partial_t P + \frac{\hat{v}_c \hat{P}_c}{\hat{l}_c} \mathbf{v} \cdot \nabla P + \frac{\hat{\mu}_c \hat{v}_c^2}{\hat{l}_c^2} \nabla \mathbf{v} : \mathbf{\Gamma} + \\ &\frac{\hat{k}_c \hat{T}_c}{\hat{l}_c^2} \nabla \cdot k \nabla T + \frac{\hat{\rho}_c}{\hat{l}_c^2} \sum_n (\hat{D}_{n_c} \hat{Y}_{n_c} \hat{h}_c) \nabla \cdot \rho D_n \nabla Y_n h + \hat{\rho}_c \hat{Q} \rho \hat{\omega} \\ \implies \frac{\hat{l}_c}{\hat{\rho}_c \hat{v}_c \hat{h}_c} \frac{\hat{\rho}_c \hat{h}_c}{\hat{t}_c} \partial_t \rho h + \frac{\hat{l}_c}{\hat{\rho}_c \hat{v}_c \hat{h}_c} \frac{\hat{\rho}_c \hat{v}_c \hat{h}_c}{\hat{l}_c} \nabla \cdot \rho \mathbf{v} h &= \frac{\hat{l}_c}{\hat{\rho}_c \hat{v}_c \hat{h}_c} \frac{\hat{P}_c}{\hat{t}_c} \partial_t P + \frac{\hat{l}_c}{\hat{\rho}_c \hat{v}_c \hat{h}_c} \frac{\hat{v}_c \hat{P}_c}{\hat{l}_c} \mathbf{v} \cdot \nabla P \\ + \frac{\hat{l}_c}{\hat{\rho}_c \hat{v}_c \hat{h}_c} \frac{\hat{\mu}_c \hat{v}_c^2}{\hat{l}_c^2} \nabla \mathbf{v} : \mathbf{\Gamma} + \frac{\hat{l}_c}{\hat{\rho}_c \hat{v}_c \hat{h}_c} \frac{\hat{k}_c \hat{T}_c}{\hat{l}_c^2} \nabla \cdot k \nabla T &+ \frac{\hat{l}_c}{\hat{\rho}_c \hat{v}_c \hat{h}_c} \frac{\hat{\rho}_c}{\hat{l}_c^2} \sum_n (\hat{D}_{n_c} \hat{Y}_{n_c} \hat{h}_c) \nabla \cdot \rho D_n \nabla Y_n h \\ &+ \frac{\hat{l}_c}{\hat{\rho}_c \hat{v}_c \hat{h}_c} \hat{Q} \rho \hat{\omega} \frac{\hat{\rho}_c \hat{Y}_{F_c}}{\hat{Y}_{F_c}} \\ \implies \frac{\hat{l}_c / \hat{v}_c}{\hat{t}_c} \partial_t \rho h + \nabla \cdot \rho \mathbf{v} h &= \frac{\hat{l}_c \hat{P}_c}{\hat{\rho}_c \hat{v}_c \hat{h}_c \hat{t}_c} \partial_t P + \frac{\hat{P}_c}{\hat{\rho}_c \hat{h}_c} \mathbf{v} \cdot \nabla P + \frac{\hat{\mu}_c \hat{v}_c^2}{\hat{\rho}_c \hat{v}_c \hat{h}_c \hat{l}_c} \nabla \mathbf{v} : \mathbf{\Gamma} + \\ + \frac{\hat{k}_c \hat{T}_c}{\hat{l}_c \hat{\rho}_c \hat{v}_c \hat{h}_c} \nabla \cdot k \nabla T + \frac{1}{\hat{l}_c \hat{v}_c \hat{h}_c} \sum_n (\hat{D}_{n_c} \hat{Y}_{n_c} \hat{h}_c) \nabla \cdot \rho D_n \nabla Y_n h &+ \frac{\hat{Y}_{F_c}}{\hat{h}_c} \hat{Q} \rho \hat{\omega} \frac{\hat{l}_c}{\hat{v}_c \hat{Y}_{F_c}} \end{aligned}$$

Considering $\hat{h}_c = \hat{c}_p \hat{T}_c$, $\hat{r}_0 = \hat{c}_p - \hat{c}_v$, $\gamma := \hat{c}_p / \hat{c}_v$, in which c_p is specific heat at constant pressure and \hat{c}_v , specific heat at constant volume. Moreover, using the constitutive equation for an ideal gas:

$$\frac{\hat{P}_c}{\hat{\rho}_c \hat{h}_c} = \frac{\hat{\rho}_c \hat{r}_0 \hat{T}_c}{\hat{\rho}_c \hat{c}_p \hat{T}_c} = \frac{\hat{r}_0}{\hat{c}_p} = \frac{\hat{c}_p - \hat{c}_v}{\hat{c}_p} = 1 - \frac{\hat{c}_v}{\hat{c}_p} = 1 - \frac{1}{\gamma} = \frac{\gamma - 1}{\gamma}$$

$$\frac{\hat{l}_c \hat{P}_c}{\hat{\rho}_c \hat{v}_c \hat{h}_c \hat{t}_c} = \frac{\hat{P}_c}{\hat{\rho}_c \hat{h}_c} \frac{\hat{l}_c / \hat{v}_c}{\hat{t}_c} = \frac{\gamma - 1}{\gamma} S_t$$

$$\frac{\hat{\mu}_c \hat{v}_c^2}{\hat{\rho}_c \hat{v}_c \hat{h}_c \hat{l}_c} = \frac{\hat{\mu}_c}{\hat{\rho}_c \hat{v}_c \hat{l}_c} \frac{\hat{v}_c^2}{\hat{h}_c} = \frac{\nu_c}{\hat{v}_c \hat{l}_c} \frac{\hat{v}_c^2}{\hat{c}_p \hat{T}_c} = \frac{1}{Re} \frac{\hat{v}_c^2}{\hat{c}_p \hat{T}_c} \frac{\gamma \hat{r}_0}{\gamma \hat{r}_0} = \frac{1}{Re} \frac{\hat{v}_c^2}{\gamma \hat{r}_0 \hat{T}_c} \frac{\gamma \hat{r}_0}{\hat{c}_p} = \frac{1}{Re} M^2 \gamma \frac{\gamma - 1}{\gamma} = \frac{1}{Re} M^2 (\gamma - 1)$$

$$\frac{\hat{k}_c \hat{T}_c}{\hat{l}_c \hat{\rho}_c \hat{v}_c \hat{h}_c} = \frac{\hat{k}_c \hat{T}_c}{\hat{l}_c \hat{\rho}_c \hat{v}_c \hat{c}_p \hat{T}_c} = \frac{\hat{k}_c}{\hat{\rho}_c \hat{c}_p \hat{l}_c \hat{v}_c} = \frac{\hat{\alpha}_c}{\hat{l}_c \hat{v}_c} = \frac{1}{Pe}$$

$$\frac{1}{\hat{l}_c \hat{v}_c \hat{h}_c} \sum_n (\hat{D}_{n_c} \hat{Y}_{n_c} \hat{h}_c) = \frac{\hat{\alpha}_c}{\hat{\alpha}_c \hat{l}_c \hat{v}_c \hat{h}_c} \sum_n (\hat{D}_{n_c} \hat{Y}_{n_c} \hat{h}_c) = \frac{\hat{\alpha}_c}{\hat{l}_c \hat{v}_c \hat{h}_c} \sum_n \frac{\hat{D}_{n_c}}{\hat{\alpha}_c} = \frac{1}{Pe} \sum_n \frac{1}{Le_n}$$

Thus

$$\begin{aligned} S_t \partial_t \rho h + \nabla \cdot \rho \mathbf{v} h &= \frac{\gamma - 1}{\gamma} S_t \partial_t P + \frac{\gamma - 1}{\gamma} \mathbf{v} \cdot \nabla P + \frac{1}{Re} (\gamma - 1) M^2 \nabla \mathbf{v} : \mathbf{\Gamma} \\ &+ \frac{1}{Pe} \nabla \cdot k \nabla T + \frac{1}{Pe} \sum_n \frac{1}{Le_n} \nabla \cdot \rho D_n \nabla Y_n h_n + Q \rho \omega \end{aligned} \quad (\text{B.1.8})$$

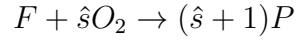
with $Q := \frac{\hat{Y}_{F_c}}{\hat{h}_c} \hat{Q}$ and ω already defined.

B.2 Mixture Fraction (Z) and Excess Enthalpy (H)

In the possession of these results, the equations for the mixture fraction and the excess enthalpy can be deduced.

It is worth to mention that the dependency of D_F , D_O , α on temperature is assumed to be the same ($D_F = D_O = \alpha$).

Considering only the one-step irreversible, infinitely fast reaction:



In which \hat{s} is the mass stoichiometric coefficient.

The chemical reactants species are only fuel, F, and oxidant, O, and the dimensionless mass balance equation of the chemical species are given by Equation (B.1.7):

$$S_t \partial_t \rho Y_F + \nabla \cdot \rho \mathbf{v} Y_F = \frac{1}{PeLe_F} \nabla \cdot \rho \alpha \nabla Y_F - s_F \rho \omega$$

$$S_t \partial_t \rho Y_O + \nabla \cdot \rho \mathbf{v} Y_O = \frac{1}{PeLe_O} \nabla \cdot \rho \alpha \nabla Y_O - s_O \rho \omega$$

But, $s_n := \frac{\hat{Y}_{F_c}}{\hat{Y}_{n_c}} \hat{s}_n$, then

- For fuel: $s_F := \frac{\hat{Y}_{F_c}}{\hat{Y}_{F_c}} = 1$
- For oxidant: $s_O := \frac{\hat{Y}_{F_c}}{\hat{Y}_{O_c}} \hat{s}$

Defining $s_O := S$,

$$S_t \partial_t \rho Y_F + \nabla \cdot \rho \mathbf{v} Y_F = \frac{1}{PeLe_F} \nabla \cdot \rho \alpha \nabla Y_F - \rho \omega \quad (\text{B.2.1})$$

$$S_t \partial_t \rho Y_O + \nabla \cdot \rho \mathbf{v} Y_O = \frac{1}{PeLe_O} \nabla \cdot \rho \alpha \nabla Y_O - S \rho \omega \quad (\text{B.2.2})$$

Multiplying Equation (B.2.1) by S and Equation (B.2.2) by (-1) :

$$S_t \partial_t \rho(SY_F) + \nabla \cdot \rho \mathbf{v}(SY_F) = \frac{1}{Pe Le_F} \nabla \cdot \rho \alpha \nabla(SY_F) - S \rho \omega$$

$$S_t \partial_t \rho(-Y_O) + \nabla \cdot \rho \mathbf{v}(-Y_O) = \frac{1}{Pe Le_O} \nabla \cdot \rho \alpha \nabla(-Y_O) + S \rho \omega$$

Adding the last two equations:

$$S_t \partial_t \rho(SY_F - Y_O) + \nabla \cdot \rho \mathbf{v}(SY_F - Y_O) = \frac{1}{Pe} \nabla \cdot \rho \alpha \nabla \left[\frac{SY_F}{Le_F} - \frac{Y_O}{Le_O} \right]$$

Which is the same that, using Equation (B.1.5):

$$S_t \partial_t \rho(SY_F - Y_O + 1) + \nabla \cdot \rho \mathbf{v}(SY_F - Y_O + 1) = \frac{1}{Pe} \nabla \cdot \rho \alpha \nabla \left[\frac{SY_F}{Le_F} - \frac{Y_O}{Le_O} \right]$$

Or,

$$S_t \partial_t \rho(SY_F - Y_O + 1) + \nabla \cdot \rho \mathbf{v}(SY_F - Y_O + 1) = \frac{1}{Pe} \nabla \cdot \rho \alpha \nabla \left(\frac{SY_F}{Le_F} - \frac{Y_O}{Le_O} + 1 \right)$$

The new variable, $SY_F - Y_O + 1$, is set as the mixture fraction Z , that is $Z := SY_F - Y_O + 1$. It is also defined the modified mixture fraction $\tilde{Z} := (SY_F/Le_F) - (Y_O/Le_O) + 1$.

$$S_t \partial_t \rho Z + \nabla \cdot \rho \mathbf{v} Z = \frac{1}{Pe} \nabla \cdot \rho \alpha \nabla \tilde{Z} \quad (\text{B.2.3})$$

In the particular case that $Le_F = Le_O = 1$, one has $\tilde{Z} = Z$.

The simplify dimensionless thermal enthalpy balance equation is given by Equation (B.1.8), disregarding the pressure and concentration contributions and by consideration that $k = \hat{k}/\hat{k}_c = (\hat{\alpha}_c \hat{c}_p \hat{\rho})/(\hat{\alpha}_c \hat{c}_p \hat{\rho}_c) = \rho\alpha$:

$$S_t \partial_t \rho h + \nabla \cdot \rho \mathbf{v} h = \frac{1}{Pe} \nabla \cdot \rho \alpha \nabla T + Q \rho \omega \quad (\text{B.2.4})$$

Multiplying Equation (B.2.4) by $\frac{(S+1)}{Q}$:

$$\frac{(S+1)}{Q} S_t \partial_t \rho h + \frac{(S+1)}{Q} \nabla \cdot \rho \mathbf{v} h = \frac{(S+1)}{Q} \frac{1}{Pe} \nabla \cdot \rho \alpha \nabla T + \frac{(S+1)}{Q} Q \rho \omega$$

Since $h = \hat{h}/\hat{h}_c = (\hat{c}_p \hat{T})/(\hat{c}_p \hat{T}_c) = \hat{T}/\hat{T}_c = T$, then:

$$\frac{(S+1)}{Q} S_t \partial_t \rho T + \frac{(S+1)}{Q} \nabla \cdot \rho \mathbf{v} T = \frac{(S+1)}{Q} \frac{1}{Pe} \nabla \cdot \rho \alpha \nabla T + (S+1) \rho \omega$$

Or,

$$S_t \partial_t \rho S_H T + \nabla \cdot \rho \mathbf{v} S_H T = \frac{1}{Pe} \nabla \cdot \rho \alpha \nabla S_H T + (S+1) \rho \omega \quad (\text{B.2.5})$$

in which

$$S_H := \frac{S+1}{Q}$$

Adding Equation (B.2.1) and Equation (B.2.2) to Equation (B.2.5):

$$S_t \partial_t \rho (S_H T + Y_F + Y_O) + \nabla \cdot \rho \mathbf{v} (S_H T + Y_F + Y_O) = \frac{1}{Pe} \nabla \cdot \rho \alpha \nabla \left[S_H T + \frac{Y_F}{Le_F} + \frac{Y_O}{Le_O} \right] \quad (\text{B.2.6})$$

The new variable, $S_H T + Y_F + Y_O$, is set as the enthalpy excess H , that is

$$H := S_H T + Y_F + Y_O$$

It also is set the modified enthalpy excess (\tilde{H}) as

$$\tilde{H} := S_H T + \frac{Y_F}{Le_F} + \frac{Y_O}{Le_O}$$

From these definitions, Equation (B.2.6) becomes:

$$S_t \partial_t \rho H + \nabla \cdot \rho \mathbf{v} H = \frac{1}{Pe} \nabla \cdot \rho \alpha \nabla \tilde{H} \quad (\text{B.2.7})$$

In the particular case that $Le_F = Le_O = 1$, one has $\tilde{H} = H$.

Therefore, the set of equations that describe the dynamics of diffusion flame is given by Equation (B.1.5), Equation (B.1.6) Equation (B.2.3) and Equation (B.2.7):

$$S_t \partial_t \rho + \nabla \cdot \rho \mathbf{v} = 0$$

$$S_t \partial_t \rho \mathbf{v} + \nabla \cdot \rho \mathbf{v} \mathbf{v} = -\frac{1}{\gamma M^2} \nabla P + \frac{1}{Re} \nabla \cdot \mathbf{\Gamma} + \sum_k \rho \mathbf{f}_k$$

$$S_t \partial_t \rho Z + \nabla \cdot \rho \mathbf{v} Z = \frac{1}{Pe} \nabla \cdot \rho \alpha \nabla \tilde{Z}$$

$$S_t \partial_t \rho H + \nabla \cdot \rho \mathbf{v} H = \frac{1}{Pe} \nabla \cdot \rho \alpha \nabla \tilde{H}$$

APPENDIX C - DETAILED FORMULATION OF TRANSITION PROBLEM

In this appendix the transition from transient, one-dimensional regime to stationary, two-dimensional regime formulation is detailed.

Description when injection and counter-flow velocities have the same magnitude order, for small Pe_c . It can be interpreted as the threshold between steady-state 2-D and transient 1-D states.

For small ε :

$$Pe_c = \varepsilon Pe_c^{(1)} \quad (C.1)$$

Considering velocity expression given by (3.4.3):

$$\begin{aligned} u &= Pe_c x - \frac{Pe_c x(x^2 - 3y^2)}{(x^2 + y^2)^3} + \frac{Pe_b x}{x^2 + y^2} \\ v &= -Pe_c y - \frac{Pe_c y(3x^2 - y^2)}{(x^2 + y^2)^3} + \frac{Pe_b y}{x^2 + y^2} \end{aligned}$$

The analysis studies the behavior of the flame far from the burner in which the flow field imposed by the counterflow is of the same order of magnitude of flow field imposed by the fuel injection. The condition of the counterflow is such that $Pe_c \ll 1$, i.e. $Pe_c = \varepsilon Pe_c^{(1)}$, with $\varepsilon \ll 1$ and $Pe_c^{(1)} = O(1)$. The region of the space determined by $x^2 + y^2 = 1/\varepsilon$ is chosen. Then the proper variables to analyze the proposed problem are $\tilde{x} = \sqrt{\varepsilon}x$ and $\tilde{y} = \sqrt{\varepsilon}y$ and the flow field is described by

$$\begin{aligned} u &= \varepsilon Pe_c^{(1)} \tilde{x} / \sqrt{\varepsilon} - \frac{\varepsilon Pe_c^{(1)} \tilde{x}(\tilde{x}^2 - 3\tilde{y}^2) / \varepsilon^{3/2}}{(\tilde{x}^2 + \tilde{y}^2)^3 / \varepsilon^3} + \frac{Pe_b \tilde{x} / \sqrt{\varepsilon}}{(\tilde{x}^2 + \tilde{y}^2) / \varepsilon} \\ v &= -\varepsilon Pe_c^{(1)} \tilde{y} / \sqrt{\varepsilon} - \frac{\varepsilon Pe_c^{(1)} \tilde{y}(3\tilde{x}^2 - \tilde{y}^2) / \varepsilon^{3/2}}{(\tilde{x}^2 + \tilde{y}^2)^3 / \varepsilon^3} + \frac{Pe_b \tilde{y} / \sqrt{\varepsilon}}{(\tilde{x}^2 + \tilde{y}^2) / \varepsilon} \end{aligned}$$

Or,

$$\begin{aligned}
u &= \sqrt{\varepsilon} Pe_c^{(1)} \tilde{x} - \frac{\varepsilon^{5/2} Pe_c^{(1)} \tilde{x} (\tilde{x}^2 - 3\tilde{y}^2)}{(\tilde{x}^2 + \tilde{y}^2)^3} + \frac{Pe_b \sqrt{\varepsilon} \tilde{x}}{\tilde{x}^2 + \tilde{y}^2} \\
v &= -\sqrt{\varepsilon} Pe_c^{(1)} \tilde{y} - \frac{\varepsilon^{5/2} Pe_c^{(1)} \tilde{y} (3\tilde{x}^2 - \tilde{y}^2)}{(\tilde{x}^2 + \tilde{y}^2)^3} + \frac{Pe_b \sqrt{\varepsilon} \tilde{y}}{\tilde{x}^2 + \tilde{y}^2}
\end{aligned}$$

In addition, the condition $Pe_b = O(1)$ must be satisfied, in order to achieve the same magnitude order for the flow imposed by the counter-flow and the flow imposed by the fuel ejection.

$$\begin{aligned}
u &= \sqrt{\varepsilon} Pe_c^{(1)} \tilde{x} - \frac{\varepsilon^{5/2} Pe_c^{(1)} \tilde{x} (\tilde{x}^2 - 3\tilde{y}^2)}{(\tilde{x}^2 + \tilde{y}^2)^3} + \frac{Pe_b \sqrt{\varepsilon} \tilde{x}}{\tilde{x}^2 + \tilde{y}^2} \\
v &= -\sqrt{\varepsilon} Pe_c^{(1)} \tilde{y} - \frac{\varepsilon^{5/2} Pe_c^{(1)} \tilde{y} (3\tilde{x}^2 - \tilde{y}^2)}{(\tilde{x}^2 + \tilde{y}^2)^3} + \frac{Pe_b \sqrt{\varepsilon} \tilde{y}}{\tilde{x}^2 + \tilde{y}^2}
\end{aligned}$$

Defining $\tilde{u} := u/\sqrt{\varepsilon}$ and $\tilde{v} := v/\sqrt{\varepsilon}$:

$$\begin{aligned}
\tilde{u} &= Pe_c^{(1)} \tilde{x} - \frac{\varepsilon^2 Pe_c^{(1)} \tilde{x} (\tilde{x}^2 - 3\tilde{y}^2)}{(\tilde{x}^2 + \tilde{y}^2)^3} + \frac{Pe_b \tilde{x}}{\tilde{x}^2 + \tilde{y}^2} \\
\tilde{v} &= -Pe_c^{(1)} \tilde{y} - \frac{\varepsilon^2 Pe_c^{(1)} \tilde{y} (3\tilde{x}^2 - \tilde{y}^2)}{(\tilde{x}^2 + \tilde{y}^2)^3} + \frac{Pe_b \tilde{y}}{\tilde{x}^2 + \tilde{y}^2}
\end{aligned}$$

The second terms are two order smaller than the others and shall be neglected:

$$\begin{aligned}
\tilde{u} &= Pe_c^{(1)} \tilde{x} + \frac{Pe_b \tilde{x}}{\tilde{x}^2 + \tilde{y}^2} + O(\varepsilon^2) \\
\tilde{v} &= -Pe_c^{(1)} \tilde{y} + \frac{Pe_b \tilde{y}}{\tilde{x}^2 + \tilde{y}^2} + O(\varepsilon^2)
\end{aligned}$$

The Z equation is described by

$$u \frac{\partial Z}{\partial x} + v \frac{\partial Z}{\partial y} = \left(\frac{\partial^2 Z}{\partial x^2} + \frac{\partial^2 Z}{\partial y^2} \right) \tag{C.2}$$

Which rewrite in the new coordinate system, is:

$$\sqrt{\varepsilon}\tilde{u}\frac{\partial\tilde{x}}{\partial x}\frac{\partial Z}{\partial\tilde{x}} + \sqrt{\varepsilon}\tilde{v}\frac{\partial\tilde{y}}{\partial y}\frac{\partial Z}{\partial\tilde{y}} = \left[\left(\frac{\partial\tilde{x}}{\partial x}\right)^2 \frac{\partial^2 Z}{\partial\tilde{x}^2} + \left(\frac{\partial\tilde{y}}{\partial y}\right)^2 \frac{\partial^2 Z}{\partial\tilde{y}^2} \right] \quad (\text{C.3})$$

Since

$$\frac{\partial\tilde{x}}{\partial x} = \sqrt{\varepsilon}, \quad \frac{\partial\tilde{y}}{\partial y} = \sqrt{\varepsilon},$$

then,

$$\begin{aligned} \sqrt{\varepsilon}\tilde{u}\sqrt{\varepsilon}\frac{\partial Z}{\partial\tilde{x}} + \sqrt{\varepsilon}\tilde{v}\sqrt{\varepsilon}\frac{\partial Z}{\partial\tilde{y}} &= \left[(\sqrt{\varepsilon})^2 \frac{\partial^2 Z}{\partial\tilde{x}^2} + (\sqrt{\varepsilon})^2 \frac{\partial^2 Z}{\partial\tilde{y}^2} \right] \\ \implies \varepsilon\tilde{u}\frac{\partial Z}{\partial\tilde{x}} + \varepsilon\tilde{v}\frac{\partial Z}{\partial\tilde{y}} &= \varepsilon \left(\frac{\partial^2 Z}{\partial\tilde{x}^2} + \frac{\partial^2 Z}{\partial\tilde{y}^2} \right) \end{aligned} \quad (\text{C.4})$$

Dividing by ε :

$$\tilde{u}\frac{\partial Z}{\partial\tilde{x}} + \tilde{v}\frac{\partial Z}{\partial\tilde{y}} = \left(\frac{\partial^2 Z}{\partial\tilde{x}^2} + \frac{\partial^2 Z}{\partial\tilde{y}^2} \right) \quad (\text{C.5})$$

A further change of coordinates system shall take place, this time for polar coordinates:

$$\tilde{x} = r \cos \theta \quad (\text{C.6})$$

$$\tilde{y} = r \sin \theta \quad (\text{C.7})$$

Which implies:

$$r = \sqrt{\tilde{x}^2 + \tilde{y}^2} \quad \text{and} \quad \theta = \arctan(\tilde{y}/\tilde{x})$$

Thus,

$$\frac{\partial r}{\partial\tilde{x}} = \frac{\tilde{x}}{\sqrt{\tilde{x}^2 + \tilde{y}^2}} = \frac{r \cos \theta}{r} = \cos \theta \quad (\text{C.8})$$

$$\frac{\partial r}{\partial\tilde{y}} = \frac{\tilde{y}}{\sqrt{\tilde{x}^2 + \tilde{y}^2}} = \frac{r \sin \theta}{r} = \sin \theta \quad (\text{C.9})$$

Derivating Equation (C.6) in relation to \tilde{x} :

$$\frac{\partial \tilde{x}}{\partial \tilde{x}} = \frac{\partial}{\partial \tilde{x}}(r \cos \theta)$$

$$\implies 1 = \cos \theta \frac{\partial r}{\partial \tilde{x}} + r \frac{\partial}{\partial \tilde{x}}(\cos \theta)$$

$$\implies 1 = (\cos \theta) \frac{\partial r}{\partial \tilde{x}} - r(\sin \theta) \frac{\partial \theta}{\partial \tilde{x}}$$

Using Equation (C.8):

$$1 = \cos^2 \theta - r(\sin \theta) \frac{\partial \theta}{\partial \tilde{x}}$$

$$\implies \frac{\partial \theta}{\partial \tilde{x}} = \frac{\cos^2 \theta - 1}{r \sin \theta}$$

$$\implies \frac{\partial \theta}{\partial \tilde{x}} = \frac{-\sin^2 \theta}{r \sin \theta}$$

Or, finally:

$$\frac{\partial \theta}{\partial \tilde{x}} = -\frac{\sin \theta}{r} \tag{C.10}$$

The procedure is the same for \tilde{y} , derivating Equation (C.7) and using Equation (C.9):

$$\frac{\partial \theta}{\partial \tilde{y}} = \frac{\cos \theta}{r} \tag{C.11}$$

Now it is time to calculate the r and θ second derivatives:

The r -derivative in relation to \tilde{x} :

From Equation (C.8):

$$\frac{\partial^2 r}{\partial \tilde{x}^2} = \frac{\partial}{\partial \tilde{x}}(\cos \theta) = -\sin \theta \frac{\partial \theta}{\partial \tilde{x}}$$

Using Equation (C.10):

$$\frac{\partial^2 r}{\partial \tilde{x}^2} = -\sin \theta \frac{(-\sin \theta)}{r}$$

Or,

$$\frac{\partial^2 r}{\partial \tilde{x}^2} = \frac{\sin^2 \theta}{r} \quad (\text{C.12})$$

Analogously for \tilde{y} , using Equation (C.9) and Equation (C.11):

$$\frac{\partial^2 r}{\partial \tilde{x}^2} = \frac{\cos^2 \theta}{r} \quad (\text{C.13})$$

The θ -derivative in relation to \tilde{x} :

From Equation (C.10):

$$\begin{aligned} \frac{\partial^2 \theta}{\partial \tilde{x}^2} &= \frac{\partial \theta}{\partial \tilde{x}} \left(-\frac{\sin \theta}{r} \right) \\ \Rightarrow \frac{\partial^2 \theta}{\partial \tilde{x}^2} &= - \left(\frac{r \cos \theta \frac{\partial \theta}{\partial \tilde{x}} - \frac{\partial r}{\partial \tilde{x}} \sin \theta}{r^2} \right) \end{aligned}$$

Using Equation (C.8) and Equation (C.10):

$$\begin{aligned} \Rightarrow \frac{\partial^2 \theta}{\partial \tilde{x}^2} &= - \left[\frac{r \cos \theta \left(-\frac{\sin \theta}{r} \right) - \cos \theta \sin \theta}{r^2} \right] \\ \Rightarrow \frac{\partial^2 \theta}{\partial \tilde{x}^2} &= - \left(\frac{-\cos \theta \sin \theta - \cos \theta \sin \theta}{r^2} \right) \end{aligned}$$

$$\implies \frac{\partial^2 \theta}{\partial \tilde{x}^2} = - \left(\frac{-2 \cos \theta \sin \theta}{r^2} \right)$$

Or, finally:

$$\frac{\partial^2 \theta}{\partial \tilde{x}^2} = \frac{2 \cos \theta \sin \theta}{r^2} \quad (\text{C.14})$$

By adopting analogous reasoning for \tilde{y} , from Equation (C.11) and using Equation (C.9) and Equation (C.11), one deduces:

$$\frac{\partial^2 \theta}{\partial \tilde{y}^2} = - \frac{2 \cos \theta \sin \theta}{r^2} \quad (\text{C.15})$$

Z-equation in terms of the new polar variables is

For an arbitrary variable w :

For the first derivatives:

$$\frac{\partial Z}{\partial w} = \frac{\partial Z}{\partial r} \frac{\partial r}{\partial w} + \frac{\partial Z}{\partial \theta} \frac{\partial \theta}{\partial w} \quad (\text{C.16})$$

For the second derivatives:

$$\frac{\partial^2 Z}{\partial w^2} = \frac{\partial}{\partial w} \left(\frac{\partial Z}{\partial w} \right)$$

Using Equation (C.16):

$$\begin{aligned} \frac{\partial^2 Z}{\partial w^2} &= \frac{\partial}{\partial w} \left(\frac{\partial Z}{\partial r} \frac{\partial r}{\partial w} + \frac{\partial Z}{\partial \theta} \frac{\partial \theta}{\partial w} \right) \\ \implies \frac{\partial^2 Z}{\partial w^2} &= \frac{\partial r}{\partial w} \left(\frac{\partial}{\partial w} \frac{\partial Z}{\partial r} \right) + \frac{\partial^2 r}{\partial w^2} \frac{\partial Z}{\partial r} + \frac{\partial \theta}{\partial w} \left(\frac{\partial}{\partial w} \frac{\partial Z}{\partial \theta} \right) + \frac{\partial^2 \theta}{\partial w^2} \frac{\partial Z}{\partial \theta} \\ \implies \frac{\partial^2 Z}{\partial w^2} &= \frac{\partial r}{\partial w} \left(\frac{\partial}{\partial r} \frac{\partial Z}{\partial w} \right) + \frac{\partial \theta}{\partial w} \left(\frac{\partial}{\partial \theta} \frac{\partial Z}{\partial w} \right) + \frac{\partial^2 r}{\partial w^2} \frac{\partial Z}{\partial r} + \frac{\partial^2 \theta}{\partial w^2} \frac{\partial Z}{\partial \theta} \end{aligned}$$

Using Equation (C.16) again:

$$\begin{aligned} \Rightarrow \frac{\partial^2 Z}{\partial w^2} &= \frac{\partial r}{\partial w} \left[\frac{\partial}{\partial r} \left(\frac{\partial Z}{\partial r} \frac{\partial r}{\partial w} + \frac{\partial Z}{\partial \theta} \frac{\partial \theta}{\partial w} \right) \right] + \\ &\quad + \frac{\partial \theta}{\partial w} \left[\frac{\partial}{\partial \theta} \left(\frac{\partial Z}{\partial r} \frac{\partial r}{\partial w} + \frac{\partial Z}{\partial \theta} \frac{\partial \theta}{\partial w} \right) \right] + \frac{\partial^2 r}{\partial w^2} \frac{\partial Z}{\partial r} + \frac{\partial^2 \theta}{\partial w^2} \frac{\partial Z}{\partial \theta} \end{aligned}$$

$$\begin{aligned} \Rightarrow \frac{\partial^2 Z}{\partial w^2} &= \left(\frac{\partial r}{\partial w} \right)^2 \frac{\partial^2 Z}{\partial r^2} + \left(\frac{\partial r}{\partial w} \frac{\partial \theta}{\partial w} \right) \frac{\partial^2 Z}{\partial r \partial \theta} + \\ &\quad + \left(\frac{\partial \theta}{\partial w} \frac{\partial r}{\partial w} \right) \frac{\partial^2 Z}{\partial \theta \partial r} + \left(\frac{\partial \theta}{\partial w} \right)^2 \frac{\partial^2 Z}{\partial \theta^2} + \frac{\partial^2 r}{\partial w^2} \frac{\partial Z}{\partial r} + \frac{\partial^2 \theta}{\partial w^2} \frac{\partial Z}{\partial \theta} \end{aligned}$$

Finally:

$$\frac{\partial^2 Z}{\partial w^2} = \left(\frac{\partial r}{\partial w} \right)^2 \frac{\partial^2 Z}{\partial r^2} + \left(\frac{\partial \theta}{\partial w} \right)^2 \frac{\partial^2 Z}{\partial \theta^2} + 2 \left(\frac{\partial r}{\partial w} \frac{\partial \theta}{\partial w} \right) \frac{\partial^2 Z}{\partial r \partial \theta} + \frac{\partial^2 r}{\partial w^2} \frac{\partial Z}{\partial r} + \frac{\partial^2 \theta}{\partial w^2} \frac{\partial Z}{\partial \theta} \quad (\text{C.17})$$

Since the deduction is for arbitrary w , from Equation (C.16) for the first derivatives and Equation (C.17) for the second, it is possible to write:

$$\frac{\partial Z}{\partial \tilde{x}} = \frac{\partial Z}{\partial r} \frac{\partial r}{\partial \tilde{x}} + \frac{\partial Z}{\partial \theta} \frac{\partial \theta}{\partial \tilde{x}} \quad (\text{C.18})$$

$$\frac{\partial Z}{\partial \tilde{y}} = \frac{\partial Z}{\partial r} \frac{\partial r}{\partial \tilde{y}} + \frac{\partial Z}{\partial \theta} \frac{\partial \theta}{\partial \tilde{y}} \quad (\text{C.19})$$

$$\frac{\partial^2 Z}{\partial \tilde{x}^2} = \left(\frac{\partial r}{\partial \tilde{x}} \right)^2 \frac{\partial^2 Z}{\partial r^2} + \left(\frac{\partial \theta}{\partial \tilde{x}} \right)^2 \frac{\partial^2 Z}{\partial \theta^2} + 2 \left(\frac{\partial r}{\partial \tilde{x}} \frac{\partial \theta}{\partial \tilde{x}} \right) \frac{\partial^2 Z}{\partial r \partial \theta} + \frac{\partial^2 r}{\partial \tilde{x}^2} \frac{\partial Z}{\partial r} + \frac{\partial^2 \theta}{\partial \tilde{x}^2} \frac{\partial Z}{\partial \theta} \quad (\text{C.20})$$

$$\frac{\partial^2 Z}{\partial \tilde{y}^2} = \left(\frac{\partial r}{\partial \tilde{y}} \right)^2 \frac{\partial^2 Z}{\partial r^2} + \left(\frac{\partial \theta}{\partial \tilde{y}} \right)^2 \frac{\partial^2 Z}{\partial \theta^2} + 2 \left(\frac{\partial r}{\partial \tilde{y}} \frac{\partial \theta}{\partial \tilde{y}} \right) \frac{\partial^2 Z}{\partial r \partial \theta} + \frac{\partial^2 r}{\partial \tilde{y}^2} \frac{\partial Z}{\partial r} + \frac{\partial^2 \theta}{\partial \tilde{y}^2} \frac{\partial Z}{\partial \theta} \quad (\text{C.21})$$

From Equation (C.18) and Equation (C.19), using Equation (C.8), Equation (C.10) and Equation (C.9), Equation (C.11), respectively:

$$\frac{\partial Z}{\partial \tilde{x}} = \cos \theta \frac{\partial Z}{\partial r} - \frac{\sin \theta}{r} \frac{\partial Z}{\partial \theta} \quad (\text{C.22})$$

$$\frac{\partial Z}{\partial \tilde{y}} = \sin \theta \frac{\partial Z}{\partial r} + \frac{\cos \theta}{r} \frac{\partial Z}{\partial \theta} \quad (\text{C.23})$$

From Equation (C.20) and Equation (C.21), using Equation (C.8), Equation (C.10), Equation (C.12), Equation (C.14) and Equation (C.9), Equation (C.11), Equation (C.13), Equation (C.15), respectively:

$$\begin{aligned} \frac{\partial^2 Z}{\partial \tilde{x}^2} = & (\cos^2 \theta) \frac{\partial^2 Z}{\partial r^2} + \left(\frac{\sin^2 \theta}{r^2} \right) \frac{\partial^2 Z}{\partial \theta^2} - \left(\frac{2 \sin \theta \cos \theta}{r} \right) \frac{\partial^2 Z}{\partial r \partial \theta} + \\ & + \left(\frac{\cos^2 \theta}{r} \right) \frac{\partial Z}{\partial r} + \left(\frac{2 \cos \theta \sin \theta}{r^2} \right) \frac{\partial Z}{\partial \theta} \end{aligned} \quad (\text{C.24})$$

$$\begin{aligned} \frac{\partial^2 Z}{\partial \tilde{y}^2} = & (\sin^2 \theta) \frac{\partial^2 Z}{\partial r^2} + \left(\frac{\cos^2 \theta}{r^2} \right) \frac{\partial^2 Z}{\partial \theta^2} + \left(\frac{2 \sin \theta \cos \theta}{r} \right) \frac{\partial^2 Z}{\partial r \partial \theta} + \\ & + \left(\frac{\sin^2 \theta}{r} \right) \frac{\partial Z}{\partial r} - \left(\frac{2 \cos \theta \sin \theta}{r^2} \right) \frac{\partial Z}{\partial \theta} \end{aligned} \quad (\text{C.25})$$

The velocity in polar terms is given by:

$$\begin{aligned} \tilde{u} = & P e_c^{(1)} r \cos \theta + \frac{P e_b \cos \theta}{r} \\ \tilde{v} = & - P e_c^{(1)} r \sin \theta + \frac{P e_b \sin \theta}{r} \end{aligned} \quad (\text{C.26})$$

Multiplying Equation (C.22) by \tilde{u} :

$$\begin{aligned}
\tilde{u} \frac{\partial Z}{\partial \tilde{x}} &= \tilde{u} \left(\cos \theta \frac{\partial Z}{\partial r} - \frac{\sin \theta}{r} \frac{\partial Z}{\partial \theta} \right) \\
\implies \tilde{u} \frac{\partial Z}{\partial \tilde{x}} &= \left(Pe_c^{(1)} r \cos \theta + \frac{Pe_b \cos \theta}{r} \right) \left(\cos \theta \frac{\partial Z}{\partial r} - \frac{\sin \theta}{r} \frac{\partial Z}{\partial \theta} \right) \\
\implies \tilde{u} \frac{\partial Z}{\partial \tilde{x}} &= \left(Pe_c^{(1)} r \cos^2 \theta \right) \frac{\partial Z}{\partial r} - \left(Pe_c^{(1)} \cos \theta \sin \theta \right) \frac{\partial Z}{\partial \theta} + \\
&\quad + \left(\frac{Pe_b \cos^2 \theta}{r} \right) \frac{\partial Z}{\partial r} - \left(\frac{Pe_b \cos \theta \sin \theta}{r^2} \right) \frac{\partial Z}{\partial \theta} \quad (C.27)
\end{aligned}$$

Multiplying Equation (C.23) by \tilde{v} :

$$\begin{aligned}
\tilde{v} \frac{\partial Z}{\partial \tilde{y}} &= \tilde{v} \left(\sin \theta \frac{\partial Z}{\partial r} + \frac{\cos \theta}{r} \frac{\partial Z}{\partial \theta} \right) \\
\implies \tilde{v} \frac{\partial Z}{\partial \tilde{y}} &= \left(-Pe_c^{(1)} r \sin \theta + \frac{Pe_b \sin \theta}{r} \right) \left(\cos \theta \frac{\partial Z}{\partial r} - \frac{\sin \theta}{r} \frac{\partial Z}{\partial \theta} \right) \\
\implies \tilde{v} \frac{\partial Z}{\partial \tilde{y}} &= - \left(Pe_c^{(1)} r \sin^2 \theta \right) \frac{\partial Z}{\partial r} - \left(Pe_c^{(1)} \cos \theta \sin \theta \right) \frac{\partial Z}{\partial \theta} + \\
&\quad + \left(\frac{Pe_b \sin^2 \theta}{r} \right) \frac{\partial Z}{\partial r} + \left(\frac{Pe_b \cos \theta \sin \theta}{r^2} \right) \frac{\partial Z}{\partial \theta} \quad (C.28)
\end{aligned}$$

Adding Equation (C.28) and Equation (C.27):

$$\tilde{u} \frac{\partial Z}{\partial \tilde{x}} + \tilde{v} \frac{\partial Z}{\partial \tilde{y}} = \left[Pe_c^{(1)} r (\cos^2 \theta - \sin^2 \theta) \right] \frac{\partial Z}{\partial r} - 2 \left(Pe_c^{(1)} \cos \theta \sin \theta \right) \frac{\partial Z}{\partial \theta} + \frac{Pe_b}{r} \frac{\partial Z}{\partial r}$$

Noting that $\cos^2 \theta - \sin^2 \theta = \cos(2\theta)$ and $2 \cos \theta \sin \theta = \sin(2\theta)$:

$$\tilde{u} \frac{\partial Z}{\partial \tilde{x}} + \tilde{v} \frac{\partial Z}{\partial \tilde{y}} = Pe_c^{(1)} r \cos(2\theta) \frac{\partial Z}{\partial r} - Pe_c^{(1)} \sin(2\theta) \frac{\partial Z}{\partial \theta} + \frac{Pe_b}{r} \frac{\partial Z}{\partial r} \quad (C.29)$$

Adding Equation (C.24) and Equation (C.25):

$$\frac{\partial^2 Z}{\partial \tilde{x}^2} + \frac{\partial^2 Z}{\partial \tilde{y}^2} = \frac{\partial^2 Z}{\partial r^2} + \frac{1}{r^2} \frac{\partial^2 Z}{\partial \theta^2} + \frac{1}{r} \frac{\partial Z}{\partial r} \quad (\text{C.30})$$

That is nothing more than the Laplacian in polar coordinates, as expected.

Finally, it is possible to rewrite the Z equation in polar coordinates, from Equation(C.29) = 1/Pe Equation(C.30):

$$Pe_c^{(1)} r \cos(2\theta) \frac{\partial Z}{\partial r} - Pe_c^{(1)} \sin(2\theta) \frac{\partial Z}{\partial \theta} + \frac{Pe_b}{r} \frac{\partial Z}{\partial r} = \left(\frac{\partial^2 Z}{\partial r^2} + \frac{1}{r^2} \frac{\partial^2 Z}{\partial \theta^2} + \frac{1}{r} \frac{\partial Z}{\partial r} \right) \quad (\text{C.31})$$

Or,

$$Pe_c^{(1)} r \cos(2\theta) \frac{\partial Z}{\partial r} - Pe_c^{(1)} \sin(2\theta) \frac{\partial Z}{\partial \theta} = \left[\frac{\partial^2 Z}{\partial r^2} + \frac{1}{r^2} \frac{\partial^2 Z}{\partial \theta^2} + (1 - Pe_b) \frac{1}{r} \frac{\partial Z}{\partial r} \right] \quad (\text{C.32})$$

Dividing by $Pe_c^{(1)}$ ($Pe_c^{(1)} \neq 0$):

$$r \cos(2\theta) \frac{\partial Z}{\partial r} - \sin(2\theta) \frac{\partial Z}{\partial \theta} = \frac{1}{Pe_c^{(1)}} \left[\frac{\partial^2 Z}{\partial r^2} + \frac{1}{r^2} \frac{\partial^2 Z}{\partial \theta^2} + (1 - Pe_b) \frac{1}{r} \frac{\partial Z}{\partial r} \right] \quad (\text{C.33})$$

$$Pe_c^{(1)} \left[r \cos(2\theta) \frac{\partial Z}{\partial r} - \sin(2\theta) \frac{\partial Z}{\partial \theta} \right] + \frac{Pe_b}{r} \frac{\partial Z}{\partial r} = \frac{1}{r} \frac{\partial}{\partial r} \left(r \frac{\partial Z}{\partial r} \right) + \frac{1}{r^2} \frac{\partial^2 Z}{\partial \theta^2} \quad (\text{C.34})$$

To search the transient period for each set of conditions ($Pe_c^{(1)}, Pe_b$), the above equation, Equation (C.28), is written in transient form,

$$\begin{aligned} \frac{\partial Z}{\partial \tau} + Pe_c^{(1)} \left[r \cos(2\theta) \frac{\partial Z}{\partial r} - \sin(2\theta) \frac{\partial Z}{\partial \theta} \right] + \frac{Pe_b}{r} \frac{\partial Z}{\partial r} = \\ \frac{1}{r} \frac{\partial}{\partial r} \left(r \frac{\partial Z}{\partial r} \right) + \frac{1}{r^2} \frac{\partial^2 Z}{\partial \theta^2} \end{aligned} \quad (\text{C.35})$$

in which $\tau = \varepsilon t$ from Equation (C.4) and $t = \hat{t}/(\hat{R}^2/\hat{\alpha})$, from the definition of t given in Section (3.1).